Life Assessment Methods for Inconel 600 as an Essential Material in Micro Gas Turbines

By

Arash Moradi

Submitted to the university of Hertfordshire in fulfilment of the requirement of the degree of

DOCTOR OF PHILOSOPHY

Department of Physics, Engineering and Computer Science

February 2024

DEDICATION

I would like to dedicate this thesis to:

My family, Especially My Wife

This work would never have been possible without their support and encouragement

Declaration

I hereby declare that work presented in this thesis titled “On Life Assessment Methods for Inconel 600 as an Essential Material in Micro Gas Turbines” is original and all sources are accordingly acknowledged in the reference also all material contained within this thesis has not been previously submitted to any degree.

Arash Moradi

University of Hertfordshire

February 2024

ABSTRACT

In this research, a comprehensive investigation was conducted to understand the mechanical behavior and fatigue characteristics of Inconel 600. The study involved a series of experimental tests and Finite Element simulations, which yielded useful information about the material's properties, fatigue life, and fracture behavior of Inconel 600.

The experiments provided crucial data on the suitability of Inconel 600 for various applications. The mechanical properties, including yield strength, ultimate tensile strength, elongation, and modulus of elasticity, were determined through quasi-static tests under uniaxial loading conditions. The stress-strain relationship beyond the elastic limits was described using the Ramberg-Osgood equation. Furthermore, microstructural analysis revealed variations in grain size and microstructures in different regions of the welded joints, with the Heat-Affected Zone (HAZ) showing distinct microstructural changes due to thermal cycling during welding. These changes significantly influenced the mechanical properties and fracture behavior of the material. The rapid heating and cooling cycles experienced by the HAZ lead to alterations in the material's microstructure, including grain growth, formation of new phases, and changes in grain boundary structures. These transformations directly impact the material's strength, ductility, and susceptibility to fracture, highlighting the intricate interplay between welding processes and microstructural evolution.

Fatigue tests were performed under both smooth and notched conditions to investigate fatigue life variations based on different loading conditions. The FE simulations, along with empirical fatigue damage models, provided accurate predictions of fatigue life and identified critical loading conditions that could lead to fatigue failure. While the FE analysis showed a good correlation with experimental fatigue data, some discrepancies were observed, likely due to internal defects associated with the welding process. The study emphasized the importance of considering notch strength reduction factors and mixed mode loading to enhance the precision of fatigue predictions.

A case study involving finite element analysis (FEA) was conducted on a KJ66 micro-turbine blade to evaluate the effects of laser shock peening (LSP). The analysis revealed

that LSP significantly reduced von-Mises stress and enhanced the fatigue life of the turbine blade by more than ten times, shifting the critical crack-prone areas away from the blade root.

The investigation into fracture behavior under tensile and fatigue loading conditions was conducted through fractographic analysis using SEM images. It was found that the presence of welding influenced the fracture mode, with welded samples exhibiting a propensity towards brittle-type fractures, in contrast to the more ductile fracture behavior observed in un-welded samples. This shift towards a brittle fracture mode in welded samples is indicative of altered material properties resulting from the welding process, such as increased susceptibility to crack initiation and propagation under applied loads. Stress concentration points introduced by welding led to preferential crack initiation along grain boundaries, contributing to brittle intergranular features.

Acknowledgments

I would also like to thank all the people of the organizations, which have participated in the research projects that are described in this thesis. I would like to thank Dr Mahmoud Chizari and Professor Yong Chen for their valuable guidance, advice and encouragement during my research project. Last but not least, to all my friends and people who directly or indirectly contributed that made this project possible.

Arash Moradi

February 2024

Contents

List of Figures

Nomenclature

A:	Coefficient of Basquin's Equation
B:	Exponent of Basquin's Equation
C:	Coefficient of Paris Law
E*:*	Elastic Modulus
F:	Applied Load
G	Shear Modulus
K:	Stress Intensity Factor
N:	Number of Cycles to Failure
R:	Stress Ratio
S:	Nominal Stress
T:	Absolute Temperature in Kelvin
El:	Elongation
FSS:	Fatigue Shear Stress
HCF:	High Cycle Fatigue
LCF:	Low Cycle Fatigue
LSP:	Laser Sock Peening
MSS:	Maximum Shear Stress
NSS:	Normalized Shear Stress
SIF:	Stress Intensity Factor
SWT:	Smith-Watson-Topper
b:	Fatigue Strength Exponent
c:	Fatigue Ductility Exponent
f:	Frequency
k:	Material constant
m:	Material-specific Constant Determined through Experimental calibration
t:	Thickness
f_{-1}:	Bending Endurance Limit
K_{IC}*:*	Toughness
K_{max}:	Maximum Stress Intensity Factor

K_t:	Elastic Stress Concentration Factor
N_f:	Fatigue Life Cycles
N_t:	Fatigue Transition Life
S_b:	Range of Bending Stress
S_{max}:	Maximum Remote Stress
S_{min}:	Minimum Stress
S_t:	Range of Torsional Stress
t_{-1}:	Torsional Endurance Limit
ΔH:	Activation Energy
ΔK:	crack-tip Stress Intensity Factor Range
$\Delta\tau$:	Shear Stress Amplitude
$\Delta\sigma$:	Stress Range
σ_y:	Yield Strength
σ_{ult}:	Ultimate Tensile Strength
$\sigma_{a,eq}$:	Equivalent Stress Range
β	Material Constant
φ	Phase Difference
σ_{eq}	Equivalent Uniaxial Stress
$\sigma_{n\,max}$	Maximum Normal Stress
σ_f'	Fatigue Strength Coefficient
τ_f'	Shear Fatigue Strength Coefficient
τ_a	Shear Stress Range
$\tau_{a,cr}$	Shear Stress Range on the Critical Plane
$\sigma_{n,cr}$	Normal Stress Range on the Critical Plane
$t_{A,B}$	Shear Endurance Limit
σ_u	Ultimate Tensile Stress
λ	Material Constant
ε_f'	Fatigue Ductility Coefficient
σ_m	Mean Stress
ε_a	Strain Amplitude
σ_{eqa}	Equivalent Stress Amplitude
σ_{xa}	Stress Amplitude in x Direction
σ_{ya}	Stress Amplitude in y Direction
σ_{za}	Stress Amplitude in z Direction
σ_{eqm}	Equivalent Mean Stress
σ_{xm}	Mean Stress in x Direction
σ_{ym}	Mean Stress in y Direction
σ_{zm}	Mean Stress in z Direction
ε_{eqa}	Equivalent Strain Amplitude
ε_x	Strain Amplitude in x Direction
ε_y	Strain Amplitude in y Direction
ε_z	Strain Amplitude in z Direction
γ_{xy}	Shear Strain Amplitude (xy component)
γ_{xz}	Shear Strain Amplitude (xz component)

γ_{yz}	Shear Strain Amplitude (yz component)
σn	Normal Stress on the Critical Plane
τ_f^*	Findley's Material Constant
$\tau_f{}'$	Shear Fatigue Strength Coefficient
$\gamma_f{}'$	Torsional Fatigue Strength Coefficient
$\boldsymbol{\varepsilon}_a$	Normal Stress
da/dN	Crack Growth Rate
γ_a	Shear Strain Amplitude
ε_c	Creep Strain
H'	Ramberg-Osgood's Constants
n'	Ramberg-Osgood's Constants
σ_{max}	Maximum Stress
ε_{max}	Maximum Strain
σ_{ar}	Equivalent Completely Reversed Stress Amplitude
σ_a	Stress amplitude at R=0
σ_{max}	Maximum Stress
K_i'	Cyclic Strength Coefficient

1.Introduction

1.1 Background

Within the field of engineering, crucial components serve as the cornerstone for a myriad of applications, each assuming a pivotal role in guaranteeing the functionality, efficiency, and reliability of diverse systems. Ranging from intricate mechanical structures to cutting-edge power generation systems, these components constitute the bedrock upon which technological progress is constructed. The significance of these elements cannot be overstated, acting as the linchpin for the seamless operation of various engineering applications. Importantly, the complexity of critical engineering components transcends their geometrical intricacies, encompassing the dynamic and diverse loadings they endure during operation. Whether facing static forces, cyclic stresses, or extreme temperatures, these components necessitate materials endowed with exceptional mechanical properties to withstand such challenging conditions. The integration of advanced materials becomes imperative to meet the multifaceted demands imposed on these components, ensuring longevity, reliability, and optimal performance. In this context, microturbine combined heat and power (CHP) systems emerge as exemplary instances of critical engineering components. Their compact design and versatility render them indispensable for power generation in environments with space constraints, illustrating the intricate interplay between geometry, applied loadings, and advanced materials within the critical engineering landscape [1-3]. Their small footprint allows for efficient placement in areas where available space is limited. Additionally, these systems exhibit rapid start-up times, enabling them to reach their maximum power output within minutes. This quick response capability allows microturbines to promptly adapt to fluctuating energy demands, ensuring an agile and responsive power generation solution [4]. Microturbines are also known for their low emissions, high reliability, and low maintenance requirements. Microturbines, which are small gas turbines typically under 100 kW in capacity, are often employed in CHP systems due to their compact size, high power density, and flexibility [5]. These systems, however, operate under demanding conditions, subjecting their components to static and cyclic loads at varying temperatures.

As a result, the materials used in fabricating microturbines must possess exceptional mechanical properties to withstand such challenging operating conditions.

In the context of CHP systems, materials play a crucial role in ensuring the performance, durability, and longevity of microturbine components [6]. One commonly used material in microturbine design is Inconel alloy, specifically Inconel 600. Inconel 600 is a nickel-chromium alloy that offers excellent high-temperature strength, corrosion resistance, and oxidation resistance [7, 8].

The turbine section of a microturbine, which converts the energy from the expanding combustion gases into mechanical power, experiences high temperatures and stresses. Inconel alloy is often chosen for turbine blades, rotor discs, and other components in this section due to its superior high-temperature properties. Inconel alloys can withstand temperatures up to approximately 1093°C (2000°F) and exhibits good resistance to thermal fatigue, corrosion, and oxidation, making them well-suited for the demanding conditions encountered in microturbine operation systems or reactor vessels [9]. In the upcoming section, the details of micro gas turbine structures, including their parts and the materials typically used, have been discussed. It will be explained why Inconel 600 alloy is chosen for assessment under different types of stress and heat. This discussion offers a clear understanding of these turbine structures and why a specific alloy like Inconel 600 is crucial for their performance.

It should be emphasized that this thesis addresses the overarching theme of critical engineering components, with a specific focus on investigating the suitability of Inconel 600, a nickel-chromium alloy, under fatigue and creep loads. While microturbine combined heat and power systems are emblematic examples of critical engineering components, it's important to note that they represent just one facet of this comprehensive study. Microturbine systems have been selectively chosen as a case study within this larger framework, serving as a representative example of the broader exploration of Inconel 600's performance in diverse critical engineering applications. The novelty of this research lies not only in its thorough examination of Inconel 600 but also in the specific attention given to microturbines, an area that, to the best of our knowledge, has not been extensively studied by other researchers. By delving into the intricacies of Inconel 600's response to fatigue and creep conditions across various critical engineering components,

this thesis aims to contribute valuable insights to the field of materials science and engineering.

1.2 Micro gas turbines structures

Micro gas turbines are compact, high-speed rotating machines that convert chemical energy from fuel into mechanical energy through combustion processes. They consist of several essential components, each playing a substantial role in the efficient operation of the turbine. Figure 1-1 illustrates a schematic view of a typical micro gas turbine.

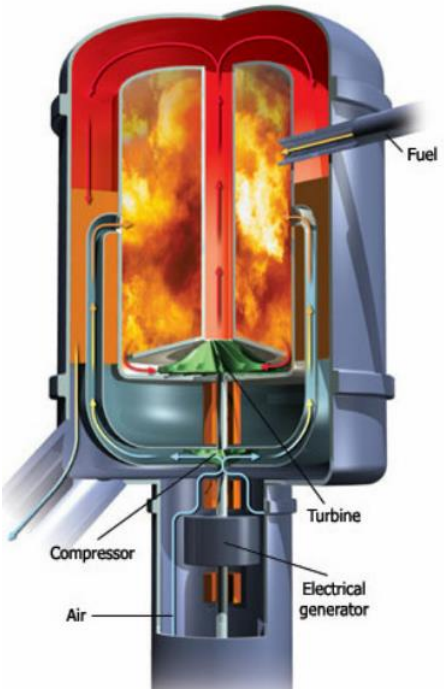

Figure 1-1. Schematic view of a typical micro gas turbine with its internal working (source: www.microturbine.com)

1.2.1 Components of micro gas turbines

Micro gas turbines typically comprise the following components:

Compressor: The compressor is responsible for drawing in and compressing the incoming air before it enters the combustion chamber. It enhances the efficiency of the combustion process by increasing the air pressure.

Combustion chamber: In the combustion chamber, the compressed air mixes with fuel and undergoes combustion. This process generates high-temperature, high-pressure gases that propel the turbine's blades.

Turbine: The turbine extracts energy from the high-temperature, high-pressure gases produced in the combustion chamber. As the gases expand through the turbine blades, they cause the turbine to rotate, generating mechanical energy.

Exhaust system: The exhaust system directs the hot gases exiting the turbine away from the turbine, converting the remaining energy into useful work.

Almost all the above-mentioned components are usually under severe complex cyclic loading. Therefore, selecting appropriate materials for different parts of the micro turbine against fatigue and creep phenomena is of great importance.

1.2.2. Common materials used in micro gas turbine components

The choice of materials for micro gas turbine components is crucial due to the extreme conditions these components endure, such as high temperatures and mechanical stresses. Common materials used in micro gas turbines include nickel-based superalloys, cobalt-based superalloys, and iron-based superalloys [10].

Nickel-Based superalloys: Nickel-based superalloys are widely used in micro gas turbines due to their excellent high-temperature strength, creep resistance, and corrosion resistance [11]. They are extensively applied in the hottest sections of gas turbines, ensuring reliable performance under extreme conditions.

Cobalt-Based superalloys: Cobalt-based superalloys are employed in components located in the combustion chamber, where temperatures can reach up to 1100℃ [10]. These alloys maintain their strength at high temperatures and are resistant to thermal shocks, making them suitable for specific micro gas turbine parts.

Iron-Based superalloys: Iron-based superalloys, evolving from austenitic stainless steels, offer a balance between strength and cost. They find applications in various micro gas turbine components, depending on the operating temperature. These alloys are categorized into different subclasses, each tailored for specific temperature ranges and properties.

1.2.3. Similarities and differences between micro gas turbines and macro gas turbines

While micro gas turbines share fundamental components with larger gas turbines, they differ in scale and application. Micro gas turbines are designed for compactness and efficiency, making them suitable for portable power generation, distributed energy systems, and small-scale aerospace applications. In contrast, larger gas turbines are used in power plants, aircraft engines, and industrial applications, where higher power output is required.

Despite the scale difference, both micro gas turbines and larger gas turbines rely on similar principles of operation, including the compression of air, combustion of fuel, and extraction of energy through turbine blades. The selection of materials remains a critical aspect in both cases, ensuring reliable and efficient performance under diverse operating conditions.

Figure 1-2 highlights various components of a typical gas turbine engine (Rolls-Royce), underscoring the strategic use of advanced superalloys throughout the system [12].

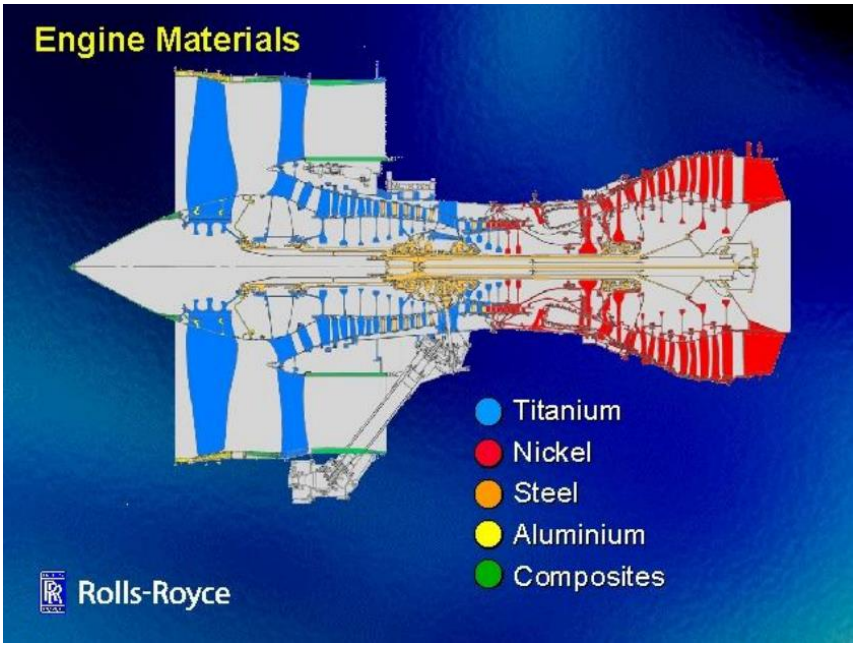

Figure 1-2. Materials used in various parts of a typical macro gas turbine engine (source: Michael Cervenka) [12]

1.2.4. Importance of material selection for micro gas turbine design

The selection of materials for micro gas turbine components is paramount to ensuring their structural integrity, durability, and overall performance. This is particularly crucial in components subjected to high temperatures, mechanical stresses, fatigue, and creep. Among the various materials available, nickel-based superalloys (Inconel alloys) play a substantial role in enhancing the efficiency and longevity of micro gas turbines.

While Inconel alloys are recognized for their suitability in microturbine components, the specific investigation of Inconel 600 under fatigue and creep conditions remains a novel aspect of research. The selection of Inconel 600 for assessment under different types of stress and heat in microturbine components forms the basis of this study. Given that the suitability of Inconel 600 for microturbine components has not been extensively explored by other researchers, this research aims to fill a crucial gap in the existing knowledge and contribute to the understanding of the material's behavior under critical conditions.

1.2.5. Significance of Inconel alloys in micro gas turbine design

Inconel alloys offer exceptional properties that are indispensable for micro gas turbine applications:

High temperature strength: These alloys maintain their strength and structural integrity at elevated temperatures, allowing micro gas turbines to operate efficiently even under extreme conditions.

Creep resistance: Inconel alloys exhibit excellent resistance to creep, which is the gradual deformation of materials under constant load and elevated temperatures. This property ensures the long-term reliability of micro gas turbine components.

Fatigue resistance: These materials possess superior fatigue resistance, enabling micro gas turbine components to withstand cyclic loading without failure, thereby enhancing their lifespan.

1.2.6. Role of Inconel alloys in fatigue and creep designs

In micro gas turbines, components such as turbine blades and disks are subjected to cyclic loading and high temperatures. Inconel alloys are specifically chosen for these

parts due to their ability to withstand fatigue and creep. Fatigue resistance ensures that components can endure repeated stress cycles without developing cracks or failures, while creep resistance guarantees structural stability over prolonged periods of continuous operation at elevated temperatures.

The careful consideration of material properties, especially fatigue and creep resistance, is essential during the design phase of micro gas turbines. Proper material selection not only ensures the structural integrity of components but also enhances the overall efficiency and reliability of the turbine system.

1.2.7. Selection of Inconel 600 alloy for fatigue and creep assessment

Inconel 600, a nickel-chromium alloy, has been chosen for our study due to its remarkable properties that make it suitable for fatigue and creep assessment in micro gas turbine components. This alloy is composed of 76% nickel, 15% chromium, and 8% iron, offering a combination of high-temperature strength, corrosion resistance, and excellent mechanical properties.

1.2.8. Properties of Inconel 600 alloy

High temperature strength: Inconel 600 exhibits exceptional strength at elevated temperatures, making it ideal for components exposed to high thermal loads.

Corrosion resistance: This alloy provides excellent resistance to corrosion, making it suitable for micro gas turbine parts exposed to aggressive environments, such as those found in combustion chambers.

Fatigue resistance: Inconel 600 possesses good fatigue resistance, enabling it to withstand cyclic loading without premature failure, a crucial characteristic for components subjected to dynamic stresses.

Creep resistance: The alloy demonstrates notable creep resistance, ensuring the structural stability of components during prolonged exposure to high temperatures and continuous loading.

1.2.9. Assessment of Inconel 600 alloy under fatigue and creep

The present study involves a comprehensive assessment of Inconel 600 alloy under fatigue and creep conditions to evaluate its performance and durability in micro gas turbine applications. Through rigorous testing and analysis, we aim to understand the alloy's behavior, including fatigue life, creep deformation, and rupture strength.

By subjecting Inconel 600 samples to controlled fatigue and creep tests, we can gather valuable data on its mechanical response under different loading conditions and temperatures. This data will contribute to a deeper understanding of the alloy's fatigue and creep characteristics, aiding in the refinement of micro gas turbine designs for enhanced reliability and efficiency.

As previously mentioned, designing microturbine parts based on fatigue and creep considerations is crucial to ensure their long-term performance and structural integrity. Fatigue analysis is employed to assess the fatigue life of critical components subjected to cyclic loading, such as turbine blades, while creep analysis is used to evaluate the time-dependent deformation and potential failure of components operating at high temperatures over extended periods.

Fatigue and creep failures can result in costly accidents, repairs, and replacements. These incidents can lead to significant financial losses for industries, affecting their profitability and competitiveness. Given the potential economic impacts of fatigue and creep failures, there is a strong case for conducting thorough investigations and research in these sectors:

- Investigating fatigue and creep behavior of the parts being used in microturbine systems can help improve the safety and reliability of the critical components, reducing the likelihood of catastrophic failures.
- Understanding the mechanisms of fatigue and creep can lead to the development of more cost-effective and durable materials and designs, ultimately saving money for the relevant industries.

Finite element analysis (FEA) is a commonly employed technique for simulating and analyzing the stress and strain behavior of microturbine components [13-16]. By incorporating an understanding of material properties, such as the fatigue and creep characteristics of Inconel 600, and carefully assessing the expected operating conditions,

engineers can significantly enhance the overall design, identify vulnerable areas, and guarantee the structural integrity and reliability of microturbine components.

The utilization of advanced materials like Inconel 600, combined with meticulous considerations for fatigue and creep resistance, plays a crucial role in securing the exceptional performance, extended durability, and steadfastness of microturbine parts, particularly under challenging and demanding operational environments. The prudent selection of materials and rigorous design analysis are paramount in optimizing the efficiency and longevity of the components used in microturbine combined heat and power systems. FEA facilitates the exploration of intricate stress distributions and the identification of potential failure modes within microturbine components. It allows for detailed analysis under various loading conditions, including thermal cycling and mechanical stresses, which are crucial factors affecting component performance and longevity.

1.3. Research Gaps

Despite the advancements in critical engineering components, such as microturbine combined heat and power systems, and the utilization of advanced materials in their specific components, there are several research gaps that require further investigation. These gaps include:

- Challenges in Micro Gas Turbines: Micro gas turbines face challenges such as high-temperature operation and fatigue failure due to cyclic loading. While materials like Inconel 780 are commonly used, they exhibit disadvantages including susceptibility to certain types of plastic deformation. In contrast, Inconel 600 offers excellent resistance to oxidation and corrosion, as well as improved mechanical properties under high-temperature conditions, making it a promising material for enhancing the durability and reliability of turbine blades.
- Mechanical Properties and Fatigue Parameters of Inconel 600: Further research is needed to characterize the basic mechanical properties of Inconel 600 parent materials and weldments. This includes determining key parameters such as yield strength, ultimate tensile strength, and fatigue behavior. Obtaining strain-based fatigue parameters for both the Inconel 600 parent material and weldments would

significantly contribute to accurate fatigue life prediction and reliability assessments.

- Fatigue Life Prediction of Inconel 600 Welded Structures: Investigating the fatigue life of Inconel 600 welded structures is essential, particularly under various loading conditions and the presence of notches. Research should focus on fatigue life prediction for welded structures, considering different types of notches, such as single-edge notches and double-sided edge notches. Understanding the influence of these notches on fatigue performance will aid in optimizing the design and reducing the risk of failure. This is important because in microturbines and other critical parts, welded structures are common. It is crucial to know how these structures hold up under repeated stress. Notches, which are common in welds, can make the components even weaker. By studying different notch types, it can be figured out how to make microturbines and other components last longer and work better.
- Fatigue Life Prediction under Multi-Axial Loading: Research efforts should explore fatigue life prediction methodologies for Inconel 600 under multi-axial loading conditions. This includes investigating energy-based models and critical plane approaches to accurately assess the effects of complex loading patterns on fatigue life. Developing reliable models and methodologies will enable better design optimization and ensure the structural integrity of microturbine components.
- Fatigue Analysis of Microturbine Blades with and without Laser Shock Peening: As a relevant case study, the fatigue analysis of microturbine blades due to their exposure to cyclic loading is studied. Research should focus on investigating the effects of laser shock peening on the fatigue performance of Inconel 600 blades. Comparing the fatigue behavior of blades with and without laser shock peening treatment will provide valuable insights into the effectiveness of this surface treatment method in enhancing fatigue resistance.
- Fatigue Crack Growth in Inconel 600 at Different Angles (Mixed Mode Fracture): Studying fatigue crack growth behavior in Inconel 600 under different angles of loading (mixed mode fracture) is necessary to understand its resistance to crack propagation. Investigating the crack growth rates, crack paths, and fracture

mechanics parameters under mixed mode loading conditions will help in developing accurate fatigue life prediction models for Inconel 600 components.

- Creep Behavior: Further research is needed to investigate the creep behavior of Inconel 600 under different operating conditions, including high temperatures. Understanding the time-dependent deformation and potential failure mechanisms due to creep will contribute to improved design guidelines and maintenance strategies for microturbine components.

Addressing these specific research gaps will provide valuable insights into the mechanical properties, fatigue behavior, and creep resistance of Inconel 600, enhancing the design, reliability, and durability of microturbine components in demanding operating conditions.

1.4. Project Aim and Objectives

The phenomenon of fatigue is a critical consideration in the design and maintenance of engineering structures exposed to cyclic loading. Fatigue failure can significantly compromise the structural integrity and reliability of components, leading to costly repairs, safety risks, and operational disruptions. Therefore, understanding and predicting fatigue behavior is of utmost importance for ensuring the longevity and performance of various structures.

In the context of this study, our focus is on investigating the fatigue phenomenon, fatigue life predictions, and related aspects in the specific context of microturbine components. Microturbines are widely used in combined heat and power (CHP) systems due to their compact size, high power density, and flexibility. However, operating under demanding conditions and subject to static and cyclic loads at varying temperatures, microturbine components require exceptional mechanical properties to withstand these challenging environments.

The objectives of this study revolve around investigating and understanding the fatigue behavior of microturbine components, specifically targeting Inconel 600 alloy, a commonly used material in their fabrication. By examining various aspects such as fatigue life predictions, the influence of different loading conditions and geometric features, creep behavior, microstructures, and fatigue damage mechanisms, this research aims to

provide valuable insights for design optimization, material selection, and maintenance strategies.

The specific objectives of the study are as follows:

- Objective 1: Investigate Fatigue Behavior of Standard and Welded Structures

The primary objective of this study is to examine the fatigue performance of both standard structural components and welded joints under cyclic loading conditions. By conducting comprehensive experimental investigations, we aim to compare and analyze the fatigue strength and life of these structures. Special attention will be given to the influence of welding processes, weld quality, and geometrical features on the fatigue behavior. This objective will provide valuable insights into the fatigue characteristics of standard and welded structures, contributing to their design optimization and enhanced reliability.

- Objective 2: Predict Fatigue Life of Structures under Uniaxial and Multiaxial Loading

The goal of this objective is to develop and validate predictive models for estimating the fatigue life of structures under both uniaxial and multiaxial loading conditions. By considering stress concentrations, stress gradients, and complex loading paths, we aim to investigate their role in fatigue crack initiation and propagation. We will evaluate the applicability of established fatigue life prediction methods, such as the Paris law and critical plane approaches, to the studied structures. Achieving this objective will enable accurate estimation of fatigue life and facilitate the design and maintenance of structures exposed to various loading conditions.

- Objective 3: Assess Fatigue Performance of Notched Specimens

This objective focuses on assessing the fatigue performance of specimens with notches, considering stress concentration factors and geometric features. Through experimental investigations, we will analyze the effects of notches on fatigue strength and life. We aim to identify the notch sensitivity and fatigue crack initiation behavior of different materials and microstructures. Additionally, we will develop empirical relationships or correction factors to account for the presence of notches in fatigue life predictions. This objective will provide insights into the influence of notches on fatigue behavior and aid in improving design practices for structures with stress concentration features.

- Objective 4: Study Creep Behavior and Its Interaction with Fatigue

The objective of this study is to investigate the creep properties of materials used in the studied structures under elevated temperature and long-term loading. We will examine the interaction between creep and fatigue, considering factors such as stress levels, temperature, and time to failure. Through experimental investigations and analysis, we aim to develop constitutive models and numerical methods to predict the combined behavior of fatigue and creep in structures. This objective will enhance our understanding of the creep-fatigue interaction, enabling more accurate lifetime predictions and ensuring the structural integrity of components subjected to prolonged loading conditions.

- Objective 5: Characterize Microstructures and Fatigue Damage Mechanisms

In this objective, we will utilize advanced microscopy techniques, such as scanning electron microscopy (SEM), to analyze the microstructural features and their influence on fatigue performance. The goal is to identify fatigue damage mechanisms, including crack initiation, propagation, and microstructural changes. By correlating microstructural characteristics with fatigue life and failure modes, we aim to gain insights into the underlying mechanisms governing fatigue behavior. This objective will enhance our understanding of the microstructural aspects related to fatigue and contribute to the development of more resilient and fatigue-resistant materials and components.

- Objective 6: Validate Experimental Results with Finite Element Analysis (FEA)

The objective of this study is to validate the experimental findings by performing finite element simulations and verifying the accuracy of fatigue life predictions. By incorporating material properties, loading conditions, and geometrical features into FEA models, we aim to capture the behavior of the studied structures under cyclic loading. Through FEA techniques, we will investigate the stress and strain distribution, crack growth, and damage accumulation. Achieving this objective will provide additional validation and a deeper understanding of the observed fatigue behavior, enhancing the reliability of fatigue life predictions.

- Objective 7: Provide Recommendations for Design and Material Selection

Based on the findings of this study, the objective is to summarize the results and draw meaningful conclusions regarding the fatigue behavior of standard and welded structures. Through a comprehensive analysis, we will provide valuable recommendations for design guidelines, including geometrical features, weld quality, and stress concentrations, to

enhance fatigue resistance. Furthermore, suitable materials and microstructural modifications will be proposed that can improve the fatigue performance of structures subjected to cyclic loading. This objective aims to bridge the gap between research findings and practical applications, assisting engineers and designers in making informed decisions to optimize design and material selection for fatigue-resistant structures.

By addressing these objectives, this study aims to advance the understanding of fatigue behavior, predict fatigue life, assess the influence of welding, stress concentrations, and microstructures, and provide valuable insights for design and material selection for microturbine blade subjected to cyclic loading. The outcomes of this research will contribute to the development of more reliable and durable structures, ensuring their safe and efficient operation in various engineering applications.

1.5. Structure of the Thesis

The thesis aims to investigate the fatigue and creep behavior of microturbine components, with a specific focus on Inconel 600 alloy. The structure of the present thesis is as follows:

Chapter 1 provides an overview of the research topic and sets the context for the study. It introduces the background of the research, highlighting the importance of investigating fatigue and creep behavior in microturbine components. The chapter also identifies the research gaps and presents the specific objectives of the study. Finally, it outlines the structure of the thesis, giving a brief overview of each chapter.

In chapter 2, a comprehensive review of the existing literature on fatigue and creep is presented. This chapter covers the fundamental concepts of fatigue, including fatigue crack initiation and propagation, as well as various methods for fatigue life prediction. The literature review also discusses fatigue crack growth models such as the Paris law and the Walker model. Additionally, the chapter provides an introduction to the creep phenomenon, influential parameters in creep deformation, and creep modeling techniques. This chapter establishes a strong theoretical foundation for the subsequent chapters of the thesis.

Chapter 3 focuses on the materials used in the study, with a particular emphasis on Inconel 600. It describes the different types of specimens used, including standard

specimens, weldments, and notched specimens. The chapter also provides details on the mechanical testing methods employed, such as quasi-static tests, hardness testing, and fatigue tests. Furthermore, it explains the setup for creep tests and discusses the fractography analysis of ruptured specimens. Additionally, the chapter introduces finite element analysis (FEA) and its application to the study, including FE modeling, boundary conditions, and the Johnson-Cook plasticity model. This chapter provides a comprehensive overview of the materials, specimens, and methodologies used in the research.

In Chapter 4, the results of the experiments and simulations conducted in the study are presented. The chapter begins with an introduction that sets the context for the results section. It then proceeds to present the findings related to fatigue life prediction of Inconel 600 parent material, weldments, and notched specimens. The fractography of the tested specimens under various loading conditions, such as tensile and cyclic loading, is also discussed. Additionally, the results of multiaxial fatigue, fatigue crack growth, and creep loading experiments are presented. This chapter provides a comprehensive analysis and discussion of the obtained results, interpreting their significance and implications within the context of the research objectives.

The final chapter of the thesis summarizes the key findings and draws conclusions based on the results and discussions presented in the previous chapters. It addresses the research objectives and assesses the extent to which they have been achieved. The chapter also provides recommendations for future research directions based on the insights gained from the study. This includes identifying areas for further investigation, potential improvements in experimental methods, and suggestions for advancing the understanding of fatigue and creep behavior in microturbine components. This chapter concludes the thesis, offering a concise summary of the research outcomes and highlighting avenues for future exploration.

The structure of the present thesis has been summarized in the following flowchart (Figure 1-3).

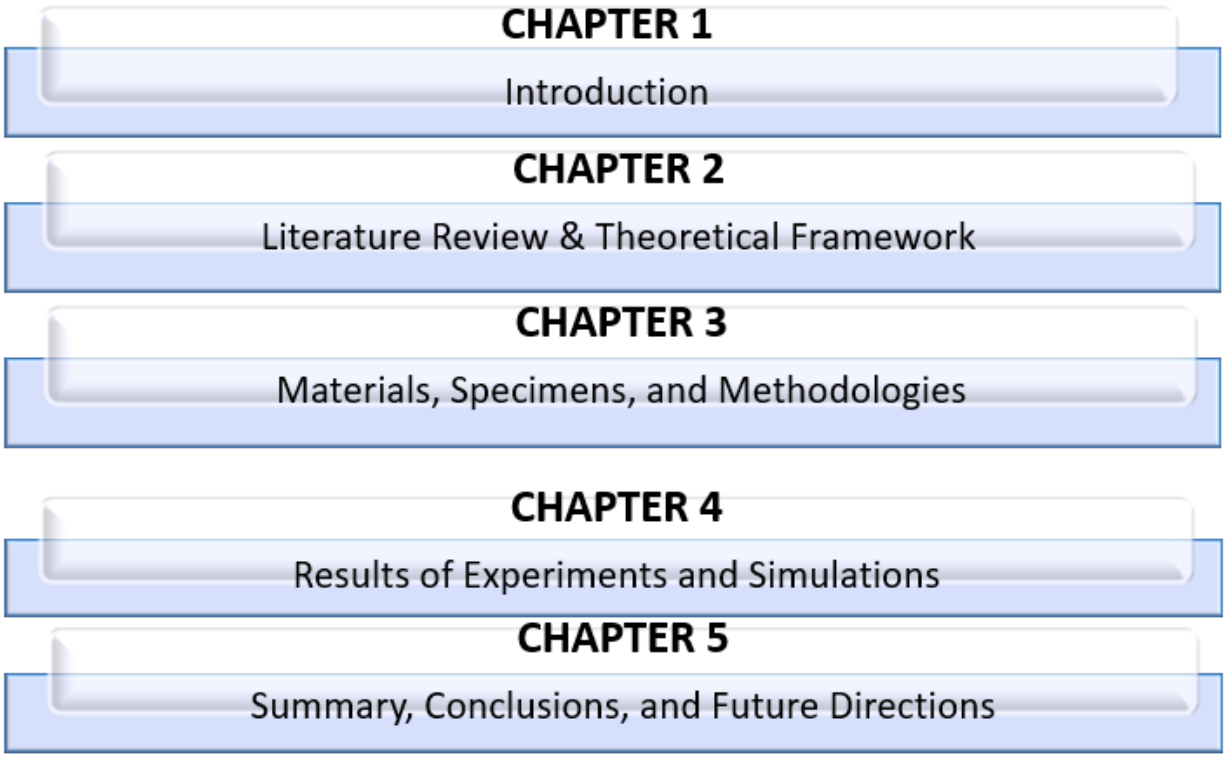

Figure 1-3. Flowchart of the thesis structure

2. Literature Review

2.1. Theoretical Background

2.1.1. Introduction to Fatigue

Fatigue failure in metals and structures refers to a specific type of failure that occurs under cyclic or repeated loading conditions. It is characterized by the progressive development of cracks and ultimately the fracture of the material, even when the applied loads are well below the material's ultimate strength.

When a metal or structural component is subjected to cyclic loading, such as repeated bending or fluctuating stress levels, the material undergoes repetitive stress cycles. Over time, these cycles can lead to the initiation and growth of small cracks, known as fatigue cracks, in areas of high stress concentration or material defects.

The fatigue failure process typically consists of several stages. Initially, microcracks form at stress concentration sites or material imperfections. As the loading continues, these cracks propagate and grow gradually under the cyclic stresses. The cracks may continue to propagate until they reach a critical size, at which point catastrophic failure occurs. Several factors influence the fatigue behavior of materials and structures. These include the stress level applied during cyclic loading [17-22], microstructures and material's properties [23-25], the presence of stress concentrators (such as sharp corners or notches) [26-29], the environment in which the component operates (e.g., temperature, humidity, corrosive substances) [30-35], and the structural design [36].

To prevent fatigue failure, engineers and designers employ various strategies. These include conducting fatigue analysis and testing during the design phase to estimate the component's expected fatigue life, avoiding stress concentrations and sharp transitions in the design, using materials with higher fatigue resistance, applying surface treatments such as laser shock peening to improve fatigue strength [37-39], and implementing regular inspection and maintenance programs to detect and address fatigue cracks before they reach critical sizes.

Understanding fatigue failure is crucial in industries such as aerospace, automotive, civil engineering, and manufacturing, where structures and components are subjected to

repetitive loading conditions. By considering fatigue behavior in the design, materials selection, and maintenance processes, engineers can ensure the safety and reliability of structures and extend their operational lifetimes.

The summary of this chapter has been summarized in the following flowchart (see Figure 2-1).

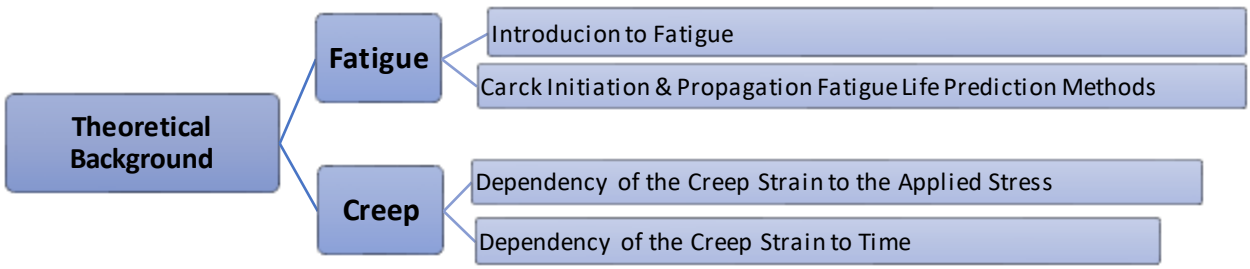

Figure 2-1. Flowchart of the present chapter

2.1.2. Fatigue Crack Initiation and Propagation

Fatigue failure consists of different stages of cracking. Fatigue crack initiation, fatigue crack propagation, and final failure in either ductile manner, involving considerable deformation, or in brittle way, involving little deformation, are three well-known stages of fatigue cracking [40]. Each above-mentioned stages have their own mechanisms and characteristics for different materials and under various conditions.

Fatigue crack initiation and propagation are important concepts in the field of materials engineering and structural mechanics. Fatigue crack initiation occurs when small cracks begin to form within a material due to repeated loading cycles. These cracks typically initiate at locations of high stress concentration, such as notches, sharp corners, or areas with material defects. The presence of stress raisers amplifies the local stresses, making the material more susceptible to crack initiation.

Once a fatigue crack initiates, it can propagate and grow through the material. This propagation occurs due to the cyclic loading, where the stress applied during each loading cycle causes the crack to extend gradually. The crack growth is influenced by factors such as the stress amplitude, stress ratio (the ratio of minimum stress to maximum stress), loading frequency, and material properties [41].

During fatigue crack propagation, various mechanisms come into play, depending on the material and environmental conditions [42]. These mechanisms include fatigue crack growth by the opening and closing of the crack faces (opening mode), shear displacement along the crack plane (sliding mode) and tearing or separation of material ahead of the crack tip (tearing mode). Engineers employ techniques like fracture mechanics analysis and design considerations to assess and mitigate the risks associated with fatigue crack growth.

Various methods have been proposed to calculate fatigue life of engineering components, which are suggested for different loading conditions. Some of these methods only consider the initiation stage and assume that the crack propagation life can be neglected compared to the initiation stage. This theory is generally applicable to high-cycle fatigue in smooth components or specimens with very small notches, accompanied by low-stress concentration. On the other hand, there are methods that consider only the crack propagation stage as the fatigue life associated with the final failure. In these models, when the initial crack is very small, linear elastic fracture mechanics (LEFM) relationships cannot be used. However, when the crack grows sufficiently large, the provided relationships can be used [43].

In metallic materials, in the absence of cracked or debonded second-phase particles or pre-existing crack-like defects, fatigue crack formation entails the concentration of permanent plastic strain within slip bands that generally lead to either the formation of intrusions or extrusions at surface grains or their impingement on grain boundaries. Through continued cyclic loading, these slip band mechanisms lead to lattice/interface disruption and the formation of a crack of either a transgranular or intergranular nature [44].

For metallic materials, the more commonly used term in engineering practice, “crack initiation,” refers to the combined processes of crack formation and growth to some predefined crack length that encompasses many grains/phases. Fatigue damage mechanisms at the macro-scale can consist of slip-bands formation, early growth of microstructurally small fatigue cracks, and fatigue crack growth beyond the first grain or phase. Two fracture modes, the mixed mode of I+II followed by pure mode I, can be seen at the early stages of crack nucleation and growth, as evidenced in Figure 2-2.

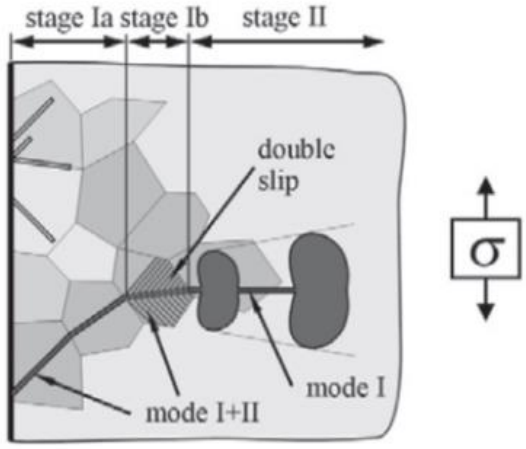

Figure 2-2. Fatigue crack formation in metallic materials under cyclic loading [44]

This figure illustrates the progression of fatigue damage mechanisms in metallic materials, including slip-band formation, early growth of microstructurally small fatigue cracks, and the transition from mixed mode I+II fracture to pure mode I fracture during crack nucleation and growth. Understanding these mechanisms is crucial for predicting and mitigating fatigue failure in engineering components.

When designing components or structures subjected to repetitive loads, it's essential to consider the various aspects of fatigue damage mechanisms. These mechanisms can lead to structural failure and reduced lifespan, making it crucial to consider them during design. One of the primary features to consider is fatigue crack initiation and growth, which occurs due to cyclic loading that causes small cracks to form and grow over time. Therefore, understanding how to detect and predict fatigue crack initiation and growth is crucial for ensuring the reliability and safety of the structure. Another critical aspect to consider is the type of applied stresses. Uniaxial and multi-axial loading conditions can lead to fatigue damage, but they affect the structure differently. Uniaxial loading, for example, can lead to cracks forming perpendicular to the applied load, while multi-axial loading can result in cracks forming in various directions.

Finally, analyzing fatigue damage can be approached from various perspectives, including stress, strain, energy, or fracture mechanics. These viewpoints can provide valuable insights into the underlying mechanisms of fatigue damage and help designers

develop more robust and reliable structures. Figure 2-3 illustrates some basic fatigue definitions and different cyclic loadings. In Figure 2-3(a), stress amplitude (σ_a), mean stress (σ_m), maximum and minimum stresses (σ_{max}) and (σ_{min}), and stress range $(\Delta\sigma)$ in a regular non-zero mean stress loading condition are shown. The following equations relate the above-mentioned terms together [45]:

$$\sigma_a = \frac{\sigma_{max} - \sigma_{min}}{2} \quad (2\text{-}1)$$

$$\sigma_m = \frac{\sigma_{max} + \sigma_{min}}{2} \quad (2\text{-}2)$$

$$R = \frac{\sigma_{min}}{\sigma_{max}} \quad (2\text{-}3)$$

In the above relation, *R* is the stress ratio. Figure 2-3(b) shows a typical irregular loading condition. Figures 2-3(c) and 2-3(d) show respectively in-phase and out-of-phase cyclic loading conditions. A typical strain history of multi-axial variable loading and fatigue crack growth rate versus stress intensity factor range are illustrated in Figures 2-3(e) and 2-3(f), respectively.

As mentioned earlier, the lifespan of a component subjected to cyclic loading can be classified into three phases: crack initiation, crack propagation, and final failure. Each of these stages can be studied using various proposed methods and criteria to analyze the fatigue life.

In summary, the first stage, crack initiation, occurs when microscopic cracks begin to form in the material due to cyclic loading. These cracks may start at stress concentration points such as notches or defects in the material. Various factors, such as material properties, loading conditions, and the geometry of the component, can affect the initiation of these cracks. The second stage, crack propagation, refers to the growth of the cracks that have already formed. This stage is the most critical as it can significantly reduce the remaining fatigue life of the component. The rate of crack growth depends on various factors, including the applied cyclic loading, the size and shape of the crack, and the material's properties. The final stage, final failure, occurs when the component can no longer sustain the applied cyclic loading and ultimately fractures. This failure can happen due to a sudden overload, a rapid crack growth, or a slow propagation of existing cracks.

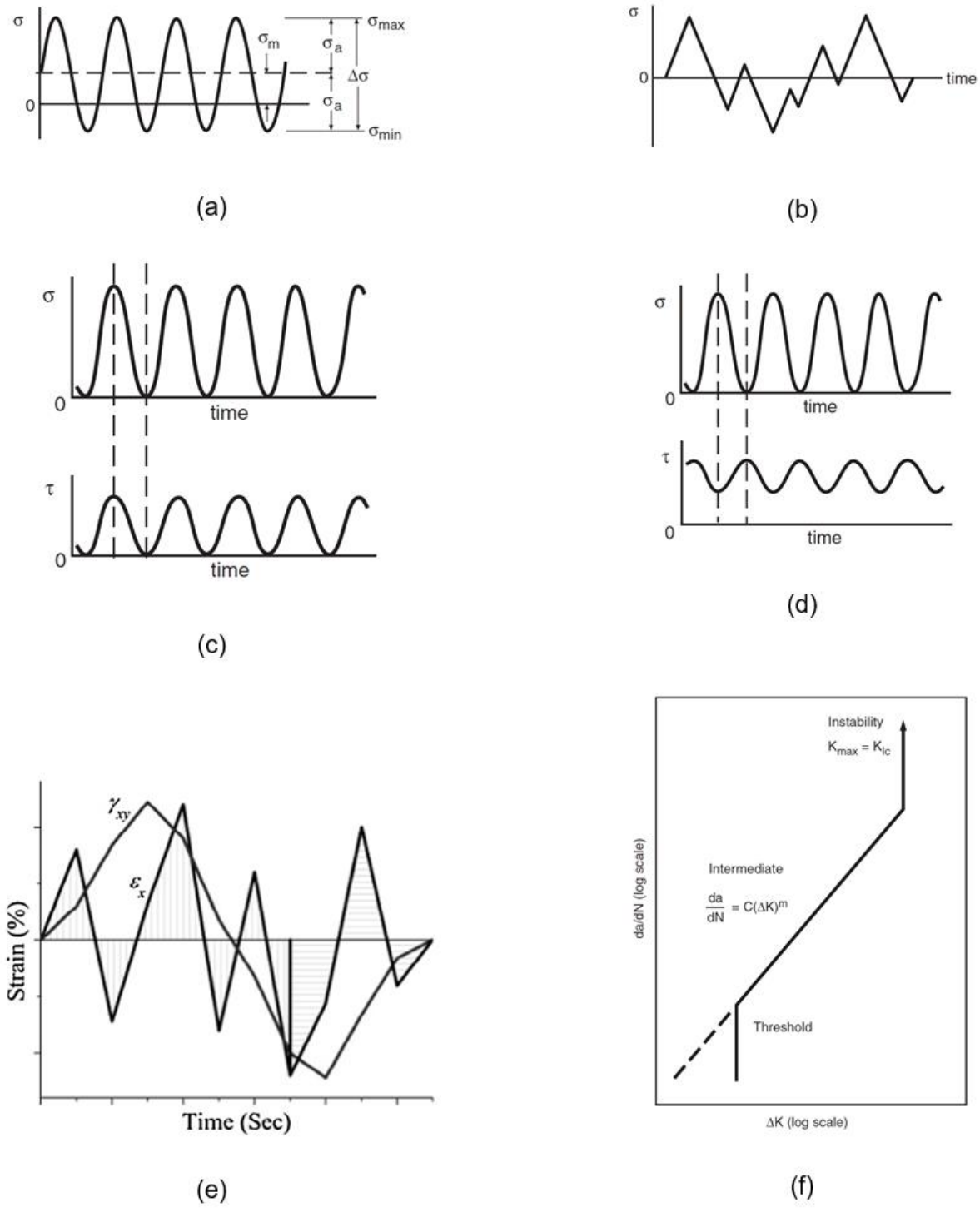

Figure 2-3. Fatigue definitions and cyclic loadings; (a) regular amplitude loading, non-zero mean stress condition, (b) variable amplitude loading, (c) a typical condition of in-phase multi-axial loading, (d) a typical condition of out-of-phase multi-axial loading

2.1.3. Fatigue Life Prediction Methods

Fatigue life prediction methods are essential tools used in materials engineering and structural design to estimate the lifespan of components subjected to cyclic loading. Fatigue failure occurs when a material or structure experiences progressive damage and ultimately fractures under repeated loading cycles, even when the applied stress is below the material's static strength.

Accurate prediction of fatigue life is crucial for ensuring the reliability and durability of various engineering systems, such as aircraft, automobiles, bridges, and machinery. Several methods have been developed to estimate the fatigue life of components, taking into account factors such as material properties, loading conditions, and environmental influences.

However, there is still no comprehensive and widely accepted criterion among researchers. The proposed criteria are either based on the principal stress/strain plane or the maximum principal strain/shear stress plane, and they are categorized into three groups: stress-based, strain-based, and energy-based approaches.

The stress-based approach considers nominal stress components for predicting the fatigue life and is usually used in situations where the plastic strain components are negligible. On the other hand, the strain-based approach uses local stresses and strains and can be employed when local yielding is involved, particularly in low cycle fatigue regimes. The energy-based approach considers the amount of energy dissipated during the loading cycle and compares it with the energy required to cause crack propagation. This approach is useful for predicting the fatigue life of components that experience high plastic strains and significant material damage.

The fracture mechanics approach focuses on the behavior of cracks and their effect on the component's strength. This approach involves analyzing the stress field around the crack tip and using fracture mechanics concepts to predict the crack growth rate and the remaining fatigue life of the component.

Fatigue life prediction methods play a crucial role in engineering design, enabling engineers to make informed decisions regarding component lifespans, maintenance schedules, and the optimization of materials and designs to enhance durability and safety.

Some of the above-mentioned approaches will be used for predicting fatigue life of the components used in the heat and power micro-turbines made of Inconel 600.

2.1.4. Stress-Based Approaches

In recent years, there has been an increasing focus on developing advanced fatigue life prediction methods that incorporate additional factors, such as variable amplitude loading, multiaxial loading conditions, and the influence of material microstructure. These methods utilize techniques like finite element analysis, damage accumulation models, and statistical approaches to improve the accuracy of fatigue life predictions.

One commonly used approach is the stress-based fatigue life prediction method. It involves assessing the fatigue strength of a material by determining the relationship between applied stress levels and the number of cycles to failure. This method relies on fatigue data from experimental tests, such as S-N curves (stress-number of cycles) generated through constant amplitude fatigue testing. The S-N curves provide a graphical representation of the fatigue behavior of a material and allow engineers to estimate the fatigue life for a given stress level. The S-N curve, also known as the Wöhler curve, is a fundamental tool in stress-based fatigue life prediction. The S-N curve is typically generated through constant amplitude fatigue testing, where specimens are subjected to various stress levels until failure. The resulting data points are plotted on a logarithmic scale to create the S-N curve, which allows engineers to estimate the fatigue life for a given stress amplitude.

The most commonly used model to describe the relationship between stress amplitude (S) and the number of cycles to failure (N) in stress-based fatigue life prediction is Basquin's equation. This equation is typically expressed in the form of a power law relationship: $S = A(N)^B$, where A and B are material constants determined through experimental testing. Basquin's equation provides an empirical fit to the S-N data and allows for estimating fatigue life under different stress amplitudes.

It is important to consider factors such as mean stress, stress concentrations, and material properties in order to improve the accuracy of fatigue life predictions. Gough and Pollard [46] proposed two equations for loading in-phase combined bending and torsion

loads. One of these equations, known as the quarter elliptical model, is suggested for soft materials.

$$(\frac{S_b}{f_{-1}})^2 + (\frac{S_t}{t_{-1}})^2 = 1 \quad (2\text{-}4)$$

In the above equation, S_b represents the range of bending stress, S_t represents the range of torsional stress, f_{-1} is the bending endurance limit, and t_{-1} is the torsional endurance limit.

Another equation called the Elliptical Bow is presented for brittle materials as follows:

$$(\frac{S_t}{t_{-1}})^2 + \left(\frac{S_b}{f_{-1}}\right)^2 \left(\frac{f_{-1}}{t_{-1}} - 1\right) + \left(\frac{S_b}{f_{-1}}\right)\left(2 - \frac{f_{-1}}{t_{-1}}\right) = 1 \quad (2\text{-}5)$$

For the case when bending and torsional loads are out of phase, Lee et al. [47] have modified the elliptical quarter model as follows:

$$\sigma_{a,eq} = S_b \left[1 + \left(\frac{f_{-1}K}{2t_{-1}}\right)^{\xi}\right]^{\frac{1}{\xi}} \quad (2\text{-}6)$$

$$\xi = 2(1 + \beta sin\varphi) \quad (2\text{-}7)$$

$$K = \frac{2S_t}{S_b} \quad (2\text{-}8)$$

In the above equations, $\sigma_{a,eq}$ represents the equivalent stress range, β is the material constant, and φ is the phase difference between the bending stress range and torsional stress. Carpinteri et al. [48] have proposed the maximum vertical stress and shear stress range on the critical plane as two parameters for modifying the elliptical quarter model for out-of-phase loading:

$$\sigma_{eq} = \sqrt{\sigma_{n\,max}^2 + (\frac{\sigma_f'}{\tau_f'})^2 \tau_a^2} \quad (2\text{-}9)$$

In this relation, σ_{eq} represents the equivalent uniaxial stress, $\sigma_{n\,max}$ is the maximum uniaxial stress, and τ_a is the shear stress range, while other parameters are fatigue constants dependent on the material properties of the component.

Matake [49] has selected the shear stress range and the maximum vertical stress on the critical plane as two parameters and proposed the following equation:

$$\tau_{a,cr} + k\sigma_{n,cr} \leq \lambda \tag{2-10}$$

$$k = \frac{t_{A,B}}{2\sigma_u} \tag{2-11}$$

$$\lambda = t_{A,B} \tag{2-12}$$

In the above equations, $\tau_{a,cr}$ represents the shear stress range on the critical plane, $\sigma_{n,cr}$ is the normal stress range on the critical plane, $t_{A,B}$ is the shear endurance limit, σ_U is the ultimate tensile stress, and the other parameters are material's constants.

Papadopoulos [50] has introduced a criterion that can be used for constant amplitude multiaxial loadings, both proportional and non-proportional, to estimate long-term fatigue life as follows:

$$\tau_{a,cr} + k\sigma_{H,max} = \lambda \tag{2-13}$$

Nevertheless, stress-based models are not as prevalent in fatigue life predictions due to their limited ability to adequately account for plastic strain components. Unlike stress, plastic strain involves irreversible deformation, affecting material response to fatigue loading differently. As a result, stress-based models may inaccurately assess fatigue life, particularly in situations where plastic deformation plays a significant role, leading to potential underestimation or overestimation of fatigue damage. Consequently, incorporating plastic strain considerations becomes essential for more accurate and reliable fatigue life predictions in engineering applications.

For more accurate results, it is advisable to opt for alternative approaches such as strain-based or energy-based models, as well as models based on critical plane analysis.

2.1.5. Strain-Based Approaches

Another approach is the strain-based fatigue life prediction method, which considers the relationship between cyclic strain and fatigue life. This method is particularly useful for materials that exhibit strain-controlled fatigue behavior, such as certain metals and alloys. Strain-based fatigue life prediction methods often utilize strain-life curves derived from experimental tests to estimate the fatigue life under different strain amplitudes.

It's important to note that fatigue life prediction methods provide estimates and are subject to some degree of uncertainty. Actual fatigue life can be affected by various factors that are challenging to fully capture in prediction models, such as stress concentrations, surface conditions, temperature fluctuations, and environmental effects.

In the context of fatigue life prediction, strain-based approaches refer to methodologies that assess the fatigue behavior and estimate the remaining fatigue life of a material or component based on the applied strains.

When applied stresses on a component are sufficiently high, and localized plastic strain under fatigue conditions with a very large number of cycles is significant, strain-based fatigue methods are suitable for low-cycle fatigue. Figure 2-4 shows a typical strain amplitude versus the number of cycles to failure in log-log scale. As seen from this representation, elastic and plastic strains versus cycles can be considered as straight lines. Data below the fatigue transition life (N_t) consists of large values of plastic strains. Therefore, it is important to consider both portions of strain values especially in low cycle fatigue (LCF) regime.

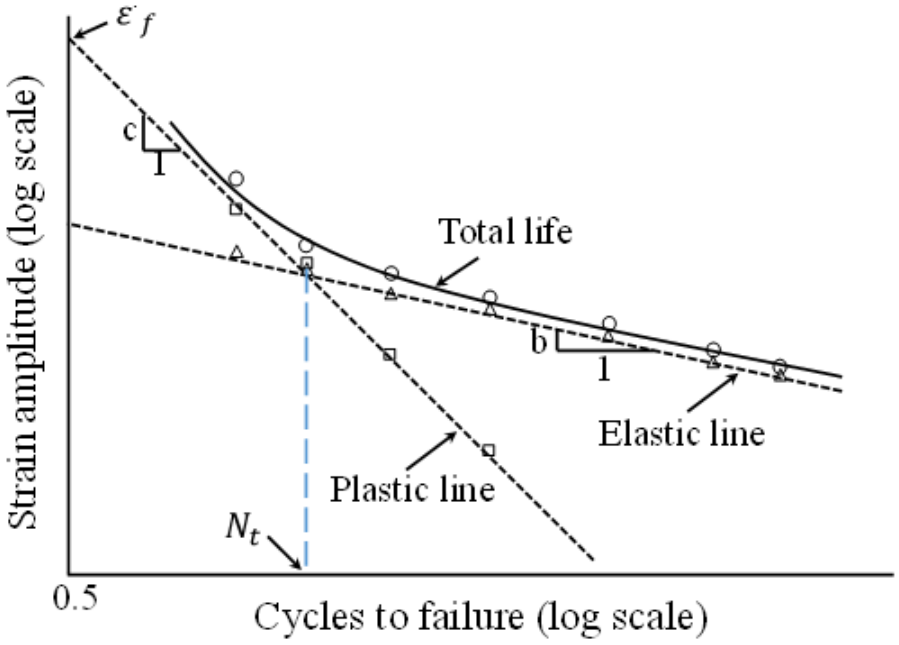

Figure 2-4. A typical strain amplitude versus the number of cycles to failure

Low cycle fatigue is a type of fatigue failure that occurs in materials subjected to a relatively small number of cyclic loading cycles. It is characterized by high-stress levels and plastic deformation. LCF is typically observed in applications where materials experience significant cyclic loading, such as in machinery, power plants, aerospace components, and structural engineering. Unlike high cycle fatigue (HCF), which involves a large number of cycles before failure, LCF is associated with a limited number of cycles typically in the range of a few thousand or less. The cyclic loading induces plastic deformation, causing microstructural changes, crack initiation, and eventually failure.

The main factors that contribute to LCF failure are the magnitude and distribution of stress, mean stress or stress ratio, strain range, strain rate, and material properties. The cyclic loading causes cyclic plastic deformation, leading to progressive accumulation of damage and the development of microcracks, which can grow and eventually cause catastrophic failure.

To assess the fatigue life in the LCF regime, various testing methods are employed, such as strain-controlled or load-controlled tests. The material's response is characterized by

hysteresis loops, where the stress-strain behavior exhibits cyclic softening due to plastic deformation.

To predict and analyze LCF behavior, several models have been developed, including the Coffin-Manson model and the Morrow model. These models take into account factors such as strain range, mean stress, and strain rate to estimate the fatigue life under LCF conditions. Additionally, advanced models, such as the Smith-Watson-Topper model and the Fatemi-Socie model, have been developed to address multiaxial LCF behavior. LCF failure is a critical concern in engineering design and maintenance, as it can lead to unexpected and catastrophic failures. Therefore, understanding and accurately predicting LCF behavior is crucial for ensuring the reliability and safety of components and structures subjected to cyclic loading in the low cycle fatigue regime.

As expected, strain-based approaches aim to understand the relationship between the applied strains and the resulting fatigue life. In this method accurate measurement of strains is crucial. To do so, strain gauges or other strain sensing techniques are used to capture the strain variations during cyclic loading. These measurements can be obtained at critical locations on the component or within the material itself. FEA analysis is another important technique to calculate the magnitudes of strains at critical locations where the fatigue cracking is most likely to occur.

Strain-life models are mathematical relationships that correlate the applied strain amplitudes or strain ranges with the number of cycles to failure. These models are derived based on experimental data and are specific to certain material types and loading conditions. Some commonly used strain-life models include the Coffin-Manson model, the Morrow model, and the Smith-Watson-Topper model.

Once the strain-life model parameters are determined, they can be used to predict the remaining fatigue life of a material or component under given strain conditions. By measuring the strains experienced during service or testing, the model can estimate the remaining cycles to failure.

It's important to note that strain-based approaches to fatigue life prediction are based on the assumption that the applied strain is the primary driving force for fatigue damage. These approaches are effective when the material exhibits a strain-controlled fatigue

behavior, where the fatigue life is predominantly influenced by the strain amplitude rather than the stress amplitude. However, in situations where other factors, such as stress concentrations or environmental effects, play a significant role, additional considerations may be necessary.

The claim that strain-controlled fatigue behavior primarily influences fatigue life in materials when strain amplitude predominates over stress amplitude is supported by various studies in the field of fatigue mechanics and materials science. Research has shown that in certain materials and loading conditions, the fatigue life is indeed more sensitive to strain amplitude rather than stress amplitude. This is particularly true for materials subjected to cyclic loading where plastic deformation dominates and strain accumulation becomes a critical factor in fatigue failure.

However, in real-world scenarios, factors beyond just strain or stress amplitude can significantly influence fatigue life. Stress concentrations, which can arise from geometric irregularities or material defects, and environmental effects such as corrosion can exacerbate fatigue damage mechanisms. Therefore, while strain-controlled approaches are effective under certain conditions, additional considerations become necessary to accurately predict fatigue life in situations where these factors play a substantial role.

2.1.5.1. Morrow's Damage Equation

Morrow's fatigue damage model and its modified version are widely used approaches to estimate fatigue life in materials subjected to cyclic loading. These models are based on strain-based fatigue theories and are particularly applicable to low cycle fatigue (LCF) conditions. This model relates the accumulated fatigue damage to the cyclic strain range experienced by the material. It assumes that the fatigue life is inversely proportional to the plastic strain range considering mean stress effect (σ_m) [45]:

$$\varepsilon_a = \left(\frac{\sigma_f{}'}{E}\right)\left(1 - \frac{\sigma_m}{\sigma_f{}'}\right)(2N_f)^b + \varepsilon_f{}'\left(1 - \frac{\sigma_m}{\sigma_f{}'}\right)^{\frac{c}{b}}(2N_f)^c \quad (2\text{-}14)$$

In the above equation, ε_a is the strain amplitude, N_f is the number of cycles to failure, and $\sigma_f', b, \varepsilon_f', c$ are respectively fatigue strength coefficient, fatigue strength exponent, fatigue ductility coefficient, and fatigue ductility exponent.

2.1.5.2. Modified Morrow's Model

In the modified Morrow's model, the second term related to plastic strain no longer depends on mean stress [45]. Consequently, this adjustment leads to a decrease in the estimated impact of mean stress, particularly for shorter fatigue life predictions.

$$\varepsilon_a = \left(\frac{\sigma_f{}'}{E}\right)\left(1 - \frac{\sigma_m}{\sigma_f{}'}\right)\left(2N_f\right)^b + \varepsilon_f{}'\left(2N_f\right)^c \quad (2\text{-}15)$$

To use this method for multiaxial fatigue condition, the multiaxial stress state should be converted to uniaxial stress using one of the methods like von Mises or other similar criteria.

2.1.5.3. Smith-Watson-Topper Model Based on Local Stress-Strain

The SWT approach suggests that the fatigue life, under any mean stress condition, is contingent on the product of $\varepsilon_a\sigma_{max} = h^{"}(N_f)$ [45]:

$$\varepsilon_a\sigma_{max} = \left(\left(\sigma_f{}'\right)^2/E\right)\left(2N_f\right)^{2b} + \varepsilon_f{}'\sigma_f{}'\left(2N_f\right)^{b+c} \quad (2\text{-}16)$$

To convert multiaxial stress and strain condition to an equivalent uniaxial stress and strain the following equations can be utilized [45]:

$$\sigma_{eqa} = \frac{1}{\sqrt{2}}\sqrt{(\sigma_{xa} - \sigma_{ya})^2 + (\sigma_{za} - \sigma_{ya})^2 + (\sigma_{xa} - \sigma_{za})^2 + 6(\tau_{xya}{}^2 + \tau_{zya}{}^2 + \tau_{xza}{}^2)} \quad (2\text{-}17)$$

$$\sigma_{eqm} = \sigma_{xm} + \sigma_{ym} + \sigma_{zm} \quad (2\text{-}18)$$

$$\varepsilon_{eqa} = \sqrt{\frac{2}{3}\left(\varepsilon_x{}^2 + \varepsilon_y{}^2 + \varepsilon_z{}^2\right) + \frac{1}{3}\left(\gamma_{yz}{}^2 + \gamma_{xz}{}^2 + \gamma_{yx}{}^2\right)} \quad (2\text{-}19)$$

In the above equations, $\sigma_{eqa}, \sigma_{eqm}, \varepsilon_{eqm}$ are effective stress amplitude, effective mean stress, and effective strain amplitude, respectively.

2.1.6. Critical Plane Approaches

Critical plane approaches are widely used methods for predicting the fatigue life of components subjected to multi-axial loading conditions, whether in-phase or out-of-phase. When a material undergoes cyclic loading in multiple directions simultaneously, it experiences complex stress states that can significantly affect its fatigue life. In such scenarios, conventional methods based solely on stress or strain amplitude may not provide accurate predictions.

Critical plane approaches address this challenge by identifying the plane or surface within the material where the most damaging stresses occur during the loading cycle. This critical plane represents the location where fatigue damage is most likely to initiate and propagate. The concept behind critical plane approaches is that fatigue failure is primarily driven by the stress state on this critical plane rather than the individual stress components.

The critical plane can be determined through different mathematical formulations and criteria, such as the Maximum Shear Stress (MSS) criterion, the Fatigue Shear Stress (FSS) criterion, or the Normalized Shear Stress (NSS) criterion, among others. These criteria consider both the amplitude and phase relationship between the principal stress components on various planes to identify the most detrimental one.

Once the critical plane is established, the fatigue life can be estimated using appropriate fatigue damage accumulation models, such as the Rainflow counting method combined with Miner's rule. These models take into account the damage caused by each stress cycle on the critical plane and accumulate it to predict the total fatigue life of the component.

In the following, the most commonly used models based on critical plane approach are discussed.

2.1.6.1. Findley Model

For a large category of components operating near or below the fatigue limit, especially those subjected to low applied stresses well below the material's yield stress, particularly components operating in the fatigue regime with a high number of cyclic cycles, fatigue models based on stress are commonly used.

The Findley model is a widely used method for assessing fatigue failure in materials under multiaxial loading conditions. This model provides a good estimation for components operating in the infinite-life regime. It offers an estimation based on the critical plane, where the critical plane is the one in which $\left(\left(\frac{\Delta\tau}{2}\right) + k\sigma_n\right)$ is maximum. In this context, the model combines shear stress and the maximum normal stress in the critical plane using a linear combination. In this parameter, $\Delta\tau$ represents the shear stress amplitude, σ_n is the normal stress on the critical plane, and k is a material constant obtained experimentally through fatigue testing of the material.

The Findley model is particularly applicable to high-strength materials that exhibit a fatigue strength that depends strongly on the stress state. It has been used in various engineering fields, including aerospace, automotive, and structural engineering, to estimate fatigue life and assess the durability of components subjected to multiaxial loading.

It's important to note that while the Findley model is widely recognized, it does have some limitations. For instance, it assumes a power law relationship for fatigue damage accumulation and may not capture all the complexities and material-specific behavior. Therefore, it is always recommended to validate the model's predictions with experimental data or consider more advanced and refined fatigue models when dealing with specific materials and loading conditions.

To predict fatigue life based on Findley's model, the following equation can be used [51]:

$$\left(\left(\frac{\Delta\tau}{2}\right) + k\sigma_n\right) = {\tau_f}^* (N_f)^b \tag{2-20}$$

In this equation, τ_f^* represents the Findley's material constant and can be obtained from the following equation:

$$\tau_f{}^* = \sqrt{1+k^2}\tau_f{}' \tag{2-21}$$

The value of $\sqrt{1+k^2}$ is usually considered to be approximately 1.04. Additionally, in the above equation, τ_f' represents the shear fatigue strength coefficient.

2.1.6.2. Fatemi-Socie Model

The Fatemi-Socie critical plane model, also known as the Fatemi-Socie multiaxial fatigue model, is a widely used method for predicting fatigue life in materials subjected to complex multiaxial loading conditions. It was developed by Fatemi and Socie in the late 1980s as an improvement over earlier fatigue models [52].

The key concept behind the Fatemi-Socie model is the consideration of the critical plane, which is the plane within the material where the fatigue damage accumulates most rapidly. Instead of evaluating the stress amplitude on a single plane, this model takes into account the orientation of the plane relative to the principal stress directions.

The Fatemi-Socie model combines elements of both stress-based and strain-based fatigue models. It utilizes the equivalent strain amplitude as the primary parameter to assess fatigue damage. The model accounts for the influence of mean stress, stress amplitude, and the interaction between shear and normal stresses on the critical plane.

The critical plane is determined by rotating the coordinate system to align the principal stress directions with the axes of the coordinate system. The strain components on the critical plane are then calculated, and the equivalent strain amplitude is determined by combining these components. The model incorporates empirical fatigue coefficients and equations to estimate the fatigue life based on the equivalent strain amplitude.

The Fatemi-Socie critical plane model provides a more accurate prediction of fatigue life under multiaxial loading conditions compared to simpler uniaxial fatigue models.

Equation below expresses Fatemi-Socie's critical plane model [52]:

$$\gamma_a\left(1+\left(\frac{\sigma_n}{\sigma_{ys}}\right)\right)=\left(\tau_f{}'/\mathrm{G}\right)\left(2N_{fs}\right)^b+\gamma_f{}'\left(2N_{fs}\right)^c \tag{2-22}$$

In this equation, τ_f' represents the coefficient of shear fatigue strength, *G* is the shear modulus of the material, $\gamma_f{}'$ is the torsional fatigue strength coefficient, and *b* and *c* are material constants. Additionally, σ_n is the normal stress on the critical plane, σ_{ys} is the yield stress of the material, and γ_a is the shear strain amplitude.

2.1.6.3. SWT Model Based on Critical Plane Approach

The SWT model assumes that the fatigue failure is controlled by the nucleation and growth of fatigue cracks on the critical plane. The model provides a means to estimate the fatigue life of materials subjected to various multiaxial loading conditions, including combinations of tension, compression, torsion, and shear.

According to this model, failure occurs on the plane where the parameter $d_t=\varepsilon_a\sigma_n$ has its maximum value, and this plane is referred to as the critical plane. The equation used based on this model is as follows:

$$d_t=\left(\left(\sigma_f{}'\right)^2/E\right)\left(2N_{ft}\right)^{2b}+\varepsilon_f{}'\sigma_f{}'\left(2N_{ft}\right)^{b+c} \tag{2-23}$$

The SWT model is specifically designed to predict the fatigue life of metallic materials subjected to complex multiaxial loading conditions. It takes into account the interaction between normal and shear stresses on the critical plane, similar to the Fatemi-Socie model. This model considers both high-cycle fatigue and low-cycle fatigue regimes and also takes into account the effects of mean stress. In the above equation, ε_a and σ_n represent the normal stress and normal strain amplitude on the critical plane, respectively.

2.1.7. Fatigue Crack Growth (FCG)

Fatigue crack growth is a phenomenon that occurs in materials subjected to cyclic loading, leading to the progressive propagation of cracks within the material. It is a common mode of failure in structural components and is a critical consideration in the design and maintenance of various engineering systems. When a material is subjected to cyclic loading, such as alternating stresses or strains, cracks can initiate at regions of high stress concentration, such as notches or flaws in the material. These cracks typically start as small microcracks, which grow incrementally with each loading cycle.

The growth of a fatigue crack is influenced by several factors, including the magnitude and distribution of cyclic loading, the stress intensity factor (SIF) at the crack tip, and the material's fracture toughness. The FCG behavior is commonly characterized by a relationship between the crack growth rate (da/dN) and the crack-tip stress intensity factor range (ΔK). The stress intensity factor K depends on the crack length a, loading type, and geometry. A typical relationship between da/dN and ΔK in a log-log plot can be illustrated in Figure 2-5, and it can be expressed by Paris equation as follows [45]:

$$\frac{da}{dN} = C(\Delta K)^m \tag{2-24}$$

where *da/dN* is the crack growth rate, *ΔK* is the stress intensity factor range, and *C* and *m* are material-specific constants determined through experimental calibration.

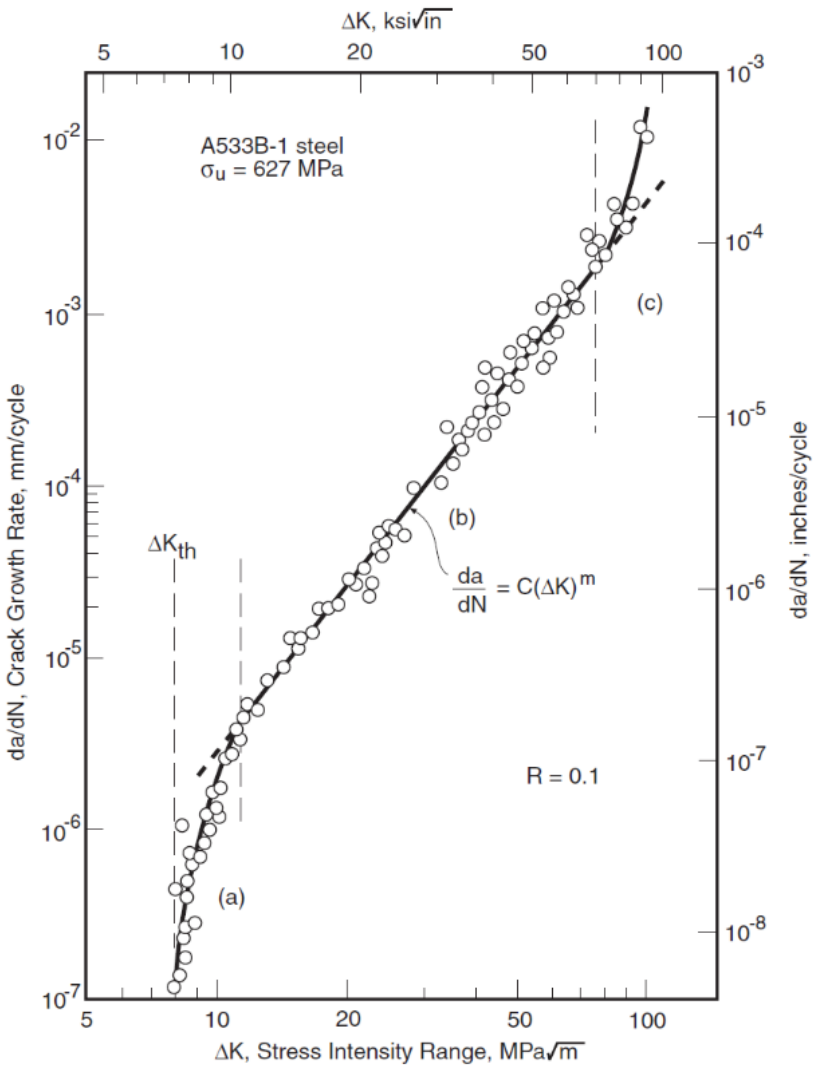

Figure 2-5. A typical representation of fatigue crack growth rates versus stress intensity factor ranges for a ductile material [45]

The values of m normally vary between the range of 2.5 to 5.5 for ductile materials [53-57] and 8 to 10 for brittle materials [58].

The value of R significantly affects the crack growth rate and the overall fatigue life of a material [59, 60]. For most materials, fatigue crack growth rates are higher under tension compared to compression. This phenomenon is commonly known as the R-ratio effect. The presence of tensile stresses during the cyclic loading accelerates crack propagation due to the development of larger plastic zones ahead of the crack tip. On the other hand,

compressive stresses tend to hinder crack growth by compressing the crack faces and closing the crack slightly during each cycle.

Furthermore, at low R-values, fatigue crack growth rates tend to be more significant due to the dominance of tensile stresses in the loading cycle. As the R-value increases towards zero and becomes positive, the crack growth rates decrease. At fully reversed loading condition, crack growth rates reach their minimum value because of the balanced presence of tensile and compressive stresses in the loading cycle.

Fatigue crack growth analysis plays a crucial role in fatigue life prediction and structural integrity assessments. By considering the crack growth rate and the initial crack size, engineers can estimate the remaining useful life of a component or determine inspection intervals to ensure safe operation. Various techniques and numerical methods, such as the finite element method, are employed to simulate and analyze fatigue crack growth behavior, aiding in the development of strategies for crack management, repair, and maintenance in real-world applications. Understanding and accurately predicting fatigue crack growth require detailed knowledge of material properties, loading conditions, and crack growth mechanisms. Empirical data, experimental testing, and sophisticated modeling techniques are typically employed to enhance the accuracy of fatigue crack growth predictions and ensure structural reliability and safety.

2.2. Creep

When a uniaxial component is simultaneously subjected to a constant tensile loading at a relatively high temperature for a long period of time, the strain progressively increases in the part [61], as shown in Figure 2-6. This strain is called creep strain which consists of three stages. The part where the strain rate decreases is called the primary creep, the stage where the strain rate is nearly constant is called the secondary or steady-state creep, and the final stage where the strain rate increases is called the tertiary creep, which occurs before failure [62]. During the primary creep stage, strain hardening takes place at temperatures below the recrystallization temperature, but due to the short duration of plastic deformation, diffusion and recovery mechanisms dominate, causing a gradual

decrease in the deformation rate with time. In the secondary stage, strain hardening increases initially due to dislocation, but as time progresses, the rate decreases as diffusion and recovery reactions occur, resulting in a steady strain rate known as the minimum strain rate. In the third creep stage, the increase in creep rate is attributed to the formation and joining of voids and cracks, leading to stress escalation. This stage may involve other metallurgical phenomena, such as recrystallization or particle coarsening, which enhance diffusion-assisted reactions and contribute to a faster strain rate until fracture occurs [63].

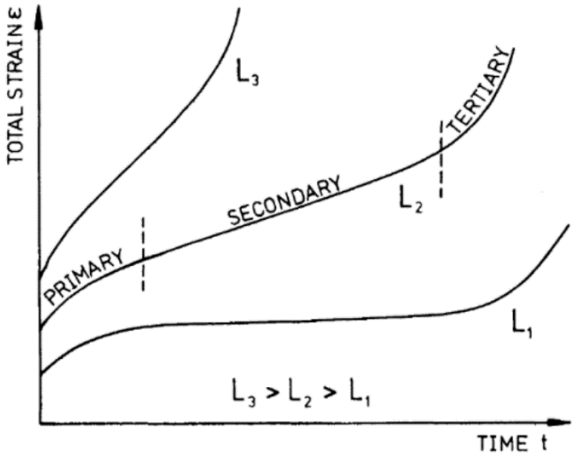

Figure 2-6. Typical creep strain versus time curves for uniaxial loading under different loads L1, L2, and L3 [61]

The creep curve slope strongly depends on the applied stress and temperature. The dependency of creep strain on the constant stress and constant temperature conditions are depicted in Figure 2-7. Due to the involvement of various factors and different mechanisms in the creep phenomenon, conducting diverse experiments under different stresses and temperatures is necessary to determine the creep characteristics of materials.

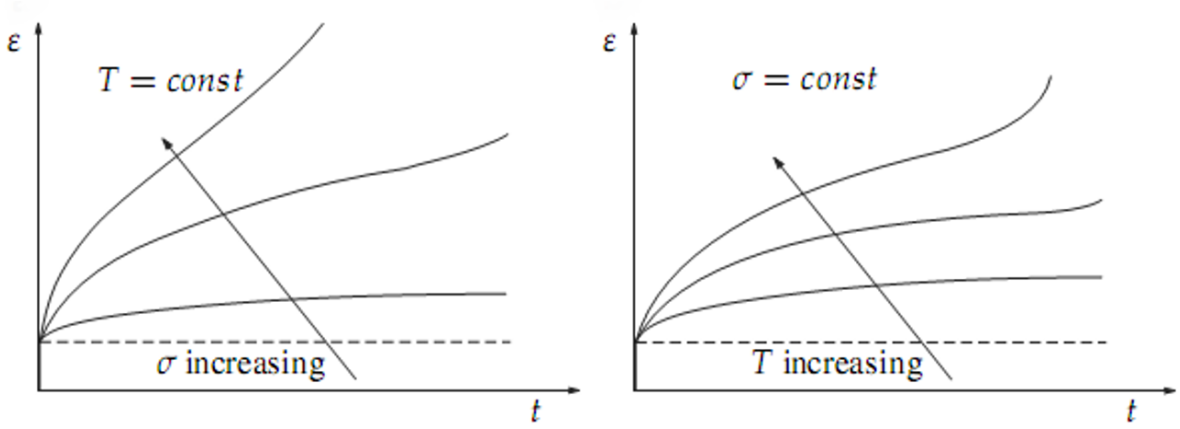

Figure 2-7. Dependency of applied stress and temperature on creep strain [64]

Under high temperature conditions, creep strain (ε_c) can be expressed as a function of applied stress, temperature, and time as follows:

$$\varepsilon_c = f(\sigma, T, t) \tag{2-25}$$

However, it is convenient to separate all the parameters and express the creep strain as follows:

$$\varepsilon_c = f_1(\sigma) f_2(t) f_3(T) \tag{2-26}$$

2.2.1. Dependency of the Creep Strain to the Applied Stress

The following relations have been proposed to express the dependency of the creep strain to the applied stress, which are Norton, Prantel, Dorn, Garofalo, and Friction Stress relations, respectively [61]:

$$f_1(\sigma) = B\sigma^n \tag{2-27}$$

$$f_1(\sigma) = Csin(\alpha\sigma) \tag{2-28}$$

$$f_1(\sigma) = Dexp(\beta\sigma) \tag{2-29}$$

$$f_1(\sigma) = A[\sin(\gamma\sigma)]^n \tag{2-30}$$

$$f_1(\sigma) = B(\sigma - \sigma_0)^n \tag{2-31}$$

The above-mentioned relations are mathematical expressions used to describe how the strain, or deformation, of a material change over time under the influence of applied stress during creep, a time-dependent deformation phenomenon observed in materials subjected to prolonged stress at elevated temperatures.

In essence, these relations provide a way to understand and predict how much a material will deform over time when subjected to a certain level of stress at elevated temperatures. They are derived from experimental observations and empirical correlations between stress, temperature, and creep strain obtained from creep testing of materials.

Each of these relations has its own set of assumptions and limitations, and they may be applicable to different materials or creep conditions. For example, some relations may be more suitable for describing primary creep (initial stage), while others may be better for secondary or tertiary creep (later stages) or for specific types of materials.

2.2.2. Dependency of the Creep Strain to Time

The following relations express the dependency of creep strain to time, which are secondary creep, Bailey, Andrade, and Graham and Walles, respectively [61]:

$$f_2(t) = t \tag{2-32}$$

$$f_2(t) = bt^m \tag{2-33}$$

$$f_2(t) = (1 + bt^{1/3})e^{kt} \tag{2-34}$$

$$f_2(t) = \sum_j a_j t^{m_j} \tag{2-35}$$

2.2.3. Dependency of the Creep Strain to the Temperature

Based on the Arrhenius rule, the creep strain dependency to the temperature is as follows [61]:

$$f_3(T) = Ae^{(-\Delta H/RT)} \tag{2-36}$$

In this relation, ΔH is the activation energy, R is the Boltzmann constant, and T is the absolute temperature in Kelvin, respectively. To describe the creep behavior of materials, constitutive equations related to creep strain or creep strain rate can be utilized. One of the most well-known equations to describe creep behavior is the Norton power law equation [61]:

$$\dot{\varepsilon}_s = Ae^{(-Q_c/RT)}\sigma^n \tag{2-37}$$

The latest equation will be used for describing creep behavior of smooth and welded samples to ensure that this material is suitable for combined heat and power micro-turbine systems. Since there are various parameters and mechanisms affecting creep phenomenon, to obtain creep characteristics of a material, creep tests must be conducted at various stress levels and temperatures.

2.3. Literature Review

2.3.1 Quasi-Static and Fatigue Failure

This section presents a comprehensive literature survey on fatigue response of superalloys, particularly Inconel alloys, with a specific focus on Inconel 600, under various loading conditions. Despite the considerable volume of existing research on these materials, there remains a need for further investigation, particularly from a fatigue failure perspective. This requirement stems from the fact that these components are utilized in various sections of microturbine systems, necessitating a thorough examination of their suitability under different conditions, including welding, notched configurations, and diverse loading scenarios. The identification of research gaps in these aspects forms the basis for this study, which aims to address and fill these gaps. The subsequent paragraphs provide concise summaries of some of the available research studies in this field.

The study conducted by Nanaware et al. [8] focuses on analyzing the turbine blades of a Gas Turbine Engine, specifically targeting the Turbine and Combustion Chamber areas, which are known for their complex problems. The objective of the project was to assess

the performance of different high-temperature alloys in terms of strength against temperature and other stress effects. Five different Ni-based alloys, specifically designed for aerospace applications, were selected for analysis. Using ANSYS software, the turbine blades made of these alloys were subjected to flow and structural analysis at various temperature levels. After comparing the results, the researchers identified the best-performing alloy for turbine blade production. They found that the alloy RR 1000 exhibited the most favorable overall results among all five alloys. On the other hand, Inconel 600 showed the minimum elongation at any temperature but did not perform as well in other properties. Based on their findings, the study suggests that Inconel 600 could be suitable for short-range aircraft, while RR 1000 is recommended for long-range aircraft due to its superior performance.

Gajalappa and colleagues [7] conducted a study on the high-temperature deformation characteristics of Inconel 600 super alloy, which possesses remarkable oxidation and corrosion resistance at elevated temperatures. Due to these exceptional properties, it is extensively used in aerospace components such as blades, shafts, and aircraft gas turbines. The researchers performed hot deformation tests on Inconel 600 at temperatures ranging from 950°C to 1100°C, with various strain rates from 0.001 s^{-1} to 1 s^{-1}. The resulting true stress-true strain curves indicated that at lower strain rates, the alloy exhibited softening behavior throughout the entire deformation temperature range. Conversely, at higher strain rates, it displayed strain hardening characteristics over the entire temperature range. The observed softening could be attributed to dynamic recrystallization (DRX) or instability in the deformed microstructure.

In their study, He et al. [65] investigated the fracture cause of a steam turbine blade root. During turbine maintenance, they identified nineteen IP-6S (Intermediate Pressure 6th Stage) blades with root cracks. The analysis involved various methods, such as macroscopic inspection, magnetic particle testing, room temperature mechanical property testing, micro-hardness testing, chemical analysis, metallographic analysis, scanning electron microscopy, and energy spectrum analysis, while simulating the blade's static stress. The results showed that the blade leaves' chemical composition and mechanical properties met the required standards, and no abnormal corrosive substances were

present in the crack initiation zone. Numerical simulations indicated that the surface of the first tooth arc experienced the highest stress in the root, and improper installation could further increase this stress level. The primary cause of root cracking was attributed to an increased gap between the blade root and leaf groove, which altered the blade root contact mode, leading to enhanced stress on the first tooth arc. This, in turn, aggravated wear between the root and leaf groove and eventually led to fatigue cracking at the stressed first tooth.

Hou et al. [14] conducted a study on blade failures in gas turbine engines, which can significantly impact engine availability. Thorough failure investigation is essential for managing engine airworthiness effectively. The researchers investigated blade fatigue failures through mechanical analyses and examination of the failed blades. They performed a series of mechanical analyses to identify potential causes of the failures by scrutinizing irregularities in the mechanical behavior of the turbine blade. Using a non-linear finite element method, they determined the steady-state stresses and dynamic characteristics of the turbine blade. By evaluating and synthesizing the steady-state stresses and dynamic characteristics, the researchers identified the root causes behind the blade failures.

Isobe and Nogami [66] conducted low cycle fatigue tests on a 12%Cr steel component specimen, resembling a turbine blade root and disc joint, at a high temperature of 600°C. The study aimed to investigate micro-crack growth behavior in the joint region to understand the damage mechanism of blade-root joints in high-temperature environments and enhance life assessment methods through finite element analysis. They observed that under conditions of relatively high total strain, the micro-crack growth behavior resembled that of smooth bar specimens, with cracks initiating at the notch region and the crack growth rate increasing with surface crack length. The fatigue life of these component specimens was similar to smooth bar specimens. However, under relatively low total strain, a different growth behavior was noticed, with no cracks observed at the notch region. Instead, microcracks initiated at the contact region's edge in the early stages, and the crack growth rate remained minimal. The fatigue life of these component

specimens was shorter than that of smooth bar specimens, possibly due to fretting fatigue at the contact edge and mean stresses.

Krechkovska et al. [67] investigated the reasons behind steam turbine rotor blade failures made of high-alloyed heat-resistant steel 15Kh11MF. Premature blade failure resulted from technological defects due to welding and surface hardening imperfections, leading to corrosion-erosion wear, uneven micro-damage distribution, and crack initiation. These cracks altered blade oscillation frequency, causing resonance and overloading. The corrosive steam-water mixture in the phase transition zone also contributed to fractures. Long-term operation led to carbide precipitation weakening grain boundaries and reducing fatigue crack growth resistance. Effective threshold values of the SIF range decreased significantly due to the crack closure effect caused by intergranular fragments formed during steel operation. To assess the steel's condition, structural and mechanical indicators were proposed, providing guidelines for safe operation of 15Kh11MF steel in steam turbine rotor blades.

2.3.2 Creep Failure

The creep response of advanced materials, such as superalloys like Inconel 600, has garnered significant interest due to their widespread use in high-temperature applications, including aerospace and power generation industries [68, 69]. However, despite their importance, studies focusing on the creep behavior of these materials, particularly in welded forms and containing discontinuities like notches, remain relatively limited in literature. Understanding the creep performance under such complex conditions is crucial for ensuring the structural integrity and reliability of components operating at elevated temperatures. This lack of comprehensive research highlights the need for further investigation to assess the long-term behavior and creep resistance of advanced materials, considering the influence of welding and other structural irregularities on their mechanical properties. The following paragraphs aim to provide a concise overview of the existing knowledge and findings available in the literature concerning the creep response of advanced materials with a focus on superalloys like Inconel 600, particularly in the presence of welds and discontinuities.

Chavez et al. [9] conducted creep and tensile tests on three materials: Inconel 600, 304 stainless steel, and SA106B carbon steel. The tests were performed at elevated temperatures and stresses, exceeding previous experiments. Inconel 600 showed a significant reduction in ultimate strength above 800 K in tensile tests. Creep data indicated failure in less than 10 hours at temperatures above 1000 K and stresses exceeding approximately 130 MPa. They reported that, stainless steel 304 exhibited consistent tensile behavior with published data up to 1366 K. However, its ultimate strength dropped rapidly beyond approximately 800 K, and creep data predicted failure in less than 10 hours at temperatures above 1089 K and stresses exceeding 80 MPa. SA106B carbon steel, not designed for high-temperature use, experienced a rapid loss of ultimate strength above approximately 600 K. Tensile testing extended up to 1150 K, and creep data showed failure in less than 10 hours at temperatures above 900 K and stresses exceeding approximately 75 MPa.

Boehlert's study [70] investigated the effect of thermomechanical processing on Alloy 690's microstructure and elevated-temperature creep behavior. They subjected commercially available sheet to four cycles of cold rolling (25% deformation) followed by annealing at 1000°C for 1 hour. The thermomechanically processed microstructure showed slightly lower twin fraction and smaller grain size compared to the original microstructure. Tensile-creep experiments were conducted at temperatures between 650 and 690°C and stresses between 75 and 172 MPa, revealing that dislocation creep with lattice self-diffusion dominated. Surprisingly, the thermomechanically processed microstructure exhibited significantly worse creep resistance than the original microstructure, suggesting that the cyclic strain and annealing processing should not be used to enhance creep resistance.

Li et al. [71] conducted a study to compare the performance of as-received and 600-hour serviced turbine blades under creep-fatigue loading. The results showed that the service-exposed blades exhibited a longer creep-fatigue life than the as-received ones, mainly due to grain size refinement and increased hardness during service. Microstructural analysis indicated no directional coarsening or rafting of γ' precipitates after 600 hours of service. Notably, the as-received blades displayed initial cyclic hardening followed by saturation and softening, while the serviced blades continuously softened until failure.

The researchers proposed a conservative service life prediction approach based on the experienced mission profile, providing a novel way to assess turbine blade durability.

Sugahara et al. [72] conducted a study to evaluate the creep and mechanical behavior of Inconel 718 superalloy, which is a new generation superalloy developed for high engine efficiency and improved elevated temperature properties, particularly creep resistance. Creep tests were performed within a temperature range of 650 to 700 °C and stress range of 625 to 814 MPa. Additionally, hot tensile and oxidation tests were carried out. The researchers used various characterization techniques, such as scanning electron microscopy (SEM) for microstructural and fracture surface analysis, transmission electron microscopy (TEM) for precipitates analysis, grazing X-ray diffraction for analyzing oxide formation, and Vickers microhardness for assessing material properties.

Vakili-Tahami and Adibeig [73] conducted a study to assess the potential of replacing IN 738LC gas turbine blades with domestically produced IN 718 superalloy, focusing on its creep behavior under various operating conditions. The domestically produced superalloy showed excellent quality and compliance with international standards based on experimental tests of its creep behavior and constitutive equation. The study used numerical optimization techniques to determine creep constitutive parameters for the alloy. The investigation also examined the creep behavior of gas turbine blades operating at different rotating speeds using the finite element method. The results indicated that due to its relatively high creep deformation, IN 718 is more suitable for use in low and medium power gas turbines.

Zhang et al. [74] conducted a study to determine the mechanical properties of nickel-based alloy 600 before and after creep using continuous indentation testing and numerical simulation. They obtained the high-stress creep constitutive equation for the alloy and found that as creep time increased, the alloy exhibited more deformations, leading to improved mechanical properties. The indentation test model offered a nondestructive approach with less than 5% relative strength error compared to traditional tests, providing valuable insights for equipment safety evaluation and material life prediction.

In this thesis, the focus shifts to the materials used in the study, with particular attention given to Inconel 600. It outlines various specimen types, including standard specimens, weldments, and notched specimens, while detailing the mechanical testing methods applied, such as quasi-static tests, hardness testing, and fatigue tests. Furthermore, it delves into the setup for creep tests and examines the fractography analysis of ruptured specimens. Additionally, finite element analysis and its application to the study, including FE modeling, boundary conditions, and the Johnson-Cook plasticity model, are introduced. This segment provides a comprehensive overview of the materials, specimens, and methodologies employed in the research.

Within this thesis, the results of the conducted experiments and simulations are outlined. The section begins with an introduction contextualizing the results, followed by discussions on fatigue life prediction for Inconel 600 parent material, weldments, and notched specimens. Moreover, it examines the fractography of the tested specimens under various loading conditions, including tensile and cyclic loading, while presenting the results of multiaxial fatigue, fatigue crack growth, and creep loading experiments. This segment offers an in-depth analysis and interpretation of the obtained results, elucidating their significance and implications within the research framework.

3. Methodology

3.1. Introduction

This chapter presents a comprehensive investigation into the mechanical properties and testing procedures of Inconel 600, a high-performance nickel-chromium alloy widely used in demanding engineering applications. The focus is on understanding the behavior of Inconel 600 through various testing methods, including quasi-static and fatigue testing, as well as characterizing its microstructure using Scanning Electron Microscopy (SEM) and assessing hardness on different types of samples. The selection of appropriate specimen geometries, such as smooth samples for basic mechanical property characterization, welded samples to evaluate the weld's integrity, and single-edge and double-edge notched samples to assess fracture toughness, is crucial for obtaining reliable and representative data. The mechanical properties of Inconel 600 play a pivotal role in determining its suitability for specific engineering applications. Key mechanical properties, including tensile strength, yield strength, elongation, and toughness, are paramount in understanding the material's ability to withstand external forces and resist deformation or fracture. Additionally, fatigue testing involves cyclic loading to simulate real-life operational conditions, offering insights into the material's resistance to crack initiation and propagation under repetitive loading. The hardness of Inconel 600 on welded samples is assessed to evaluate the material's properties of different regions of the samples. These data will then be used in FEA analysis for fatigue life predictions of the welded specimens. Finally, understanding the microstructure of Inconel 600 is crucial to link its mechanical properties to its crystal structure and grain boundaries. SEM analysis offers high-resolution imaging, enabling the identification of grain boundaries, precipitates, and defects that impact its mechanical performance.

The following flowchart provides a concise overview of the key steps undertaken throughout this chapter (see Figure 3-1).

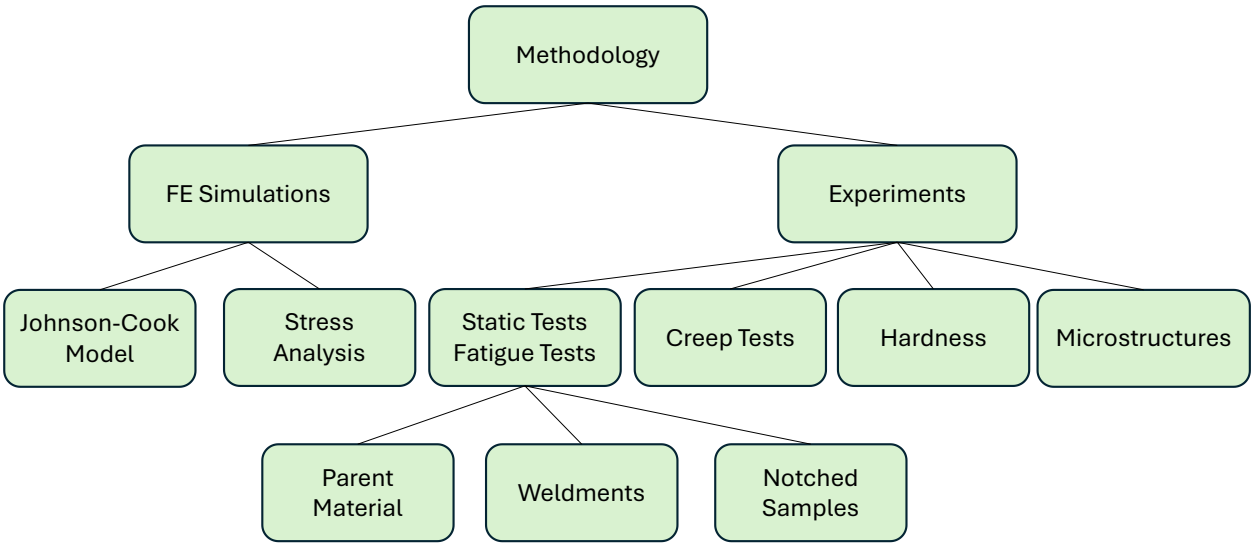

Figure 3-1. Flowchart of the steps done in the present chapter.

3.2. Materials Selection and Test Procedure

3.2.1. Inconel 600

The material used in this study was Inconel 600 alloy, which its chemical composition has been summarized in Table 3-1.

Table 3-1. Chemical composition of Inconel 600 [75]

Comp (%)	Ni	Cr	Fe	C	Mn	S	Si	Cu
Inconel 600	73.63	15.68	8.79	0.054	0.33	0.006	0.24	0.028

Inconel 600 alloy is known for its high strength and toughness, high oxidation resistance and high ductility [76]. These characteristics make it an ideal choice for the components used in CHP micro-turbines in which resistivity against high temperatures and cyclic loadings are essential. Hence, essential mechanical tests have been carried out and material properties have been extracted. The exact experimental tests are as follows:

1- Tensile tests for the Inconel 600 parent material (PM) and the weldment.
2- Hardness distribution in the cross-sectional area of the welded samples.
3- Microstructural images of different regions of the welded specimens, including nugget zone, heat-affected-zone (HAZ) and PM.
4- Fatigue tests of Inconel 600 PM and the weldment.
5- Creep tests at different loadings under a constant temperature.

3.2.2. Sample Preparation

In this study, samples for both quasi-static and fatigue tests were meticulously prepared following the guidelines provided by the ASTM-E8-04 [77]. For the quasi-static and fatigue tests, samples were obtained from Inconel 600 sheets with a uniform thickness of 3 mm. The choice of sheet material ensured homogeneity and minimized variations in mechanical properties throughout the samples. The use of standardized sample dimensions and geometries, as per the designated ASTM E8-04 standard, allowed for direct comparison with existing data and ensured the reproducibility of results.

Welded samples were prepared to investigate the mechanical behavior of Inconel 600 in welded conditions. To create the welded samples, two Inconel 600 sheets were carefully aligned and placed side by side, mimicking a butt joint configuration. Subsequently, a high-quality Tungsten Inert Gas (TIG) welding operation was performed to join the two sheets seamlessly.

After the welding process, the welded sheets were allowed to cool down to ambient temperature to prevent any heat-affected zone variations. The samples were then cut from the welded sheets using precise wire-cut technique. This ensured that the welded samples retained the intended joint configuration and avoided any detrimental effects on the material's microstructure and mechanical properties during the cutting process.

3.3. Quasi-Static Tests

Quasi-static tests were conducted on Inconel 600 samples to characterize its response to static loading conditions. During the tests, the samples were subjected to uniaxial loading at a constant and controlled speed of 1 mm/min. This loading rate allows for the accurate measurement of material deformation and stress-strain behavior, capturing critical mechanical properties such as yield strength, ultimate tensile strength, elongation, and modulus of elasticity.

Engineering and true stress-strain curves are illustrated in Figures 3-2 and 3-3. The mechanical properties of the Inconel 600 alloy and the weldment has been presented in Table 3-2.

Table 3-2. Mechanical properties of Inconel 600 and the weldment

	UTS (MPa)	Yield Strength (MPa)	Elongation (%)
Inconel 600 PM	671	345	50.8
Weldment	641	320	15.2

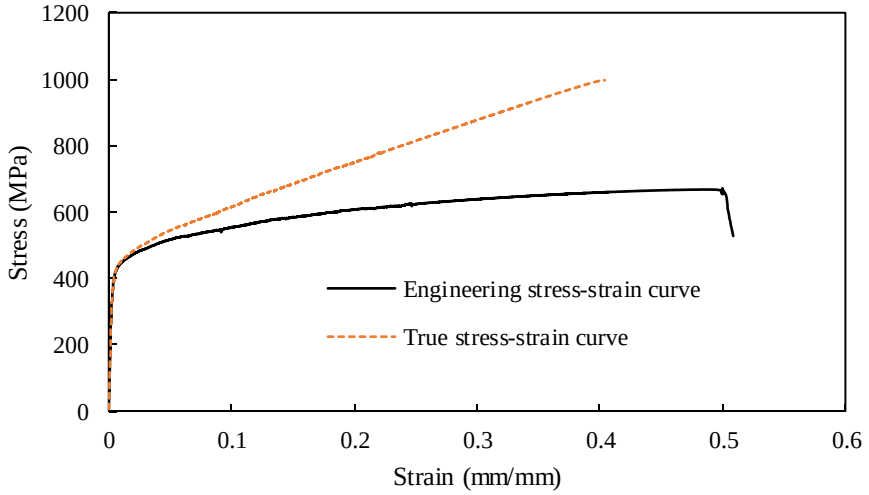

Figure 3-2 Engineering and true stress-strain curves for Inconel 600 PM

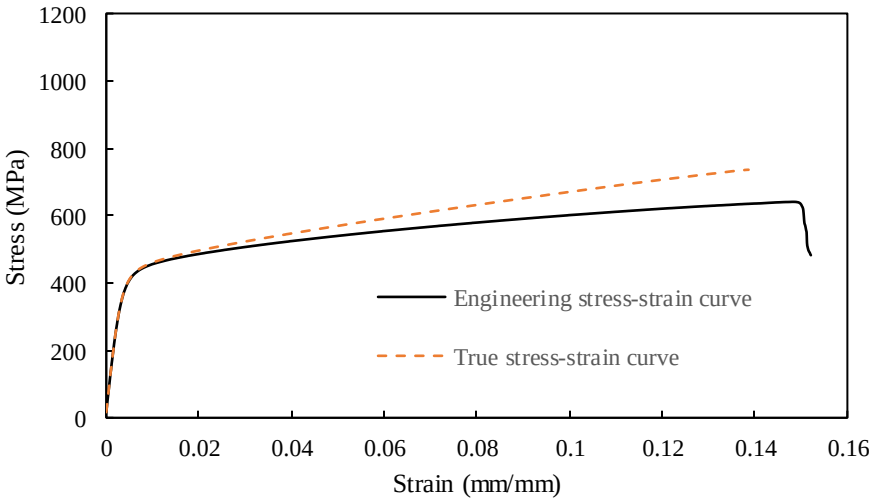

Figure 3-3. Engineering and true stress-strain curves for Inconel 600 weldment

By plotting true stress versus true plastic strain, one can extract the Ramberg-Osgood's constants. The Ramberg-Osgood equation is a widely used mathematical model in

engineering mechanics to describe the stress-strain relationship in materials beyond their elastic limits (refer to Figure 3-4).

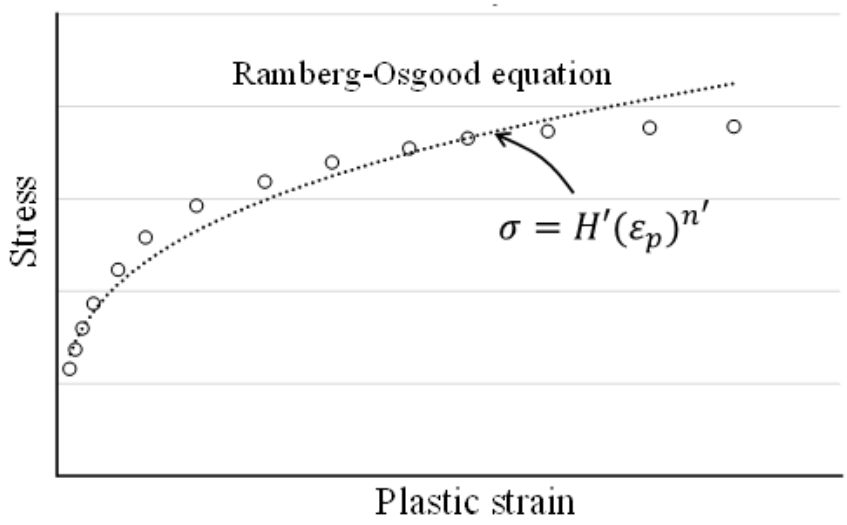

Figure 3-4. A typical Ramberg-Osgood relation, showing the power-law relationship between stress and plastic strain components

The Ramberg-Osgood relation is presented in one of the following forms [78, 79]:

$$\varepsilon = \frac{\sigma}{E} + (\frac{\sigma}{H'})^{1/n'} \quad (3\text{-}1)$$

$$\sigma = H'(\varepsilon_p)^{n'} \quad (3\text{-}2)$$

where H' and n' are Ramberg-Osgood's constants. The Ramberg-Osgood equation is valuable for predicting the non-linear deformation of materials under various loading conditions, making it essential in structural analysis and design. The Ramberg-Osgood's constants are summarized in Table 3-3.

Table 3-3. Ramberg-Osgood's constants of Inconel 600

	H' (MPa)	n'	R^2
Inconel 600 PM	771	-0.113	0.98
Weldment	869	-0.135	0.97

True stress versus true plastic strain for both Inconel 600 PM and the weldment are shown in Figures 3-5 and 3-6. Knowing the Ramberg-Osgood parameters are very important to evaluate fatigue life of notched components with different geometries using strain-based approaches. These parameters, along with the Neuber formula (Eq. 3-3) [80] are used to obtain the essential parameters, including strain amplitudes and mean stresses to be used in any strain-based fatigue life prediction models such as SWT equation (Eq. 2-16).

$$\sigma_{max}\,\varepsilon_{max} = \frac{(K_t S_{max})^2}{E} \tag{3-3}$$

In this equation, σ_{max} and ε_{max} are maximum stress and strain at the notch root of a notched component, S_{max} is the maximum remote stress, K_t is the elastic stress concentration factor, and *E* is Young's modulus.

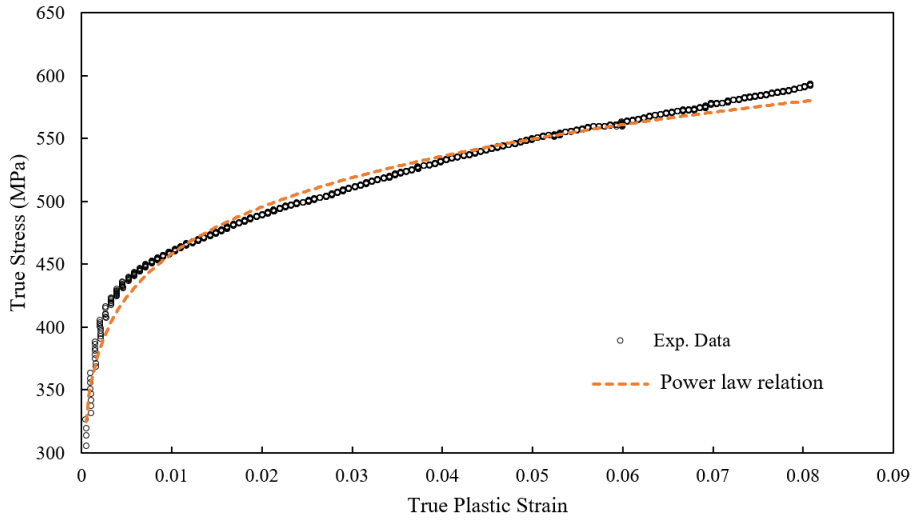

Figure 3-5. True stress versus true plastic strain for the Inconel 600 PM

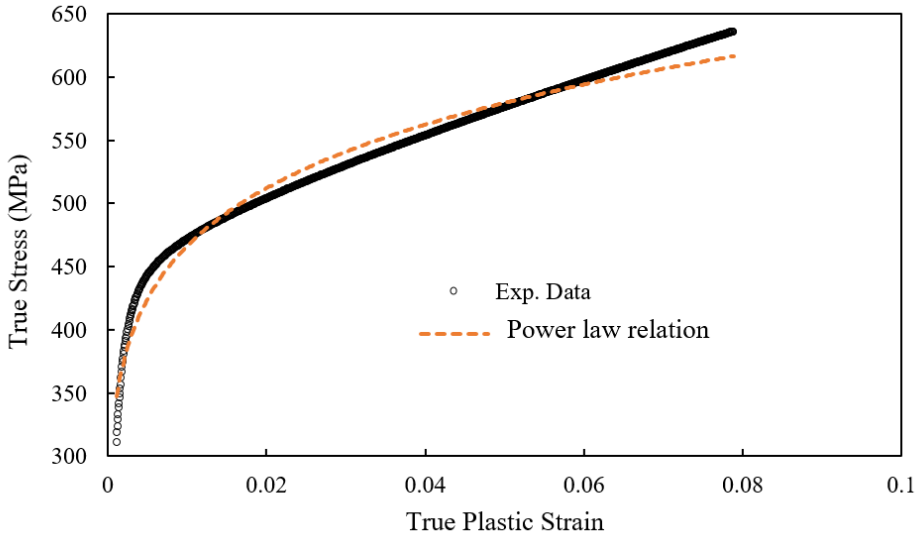

Figure 3-6. True stress versus true plastic strain for the Inconel 600 weldment

3.4. Hardness tests

To assess the hardness distribution within the welded sample, a series of hardness measurements were performed at regular intervals of 1 mm along the cross-sectional area. Figure 3-7 presents a schematic view of the cross-sectional area, showcasing the weld's geometry and boundaries. The hardness distribution will be utilized to determine the mechanical properties of different regions on the weldment based on the uniform material law [81, 82].

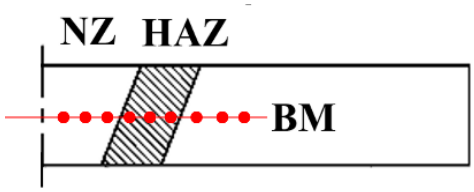

Figure 3-7. Cross-sectional area of the weldment and the points of hardness measurements

3.5. Fatigue Tests

Fatigue tests on both the smooth and welded samples were performed using a state-of-the-art Zwick/Roell servo-hydraulic fatigue testing machine with a load ratio R=0 and a

testing frequency of 10 Hz, according to ASTM E466 standard [83]. The fatigue behavior of Inconel 600 PM and the weldment were thoroughly examined to assess their resistance to cyclic loading. It should be noted that all fatigue tests were conducted at room temperature, with cyclic loads applied between 40% and 80% of the specimens' ultimate tensile strength.

For each static and fatigue test, at least two samples were tested, and the average of the results was reported. This approach was taken to account for uncertainties and ensure the reliability of the data. By averaging the results, we aimed to minimize the impact of any potential uncertainties and provide a more accurate representation of the material's performance.

3.6. Creep Tests

Before conducting the creep tests, the test sample configuration and test setup apparatus were carefully prepared to ensure accurate and reliable results. Figure 3-8 provides a visual representation of the test sample used in the experiment.

Fig. 3-9 illustrates the test setup apparatus used for the creep testing. The apparatus was designed to control and maintain a constant temperature of 650℃ throughout the testing process. Additionally, it allowed for the precise application of different loads to each type of sample. For the smooth sample, a stress level of 400 MPa was utilized, while the welded specimens were tested at stress levels of 250 and 400 MPa. These stress levels were chosen based on the material properties and the intended application of the samples.

Figure 3-8. Creep test sample

Figure 3-9. Test setup apparatus used for the creep testing

During the testing, the creep strain values were continuously monitored at regular intervals over a predetermined time duration. The strain-time data were collected, and the resulting creep strain-time curves were plotted for both smooth and welded samples under their respective stress conditions.

3.7. FE Simulations

To ensure the accuracy of FE simulations, it is essential to take into account the temperature-dependent physical, mechanical, and thermal properties of the material

being used. In the case of Inconel 600, these properties are known to vary with temperature, which can significantly affect the results obtained from FE analyses.

To account for these variations, the physical, mechanical, and thermal properties of Inconel 600 are assigned to the geometry in a temperature-dependent manner. This ensures that the FE simulations accurately reflect the behavior of the material under different thermal and structural conditions. In addition to assigning temperature-dependent properties, the Johnson-Cook plastic model [84, 85] (Eq. 3-4) is utilized in the FE simulations. This model is particularly suitable for materials that exhibit temperature-dependent plastic behavior and structures undergoing relatively severe thermal and structural loading. By considering the variations in temperature, the Johnson-Cook model provides a more accurate representation of the material's response to loading, which is crucial for predicting its behavior in real-world applications such as those in micro-turbines.

$$\sigma_0 = \left(A + B\,\bar{\varepsilon}_{Pl}^{\,n}\right)\left(1 + C\ln\frac{\dot{\bar{\varepsilon}}_{pl}}{\dot{\varepsilon}_0}\right)\left(1 - \left(\frac{T - T_{ref}}{T_{ref} - T_{melt}}\right)^m\right) \tag{3-4}$$

Constants of Johnson-Cook plasticity model for Inconel 600 was obtained and summarized in Table 3-4.

Table 3-4. Johnson-Cook constants for Inconel 600

Material	A (MPa)	B (MPa)	n	m	C	Tref (°C)	Tmelt (°C)
Inconel 600	450	1300	0.94	1.3	0.017	26	1413

Figure 3-10 depicts the variations in true stress versus true strain as a function of temperature. The data from these curves are extracted and assigned to the FE software to account for the strain hardening effects.

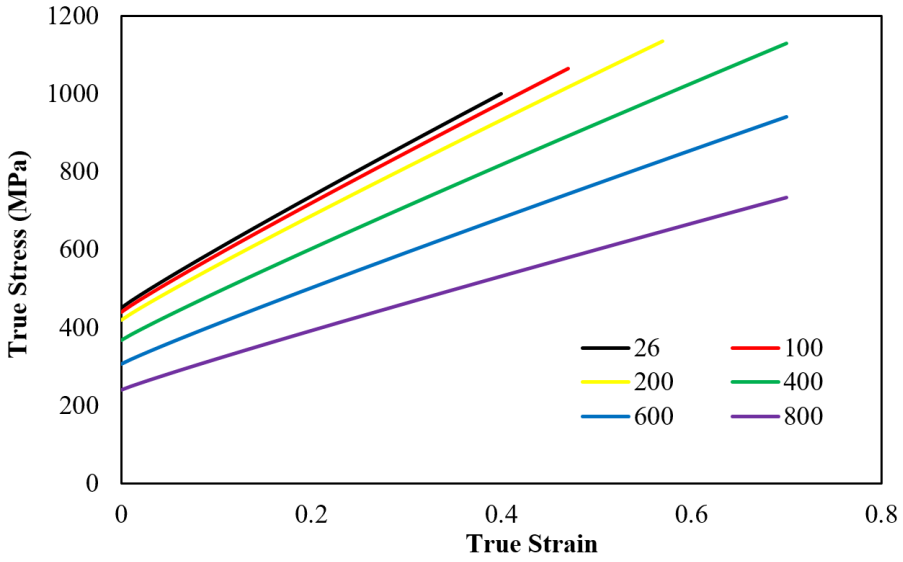

Figure 3-10. True stress-strain curves obtained using Johnson-Cook model for Inconel 600

In all the FE simulations, the samples were modeled in three dimensions and meshed using C3D8R elements. In the first stage, mesh sensitivity analysis was conducted using six different mesh sizes. Ultimately, a mesh size of 0.5 mm was selected as the optimal mesh size.

3.8. Multiaxial Fatigue

Multi-axial fatigue refers to the phenomenon of material failure under cyclic loading in more than one direction simultaneously. This means that when a mechanical component is subjected to a complex loading history, such as combined tension and torsion, its behavior cannot be fully predicted by considering only the individual stress components acting on it. Instead, the combination of stresses acting on multiple planes must be taken into account to accurately predict the fatigue life of the component.

Critical plane approaches are a set of methods used to assess multi-axial fatigue failure. These methods are based on the idea that the location of the critical plane, where the maximum damage occurs, is an important factor in predicting the fatigue life of a component subjected to complex loading. In general, critical plane approaches involve calculating the damage induced on each plane in the material, and then determining the

location of the critical plane where the maximum damage occurs. This critical plane is then used to calculate the fatigue life of the component.

The importance of critical plane approaches lies in their ability to accurately predict the fatigue life of mechanical components subjected to complex loading histories. By accounting for the combined effects of stresses acting on multiple planes, these approaches can provide more accurate and reliable fatigue life predictions than traditional methods that consider only individual stress components. This is particularly important in engineering applications where components are subjected to complex loading histories, such as aircraft and automotive structures, where safety and reliability are critical concerns.

There are several different critical plane approaches that have been developed to analyze multi-axial fatigue. Fatemi-Socie (FS) (Eq. 2-22) approach is a widely used critical plane method for predicting the fatigue life of metallic materials subjected to complex loading histories. This approach is based on the concept of a "damage parameter" that takes into account the combined effects of both shear and normal stresses on the critical plane. The FS approach uses a set of empirical equations to predict the fatigue life of a material based on the value of the damage parameter. Brown-Miller approach is another popular critical plane method for analyzing multi-axial fatigue. This approach is based on the assumption that the critical plane is the plane where the shear stress is maximum. The BM approach uses a set of empirical equations to predict the fatigue life of a material based on the maximum shear stress on the critical plane. Smith-Watson-Topper (SWT) approach (Eq. 2-23) is a method that is commonly used to analyze fatigue in ductile materials such as aluminum alloys. This approach is based on the assumption that the critical plane is the plane where the maximum shear strain energy density occurs. The SWT approach uses a set of empirical equations to predict the fatigue life of a material based on the value of the shear strain energy density on the critical plane.

All of the above-mentioned approaches have their own strengths and limitations, and the choice of which method to use will depend on the specific application and material being analyzed. It's worth noting that there are many other critical plane approaches as well, and ongoing research is focused on improving and refining these models to better predict the fatigue life of mechanical components under multi-axial loading.

4. "Results and Discussion - Mechanical Properties, Fatigue and Creep "

In this chapter, we conducted a comprehensive set of tests to evaluate the mechanical properties and microstructural characteristics of welded Inconel 600 samples. These tests included hardness measurements across the weldment, microstructural analysis using optical microscopy to examine variations within different regions of the weldment, and fatigue testing to assess the materials' responses under cyclic loading. Additionally, we performed creep tests to understand the behavior of the material under high-temperature conditions. The results of these tests will be discussed in detail throughout this chapter.

4.1. Hardness Test Results

Figure 4-1 displays the hardness values obtained from these measurements, illustrating how the hardness varies across the weldment.

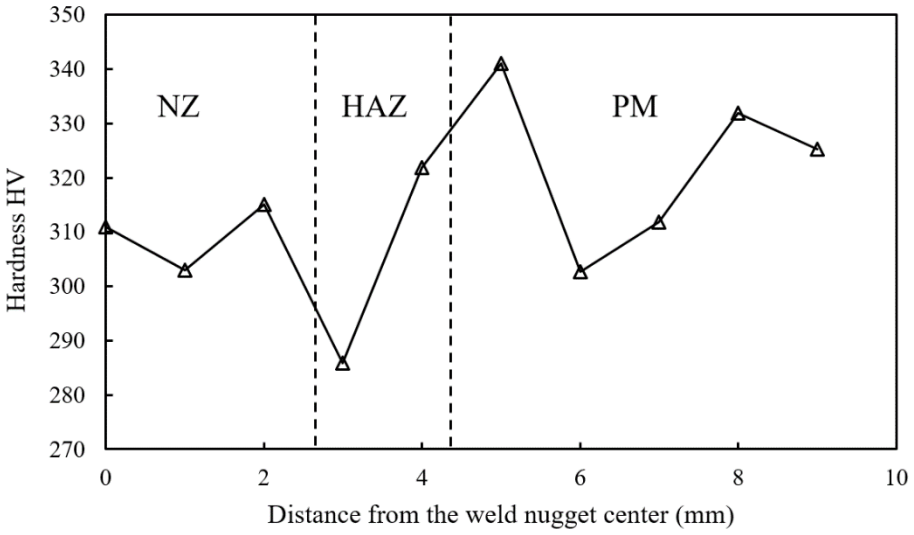

Figure 4-1. Hardness distribution in the cross-section of the weldment

As seen in Figure 4-1, the hardness value in the HAZ is less than those on fusion zone (nugget) and PM.

4.2. Microstructures

A detailed microstructural analysis was conducted using an optical microscope to investigate the grain size and other microstructural features within different regions of the welded joints, namely the Heat-Affected Zone (HAZ), the nugget zone, and the parent material.

To prepare the microstructural images, specimens were carefully cut from the cross-sectional area of the welded samples to capture representative regions of interest. These specimens were then subjected to a meticulous sample preparation procedure. First, the specimens were ground using different grades of sandpaper to remove any surface irregularities and obtain a smooth and uniform surface. Subsequently, a polishing step was carried out to create a mirror-like finish, ensuring optimal image clarity and minimizing surface artifacts during microscopy.

Etching was then performed to reveal the microstructure effectively. The chosen etchant selectively reacted with the material's constituents, making the grain boundaries and other microstructural features more distinguishable under the optical microscope. This etching process enabled the visualization of various microstructural characteristics, such as grain size, grain boundaries, inclusions, and phases, in the different regions of the weldment.

The microstructural images obtained from the optical microscope, presented in Figures 4-2 to 4-5, showcased the microstructural variations within the HAZ, nugget zone, and parent material at different magnifications. The microstructural analysis of the welded samples, as depicted in Figures 4-2 to 4-5, revealed distinct variations in the microstructures across different regions of the weldment. These differences in microstructure were observed to be associated with varying grain sizes, and consequently, they significantly impacted the mechanical properties of the welded joints. Figure 4-2 depicts the distinct microstructures of all welded regions.

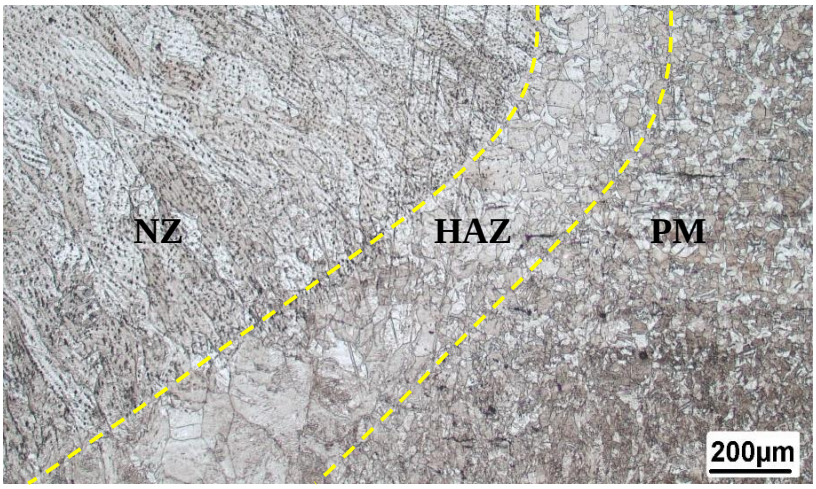

Figure 4-2. Microstructure images of all regions of the weldment

In Figure 4-3, the Heat-Affected Zone (HAZ) exhibited a different microstructure compared to the nugget zone and the parent material. The HAZ, being the region adjacent to the weld where the base metal experienced thermal cycling during welding, showed altered grain structures due to the influence of temperature gradients. This resulted in changes in grain size, which in turn influenced the mechanical properties, such as hardness, tensile strength, and ductility.

Figure 4-4 demonstrated the microstructure of the nugget zone, which is the central region of the weld where the welding operation generates the highest heat and fusion. The microstructural characteristics here were notably distinct from those observed in the HAZ and parent material. The rapid cooling and solidification during welding contributed to the formation of unique grain structures, impacting the mechanical properties differently.

Figure 4-3. Microstructural image of nugget zone

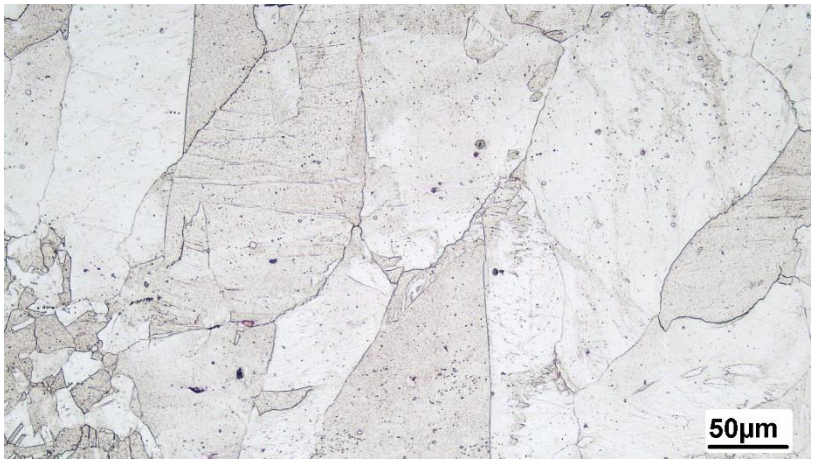

Figure 4-4. Microstructural image of HAZ

The microstructure of the parent material, shown in Figure 4-5, served as a reference point for comparison. This region exhibited the original, as-received microstructure of the base material before welding. The presence of a different grain size and distribution in this region compared to the HAZ and nugget zone influenced the overall mechanical behavior of the welded joint.

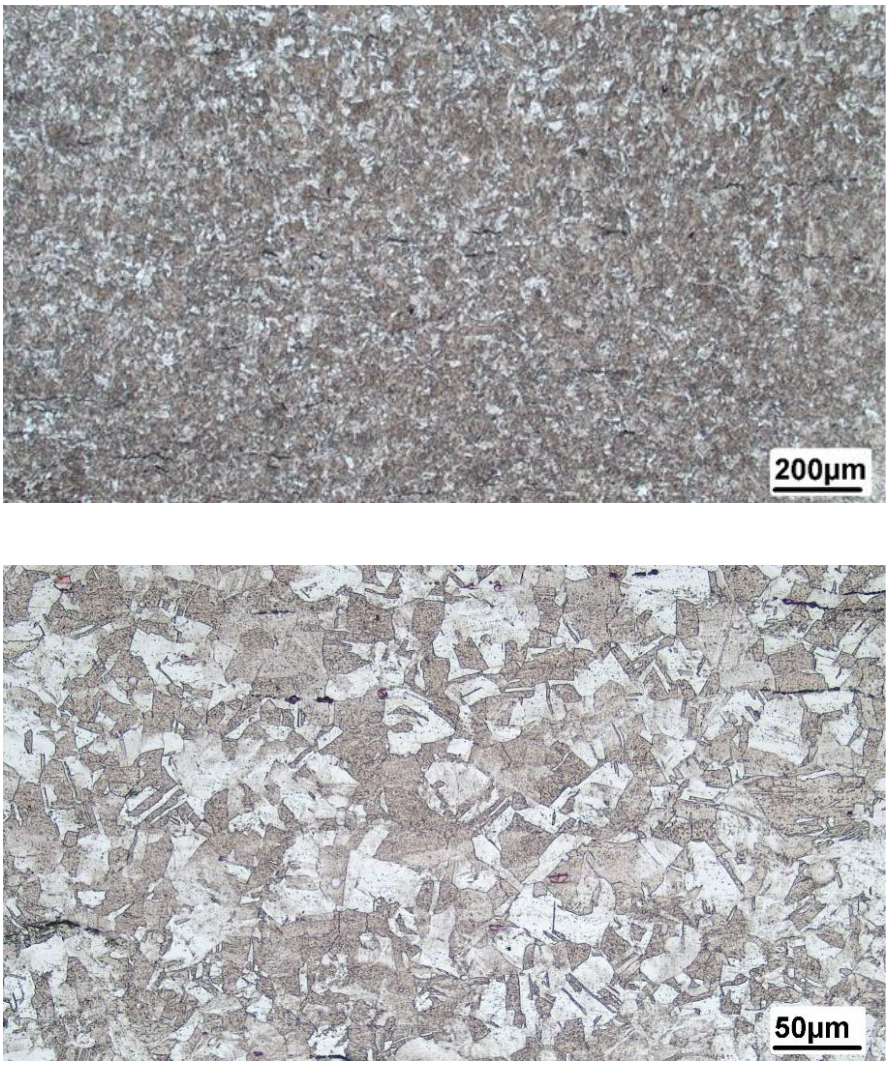

Figure 4-5. Microstructure images of PM with different magnifications

The variations in microstructure and grain size among these different regions of the welded samples led to different mechanical properties throughout the weldment. These differences included variations in strength, toughness, fatigue resistance, and other relevant mechanical characteristics.

4.3. Fatigue Test Results

Figure 4-6 presents the comprehensive fatigue test data for both Inconel 600 PM and the weldment, showcasing their respective fatigue responses under the applied loading conditions.

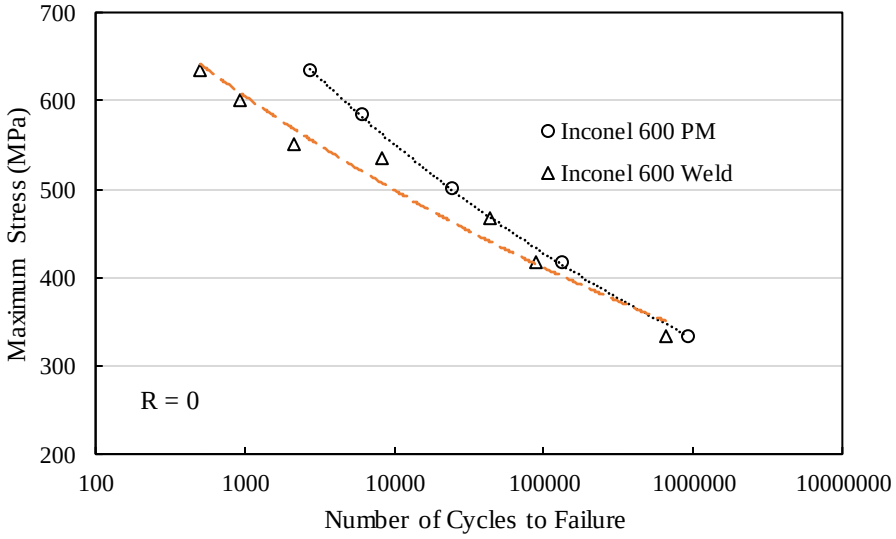

Figure 4-6. Fatigue test data for Inconel 600 PM and the weldment

Figures 4-7 and 4-8 illustrate the relationship between strain amplitude and the number of cycles to failure for both specimens. To facilitate accurate fatigue life predictions, the study summarizes the essential strain-based fatigue parameters in Table 4-1. These parameters are crucial for evaluating the materials' fatigue performance and making reliable assessments of their durability under cyclic loading. To obtain strain-based fatigue parameters, first, the data at the equivalent completely reversed stress condition (R=-1) was obtained using the SWT parameter as follows [45]:

$$\sigma_{ar} = \sqrt{\sigma_{max}\,\sigma_a} \tag{4-1}$$

In this equation, σ_{ar} is the equivalent completely reversed stress amplitude, σ_{ar} is the stress amplitude at R=0, and σ_{max} is the maximum stress.

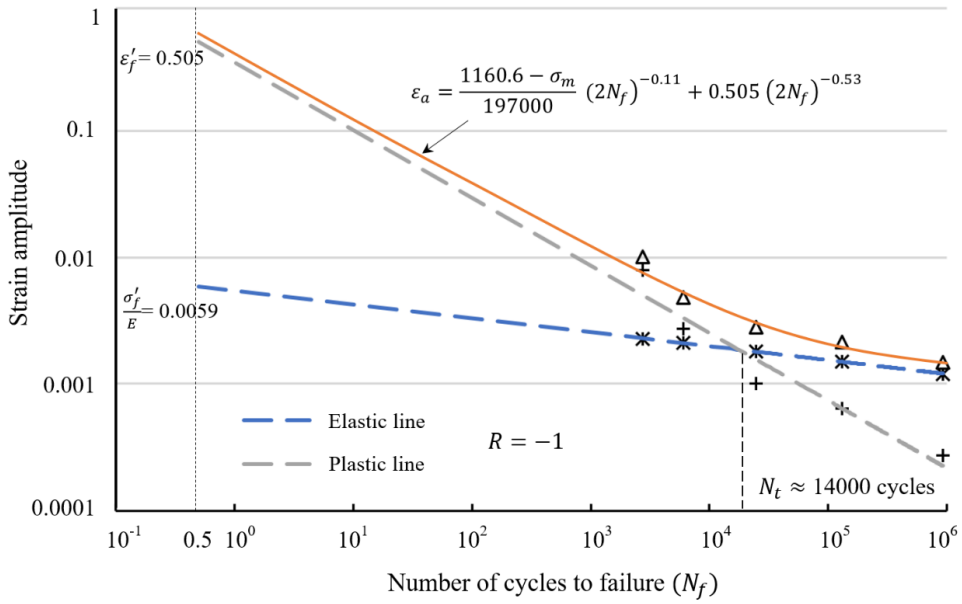

Figure 4-7. Strain-based fatigue parameters of Inconel 600 PM

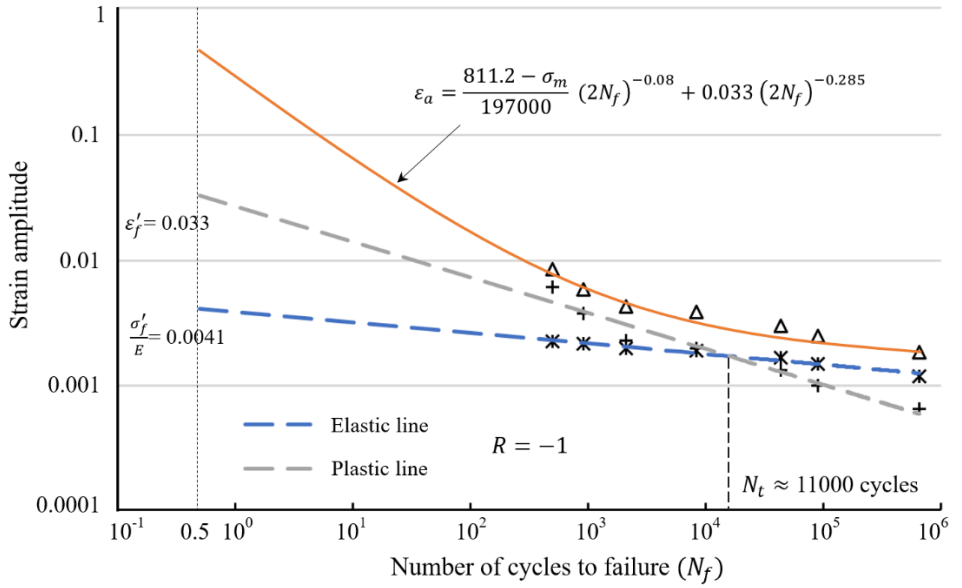

Figure 4-8. Strain-based fatigue parameters of Inconel 600 weldment

Table 4-1. Strain-based fatigue parameters of Inconel 600 PM and weldment

Material	σ_f'	b	ε_f'	c
Inconel 600 PM	1160.6	-0.11	0.505	-0.53
Weld	811.2	-0.08	0.033	-0.285

4.4. Fatigue of Notched Samples

In this stage, two distinct notch geometries: (i) single-edge and (ii) double-sided V-shaped notch were selected. Subsequently, the specimens with these chosen notch designs were fabricated. The notches were skillfully created in the weld seam of the samples utilizing a wire cut technique, with the angle of the V-shaped notches set precisely at 60 degrees. For visual reference, refer to Figure 4-9, which depicts the samples featuring both the single-edge and double-sided V-shaped notches in the welded joints.

Figure 4-9. Notched samples prepared for cyclic tests: (a) single-edge, (b) double-sided V-shaped notch.

Subsequently, fatigue tests were conducted on the notched samples using a Zwick/Roell servo-hydraulic fatigue testing machine (Fig. 4-10) at a frequency of 10 Hz and a load ratio of R=0. The obtained data was utilized to generate S-N curves, allowing for a comprehensive evaluation of the fatigue response exhibited by the notched welded samples. It is worth mentioning that the nominal stress is defined as the follows:

$$S = \frac{P}{w \times t} \tag{4-2}$$

In which S is the nominal stress, F is the applied load, and w and t are the width and thickness of the samples, respectively.

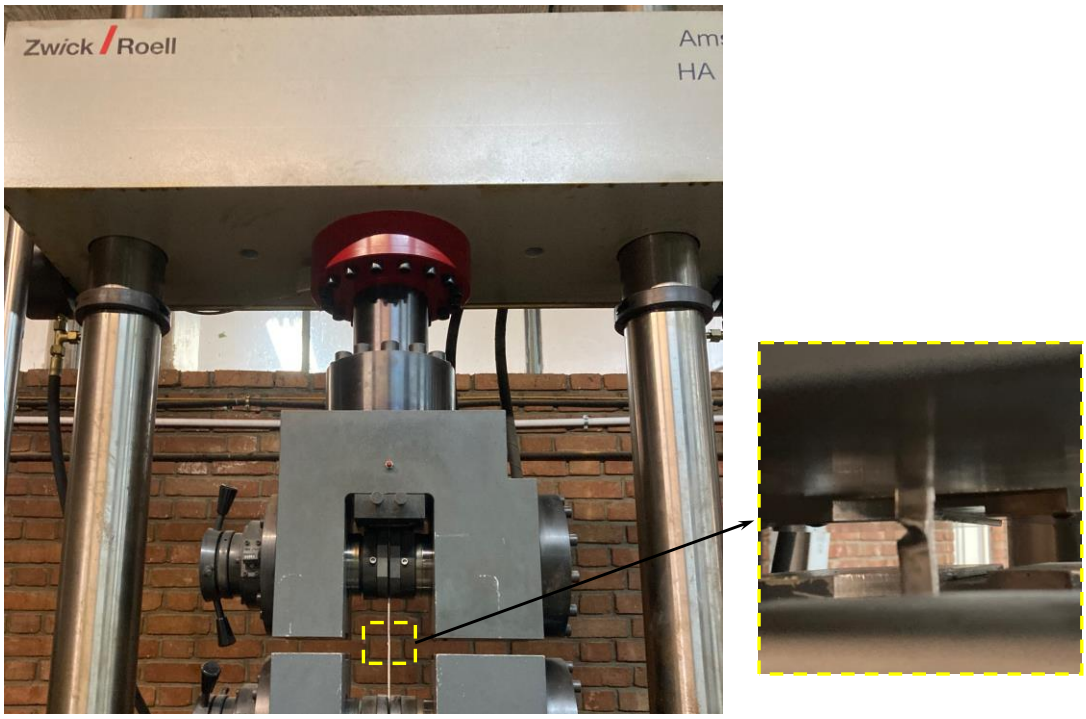

Figure 4-10. Fatigue testing machine and the close-up view of a test sample

Figure 4-11 illustrates the S-N curves representing the fatigue behavior of both single-edge and double-sided-edge notched welded samples. Remarkably, the single-edge notched samples exhibited higher fatigue lives compared to the double-sided-edge notched specimens, as depicted in the graph.

The next chapter will delve into predicting the fatigue lives of both un-welded and welded notched samples. These predictions will be thoroughly compared with the experimental results obtained so far, offering valuable insights and validating the accuracy of the conducted experiments. This comparative analysis will contribute significantly to our understanding of the fatigue characteristics of the notched samples under different conditions.

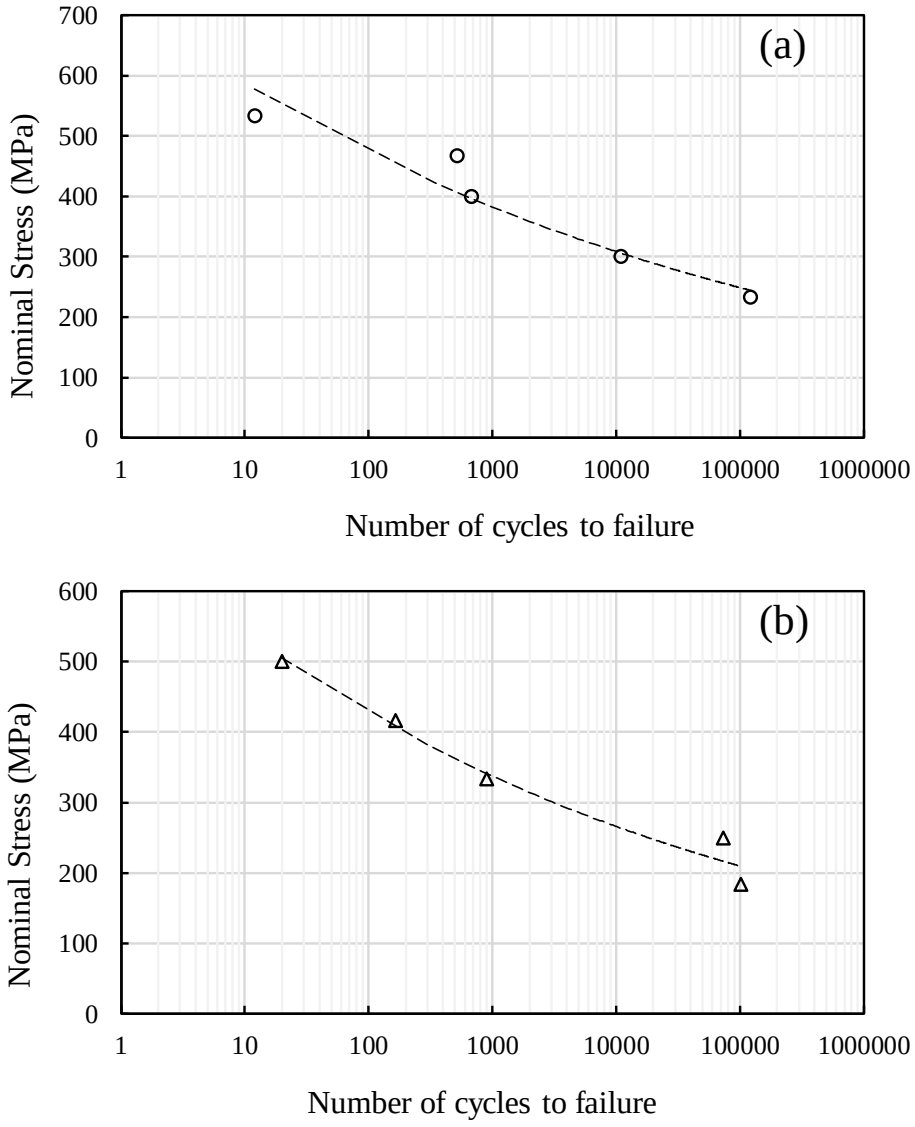

Figure 4-11. Fatigue test data and S-N curves of the samples with (a) single-edge notch, and (b) double-sided edge notch

4.5. Creep Test Results

Figure 4-12 depicts the creep strain-time response for the smooth sample subjected to a stress of 400 MPa and a temperature of 650°C, while Figures 4-13 and 4-14 illustrate respectively the corresponding creep behavior of the welded specimen under stresses of 250 and 400 MPa and the same temperature conditions.

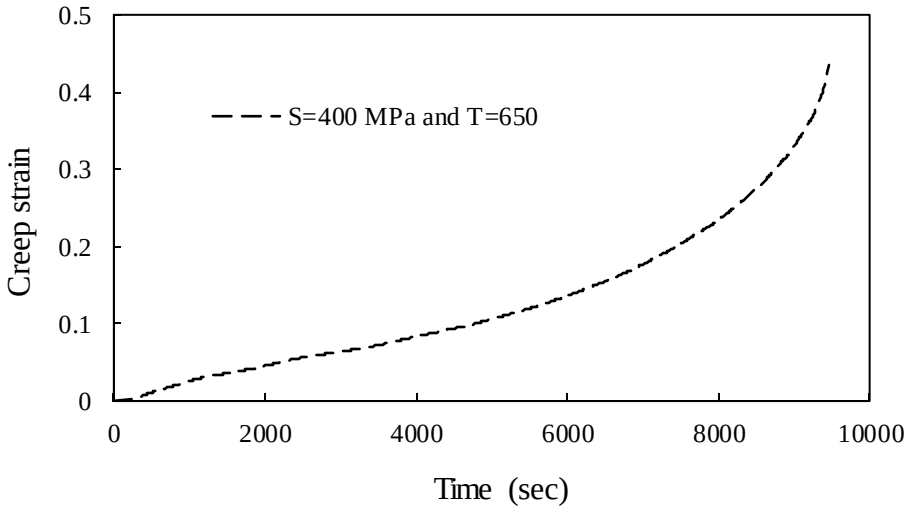

Figure 4-12. Creep strain versus time for smooth sample at S=400 MPa and T=650 ℃

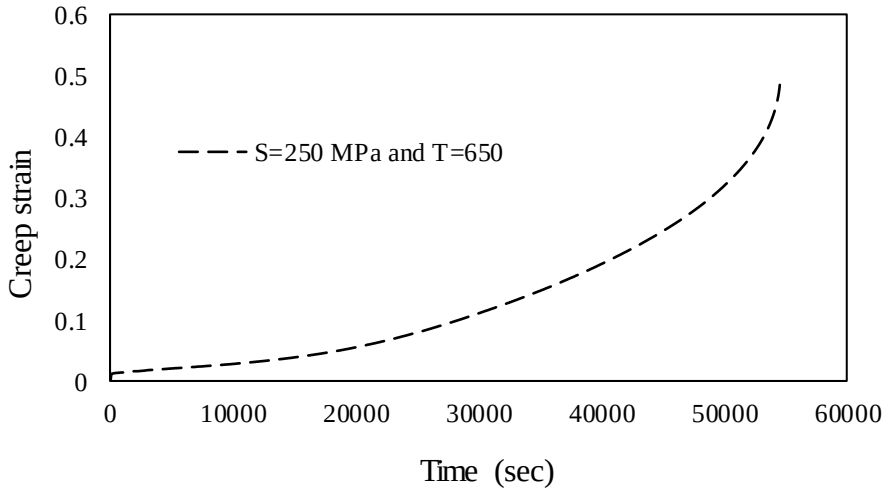

Figure 4-13. Creep strain versus time for welded sample at S=250 MPa and T=650 ℃

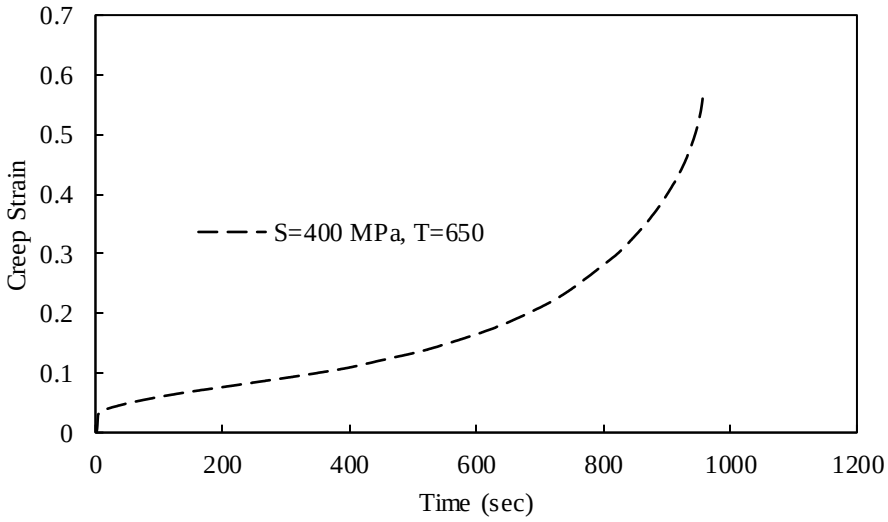

Figure 4-14. Creep strain versus time for welded sample at S=400 MPa and T=650℃

As seen in Figures 4-12 to 4-14, both smooth and welded samples failed under creep environment at 650℃, very quickly, indicating that Inconel 600 alloy is not suitable for the applications where creep may occur at high temperatures even at low load levels. However, it has been shown through research studies that, it can tolerate creep loading at lower temperatures like 300-400℃ [74]. The comparison between Figures 4-12 and 4-14 shows that creep life of smooth sample is much higher than that of welded sample at the same creep environment.

The analysis of these creep curves will help in understanding the materials' time-dependent deformation characteristics and their ability to withstand sustained loads at elevated temperatures, which is crucial in various engineering applications.

5. "Results and Discussion - FE Simulations, Comparison and Validation"

5.1. Introduction

In this chapter, a comprehensive investigation into the mechanical behavior of Inconel 600 is presented, incorporating a combination of experimental tests and FE simulations. The response of the material under various loading conditions is examined by employing standard test specimens as well as welded samples with and without notches. FE simulations are conducted on the standard Inconel 600 test specimens, subjecting them to both static and cyclic loads, and the obtained fatigue test results are compared with experimental data. Furthermore, FE simulations are extended to welded samples, allowing for an assessment of their mechanical performance under similar loading conditions, and the predicted results are meticulously compared with experimental data to ascertain the efficacy of the simulation approach. Multi-axial fatigue analysis is performed on Inconel 600 bars undergoing combined tension and torsion loadings, and fatigue life predictions are made using critical plane approaches. Moreover, SEM images of the fractured surfaces of ruptured samples under static and cyclic loadings for both standard and welded specimens are provided and used for fractography of the specimens. This comprehensive study significantly contributes to the understanding of Inconel 600's mechanical response, and it offers essential guidance for future engineering applications of this high-performance material.

5.2. Fatigue life prediction of Inconel 600 PM

To obtain S-N curve of the Inconel 600 standard specimen, the stress and strain distributions in the sample must be obtained at each load levels. The required stress and strain values obtained in a complete loading-unloading cycle are then utilized to predict fatigue lives according to the strain-based Basquin fatigue damage model (Eq. 5-1) in the MSC fatigue software. Finally, the predicted results are plotted versus the applied stresses to obtain the S-N curves.

$$\varepsilon_a = \sigma_f'(2N_f)^b + \varepsilon_f'(2N_f)^c \quad (5\text{-}1)$$

The strain-based fatigue parameters obtained from the previous chapter (Table 4-1) are used in the above equation to obtain fatigue lives. The stress distributions along the longitudinal and transverse paths, and in the directions of S_{11} and S_{22} undergoing remote stress equals to 630 MPa has been shown in Fig. 5-1.

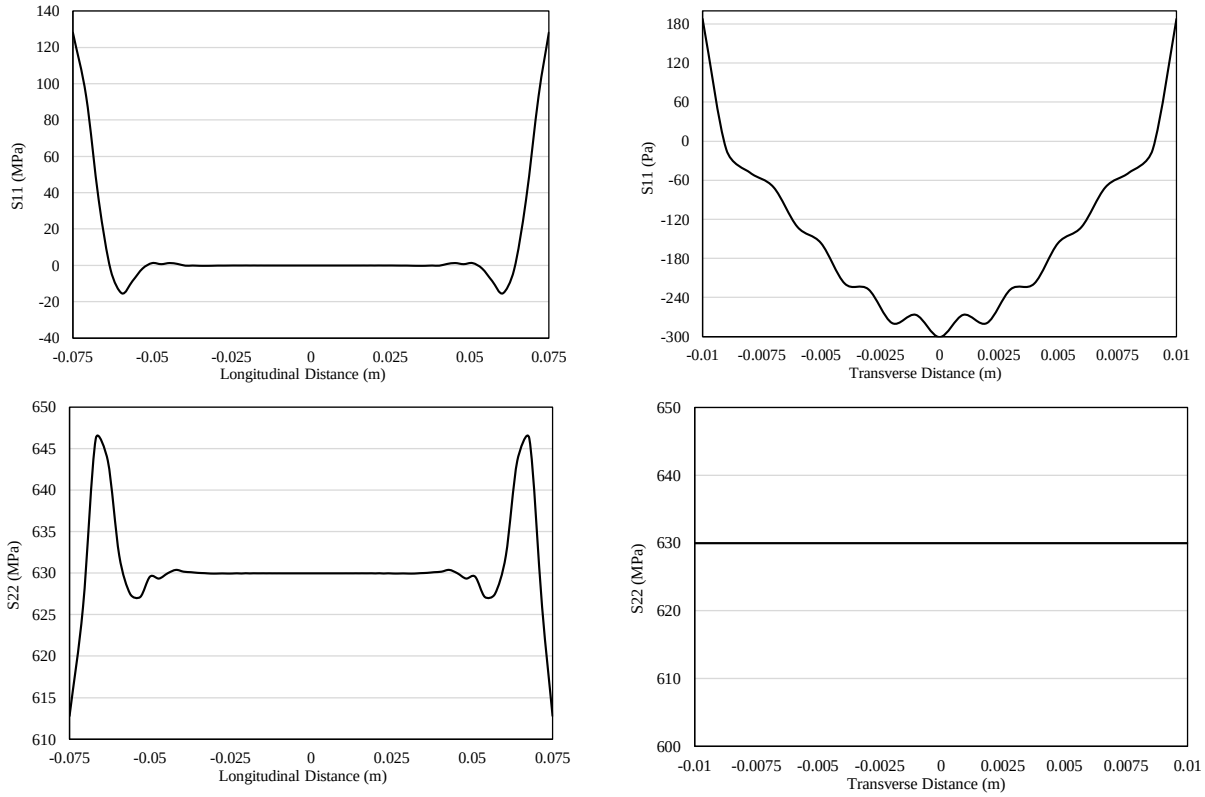

Figure 5-1. S11 and S22 stress distribution along the longitudinal distance (top left and bottom left), S11 and S22 stress distribution along the transverse path (top right and bottom right).

The von-Mises stress, maximum principal strain, and S_{11} and S_{22} stress contours have been also illustrated in Figure 5-2. As seen in this figure, the stress and strain distributions in the middle of the samples are smooth and unchanged, as expected due to the absence of a notch. However, discrepancies in stress and strain at the ends are observed, resulting from the application of concentrated loads at one end and a constraint at the other. Since the fatigue phenomenon occurs in the middle of the samples, the stress and strain values in this central part were considered for fatigue life predictions.

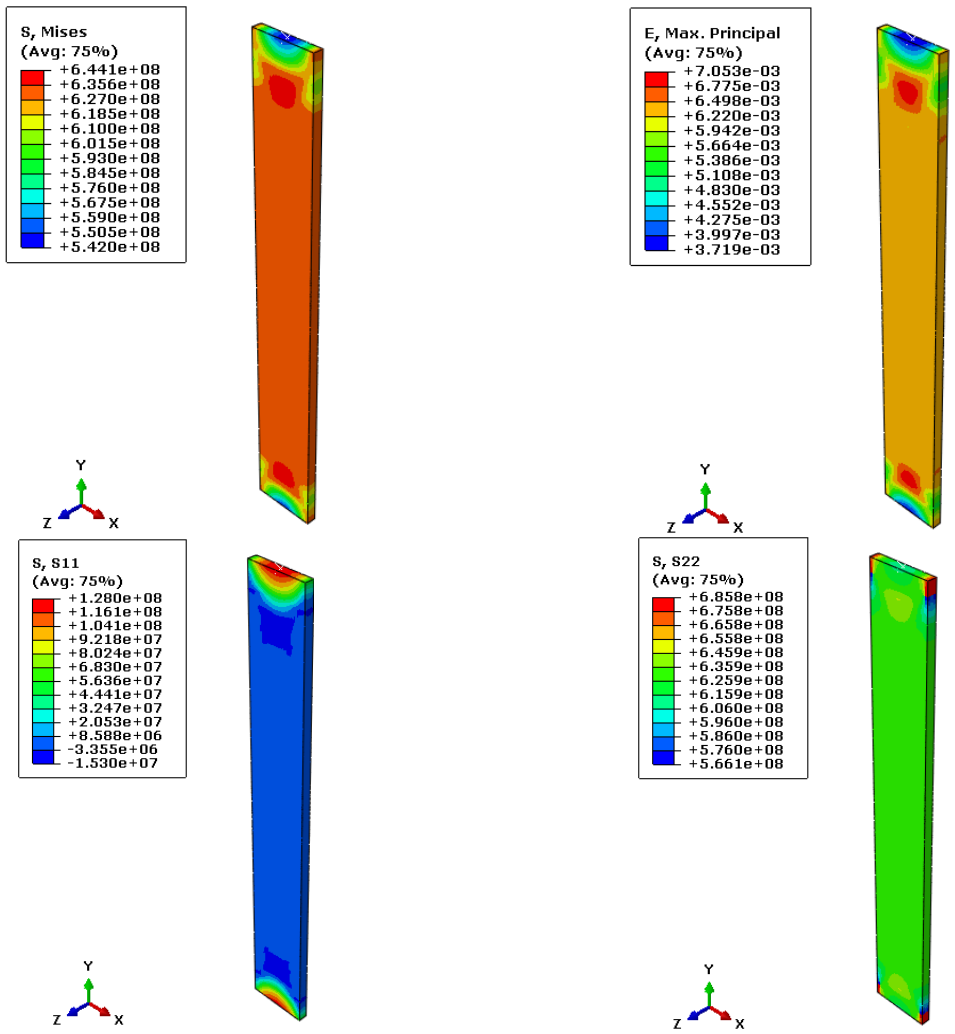

Figure 5-2. Von-Mises stress, maximum principal strain, and S11 and S22 stress contours of Inconel 600 PM

Figure 5-3 shows the comparison between the fatigue life obtained using FE method with those obtained empirically.

As seen in Fig. 5-3, there is a reasonable agreement between the fatigue life results obtained using FE method and experiments. A small discrepancy in the result could be attributed to the fact that accuracy of the empirical-based fatigue life prediction models varies with materials. Some models that can predict fatigue life well for a particular material may not be very suitable for others.

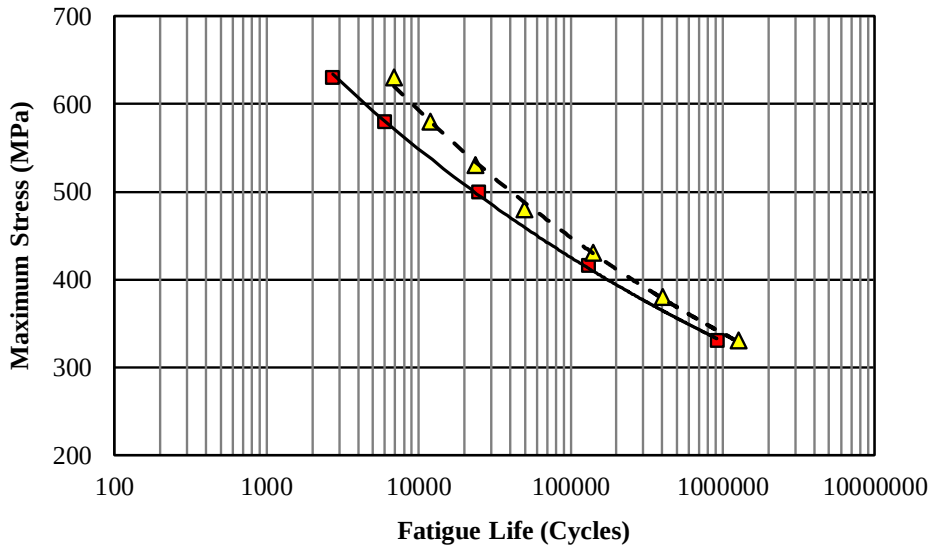

Figure 5-3. Comparison between the predicted fatigue life of the Inconel 600 standard samples with experimental fatigue test data

5.3. Fatigue Response of Inconel 600 Weldment

To predict fatigue life of the Inconel 600 weldments, stress and strain values in the vicinity of the weld seam as well as the strain-based fatigue parameters for welded samples listed in Table 4-1 of the previous chapter are required. These values as input data will be introduced to MSC fatigue software to predict the fatigue life of the samples at each applied remote stress. The applied stresses are plotted versus the predicted fatigue lives in a semi-logarithmic plot, and the results are compared with experimental test data.
The cyclic stress–strain parameters are derived from hardness distribution and parent material parameters as follows:

$$K_i' = K_1' . \frac{H_i}{H_1} \ , \ i = 1, 2, \dots, n \qquad (5\text{-}2)$$

In which K_i' and H_i are the cyclic strength coefficient and hardness value in the i th zone of the weld seam, respectively. For i = 1 data were extracted from parent material properties. Based on the above relation, the mechanical properties of different regions of the welded samples were obtained and assigned to the FE model, as observed in Figure 5-4.

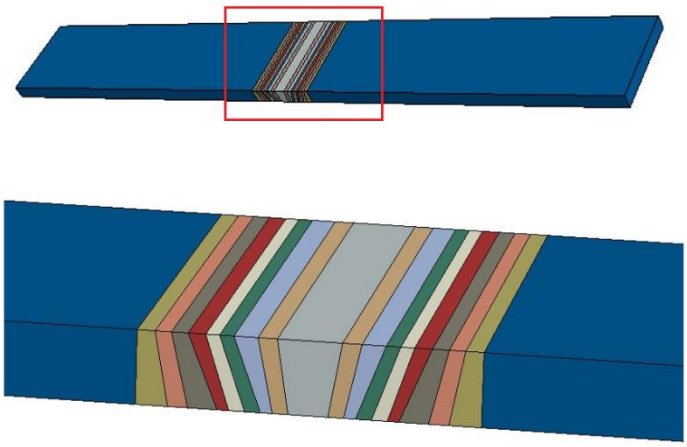

Figure 5-4. Dividing the weld region to different stripes to assign various mechanical properties.

Figures 5-5 and 5-6 illustrate the stress and strain distributions and contours required for the fatigue life predictions.

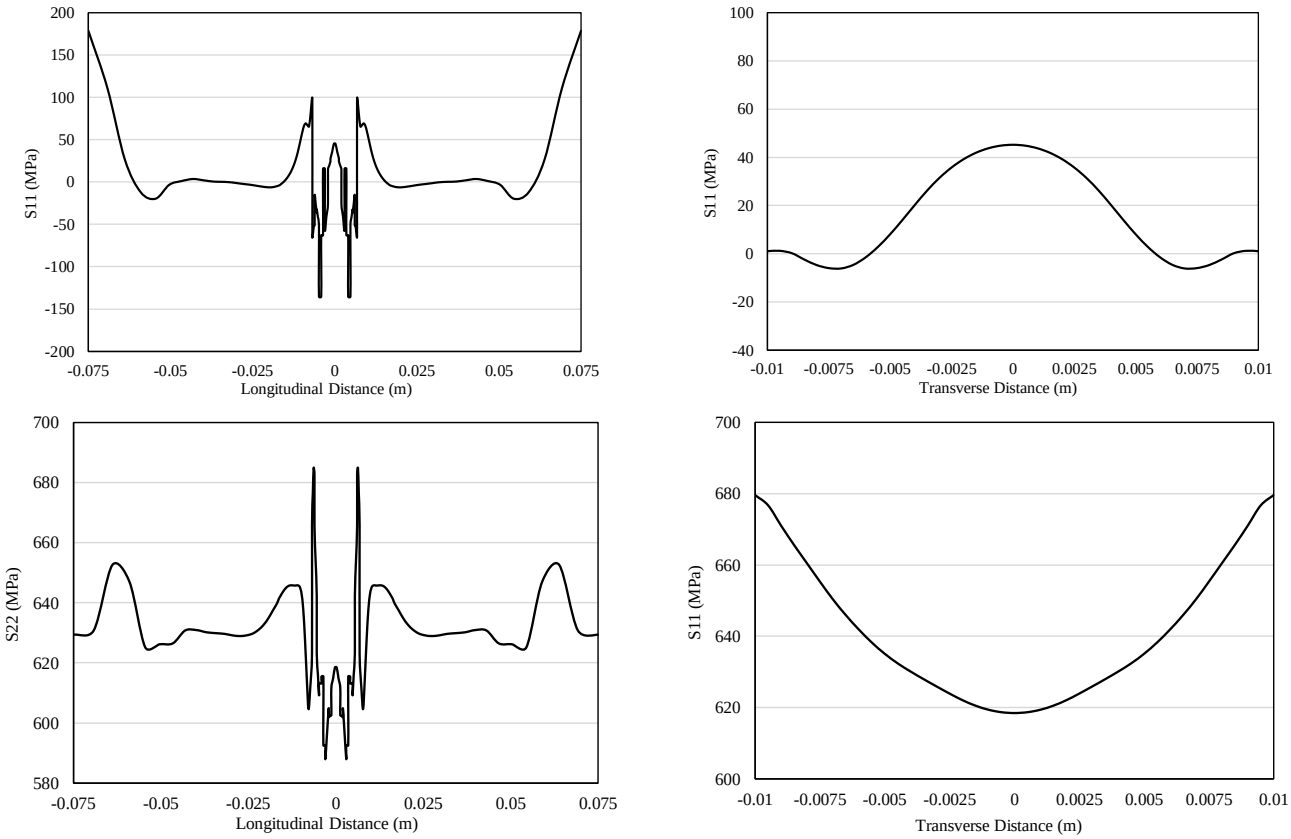

Figure 5-5. S11 and S22 stress distribution along the longitudinal distance (top left and bottom left), S11 and S22 stress distribution along the transverse path (top right and bottom right), applied stress = 630 MPa.

As seen in Figure 5-5, the values of S_{11} and S_{22} normal to the weld seam are fluctuating due to the variations in mechanical properties in different weld regions, resulting in different values of predicted fatigue life as compared to that of standard specimens. The variations in stress and strain values in the weld regions and along the different paths of the samples can simply be observed in stress and strain contours shown in Figure 5-6.

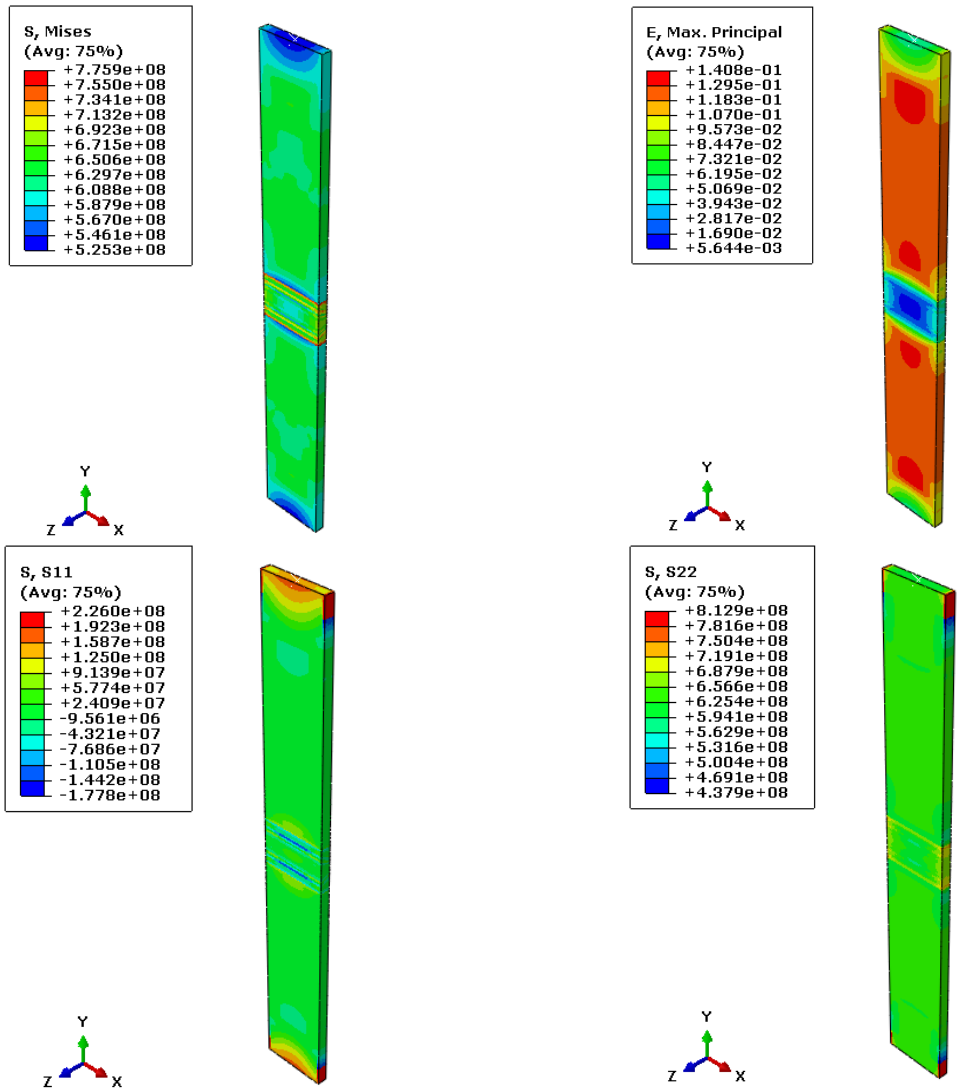

Figure 5-6. Von-Mises stress, maximum principal strain, and S11 and S22 stress contours of Inconel 600 welded samples

Figure 5-7 illustrates the critical regions near the weld seam prone to cracking and exhibiting the shortest fatigue lives. Each contour represents an area with similar fatigue

life, with the minimum fatigue life contour selected as representative for the sample. In the fatigue life prediction process, stress/strain values obtained from stress analysis are used alongside previously determined fatigue parameters. These values are then substituted into fatigue models, such as Morrow's fatigue damage model, to predict fatigue life accurately. Figure 5-8 shows the S-N curve obtained from the mentioned FE simulations and has been compared with those obtained from the experiments.

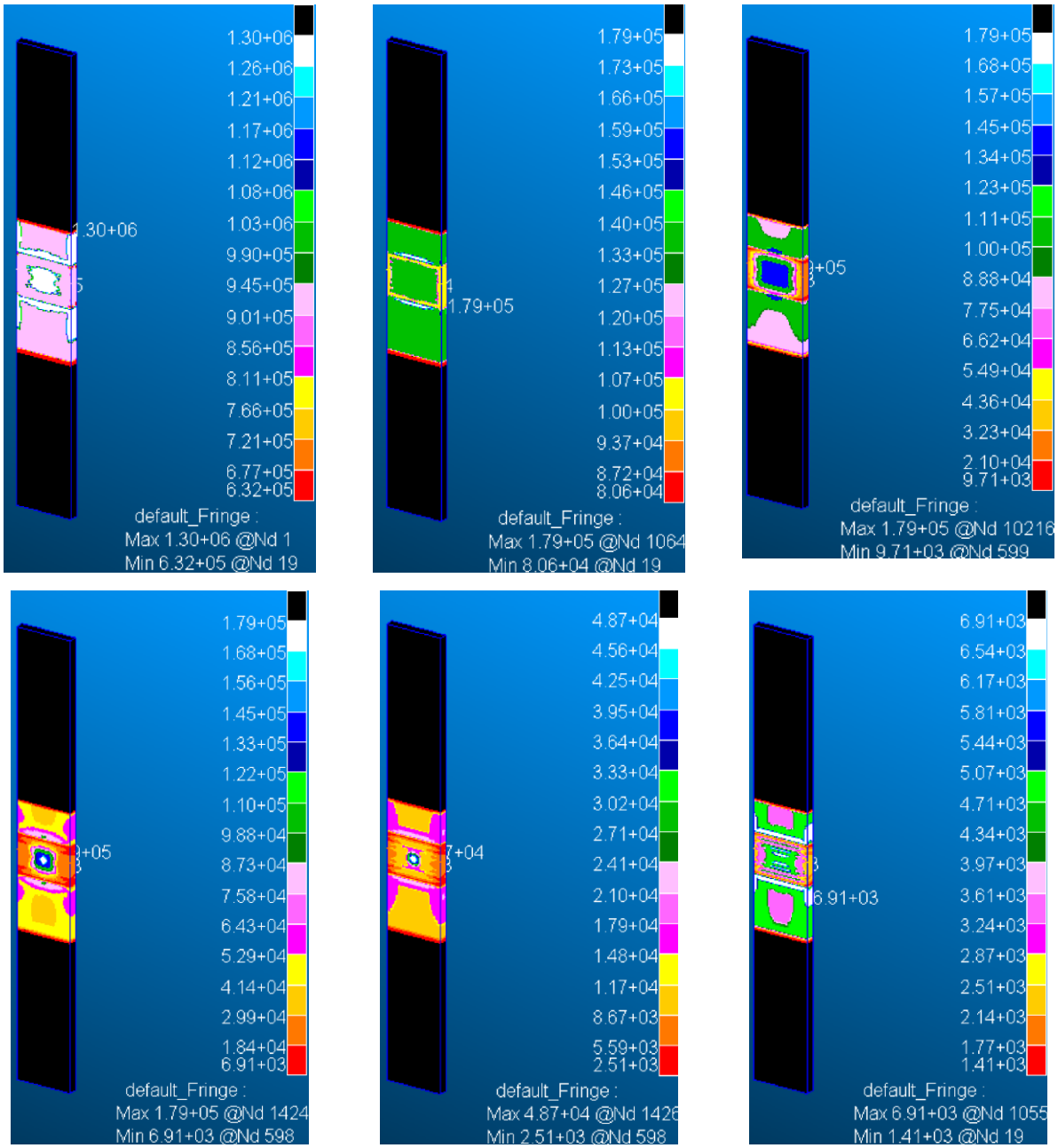

Figure 5-7. Fatigue life contours around the weld seam for the samples subjected to various load levels of (a) 330 MPa, (b) 380 MPa, (c)430 MPa, (d) 480 MPa, (e) 530 MPa, (f) 580 MPa.

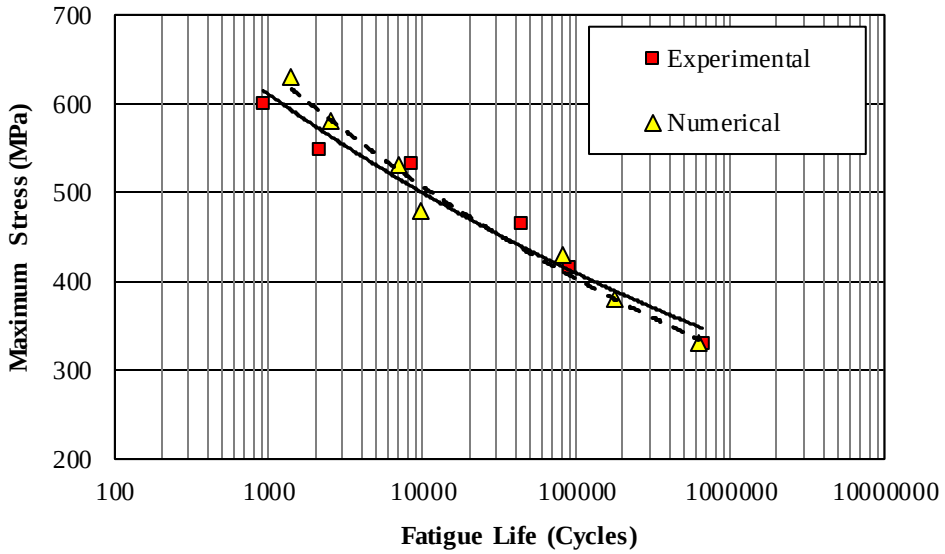

Figure 5-8. Comparison between the predicted fatigue life of the Inconel 600 welded samples with experimental fatigue test data

As seen in Figure 5-8, a very good agreement is observed between the predicted fatigue lives and experimentally obtained fatigue test data, indicating that the method upon which the mechanical properties and cyclic behavior has been assigned to the weld regions based on the changes in hardness values is an appropriate method for stress analysis and fatigue life predictions.

5.4. Fatigue Life of Inconel 600 Weldment with Single-Edge Notch

To assess the fatigue life of notched samples, first, the weldments with single-edge notch was simulated in ABAQUS software. Then, the mechanical properties of each distinct zone were assigned based on the relationship between the property and hardness distribution. The required stress and strain values shown in the forms of distributions (Figure 5-9) and contours (Figure 5-10) are used for fatigue life predictions. Figure 5-9 (a) also illustrates the longitudinal and transverse directions as well as the S11 and S22 stress components. The fatigue life contours indicate that the minimum fatigue lives occurred in the vicinity of the notch tips. The minimum values of fatigue cycles were plotted versus the applied remote stresses.

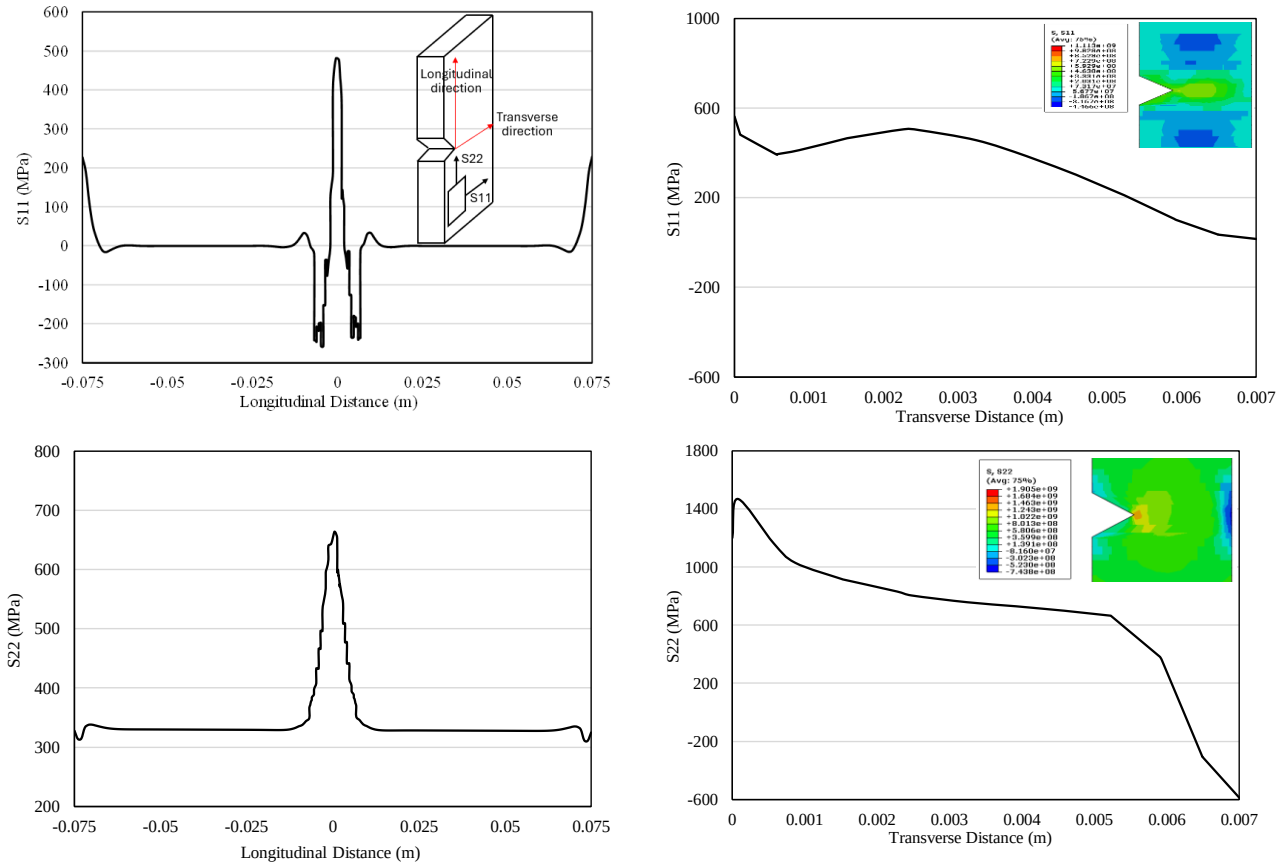

Figure 5-9. S11 and S22 stress distribution along the longitudinal distance (top left and bottom left), S11 and S22 stress distribution along the transverse path (top right and bottom right), applied stress = 630 MPa.

Single-edge notch and double-edge notch specimens were used to simulate the effect of damage and defects on the mechanical behavior and response of the specimens. These notch edges are characterized by high concentrations of residual stresses, which are critical for understanding the initiation and propagation of cracks. The FE simulations, as shown in Figures 5-9 and 5-10, revealed how these notches influenced stress distribution and strain concentration. This information helps in predicting the material's performance under realistic conditions and assessing its durability and reliability.

In Figure 5-11, the S-N curves obtained through Finite Element (FE) analysis for single-edge notch welded samples are compared with experimental data. The results show a close correlation, indicating the reliability of the FE analysis in predicting fatigue behavior.

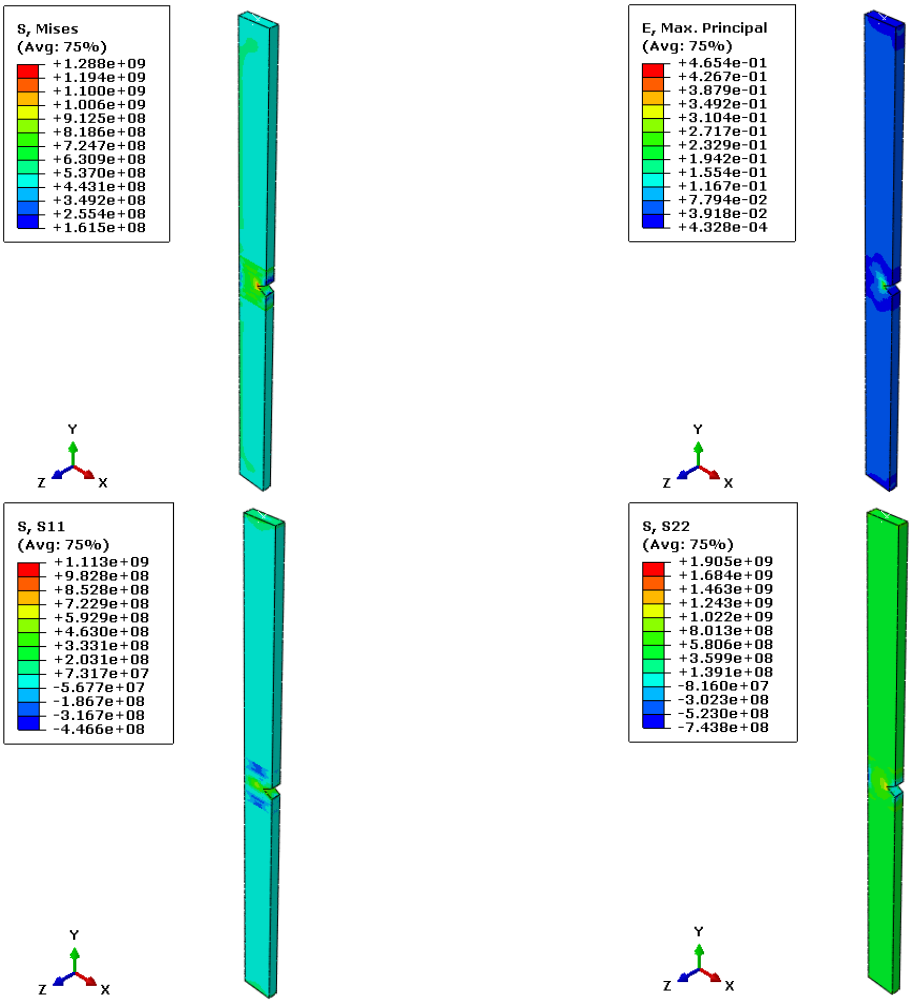

Figure 5-10. Von-Mises stress, maximum principal strain, and S11 and S22 stress contours of Inconel 600 single-edge notch welded samples.

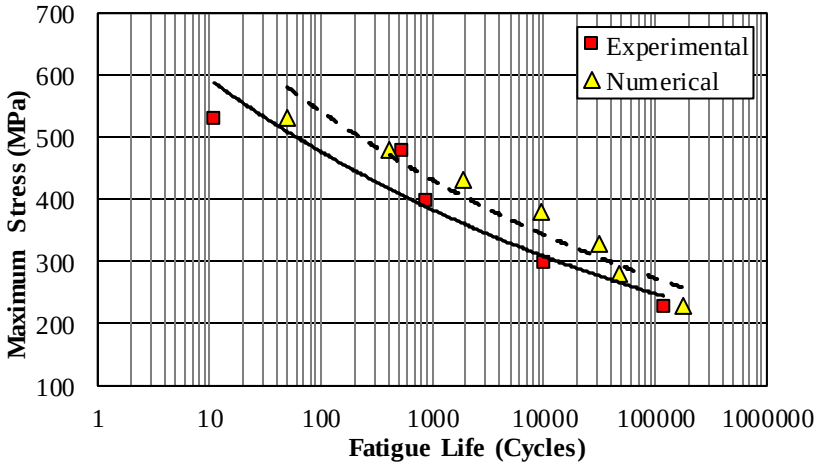

Figure 5-11. Comparison between the predicted fatigue life of the Inconel 600 single-edge notch welded samples with experimental fatigue test data.

A small discrepancy is observed between the FE results and experimental data. This discrepancy can be attributed to the fact that the FE analysis does not precisely consider the effects of the notch strength reduction factor. To address this limitation, alternative approaches can be considered. One such approach is the volumetric method based on the critical distance theory. This method takes into account the effects of the notch strength reduction factor in assessing fatigue life. By considering the critical distance from the notch tip, this approach provides a more accurate representation of the stress distribution and accounts for the notch's influence on fatigue performance. By incorporating the volumetric approach based on the critical distance theory, the FE analysis can be enhanced to provide more precise fatigue predictions for single-edge notch welded samples. This improved analysis will enable a better understanding of the fatigue behavior and help optimize the design and performance of welded structures.

5.5. Fatigue Life of Inconel 600 Weldment with Double-Edge Notch

The estimation process for the fatigue life of double-edge notch welded samples bears similarities to that of single-edge notch specimens. However, the key distinction lies in the stress and strain results due to the unique geometry, resulting in varying fatigue lives for each specimen. In Figures 5-12 to 5-14, we observe the stress and strain distributions, contours, and S-N curves, respectively, which provide useful information about the mechanical behavior of the double-edge notch welded samples.

Analyzing these data allows us to identify critical areas of localized stress concentrations and understand the relationship between applied stress amplitude and the number of cycles to failure under different conditions. These findings contribute significantly to optimizing the design and performance of welded structures, especially when double-edge notches are involved.

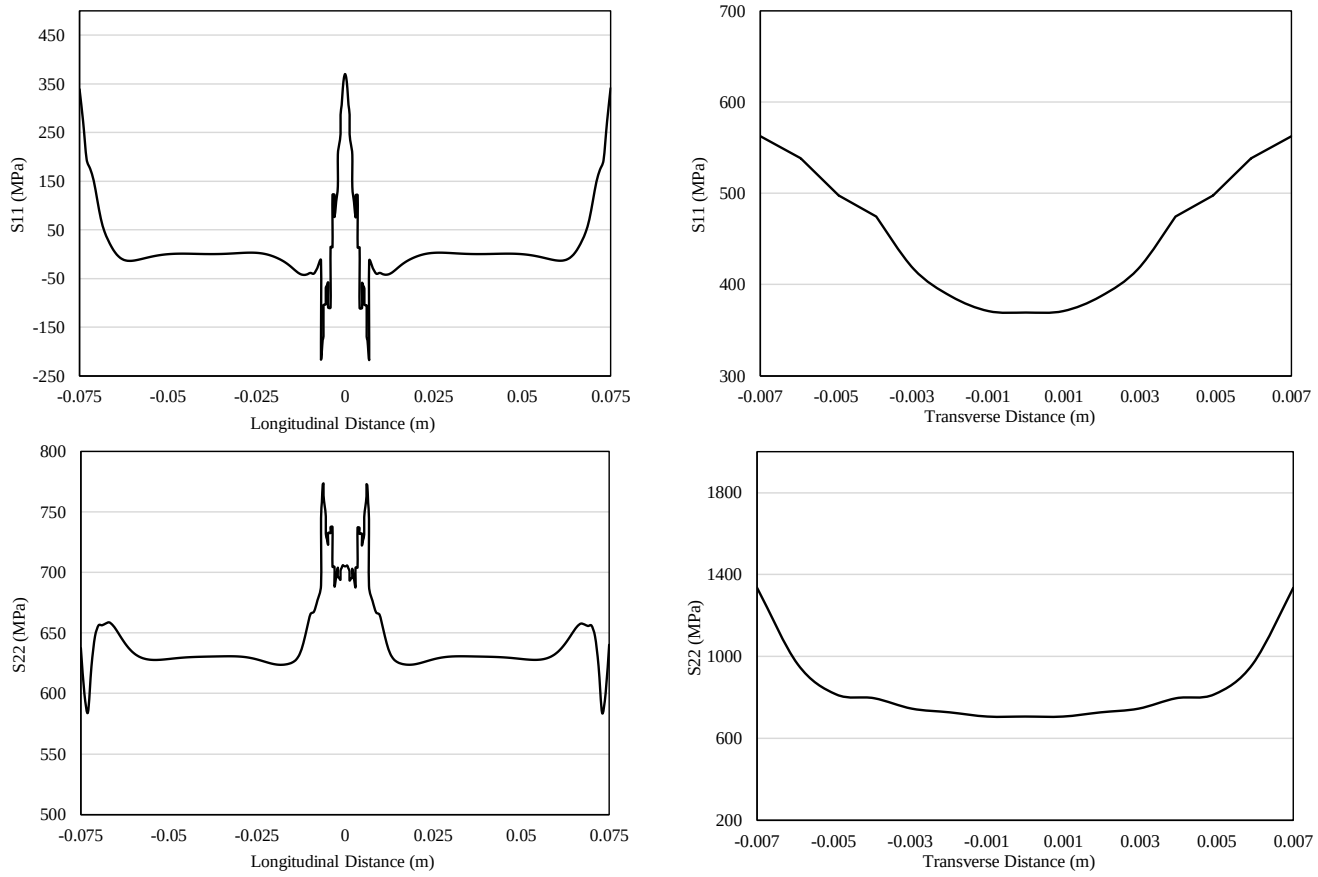

Figure 5-12. S11 and S22 stress distribution along the longitudinal distance (top left and bottom left), S11 and S22 stress distribution along the transverse path (top right and bottom right), applied stress = 630 MPa.

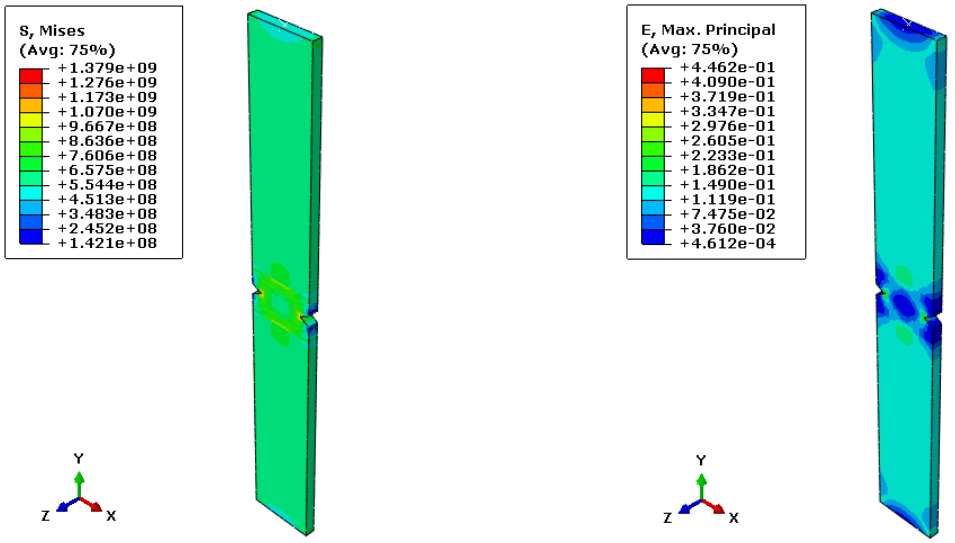

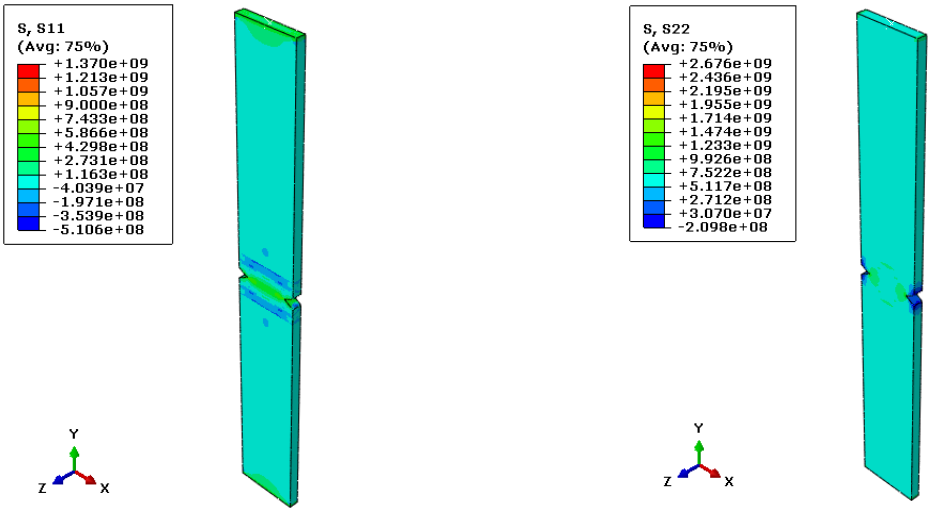

Figure 5-13. Von-Mises stress, maximum principal strain, and S11 and S22 stress contours of Inconel 600 double-edge notch welded samples.

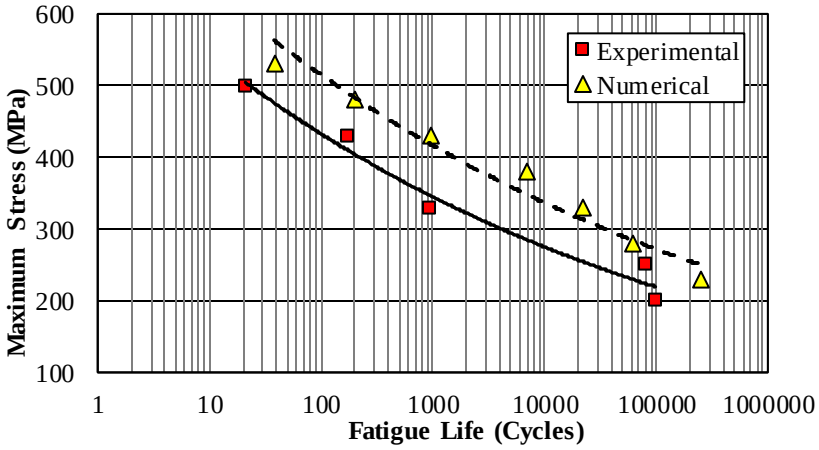

Figure 5-14. Comparison between the predicted fatigue life of the Inconel 600 double-edge notch welded samples with experimental fatigue test data.

As seen in Figure 5-14, the FE analysis over predicts the fatigue lives. This can be attributed to the fact that there are internal defects related to the welding process in the actual specimen that FE is unable to consider them. As mentioned earlier, the proposed method for fatigue life prediction only considers the effects of varying mechanical properties in the weld regions as well as the effects of notches. The influence of any metallurgy-related internal defects has been neglected.

5.6. Fractography of the Samples

In this section, fractography of the ruptured samples undergoing quasi-static and cyclic tests will be presented using SEM images. In tensile loading, the fracture surface of Inconel 600 typically exhibits a ductile appearance as shown in Figure 5-15. This is because the material undergoes plastic deformation before it finally fractures. The ductile appearance of the fracture surface indicates that the material was able to absorb a significant amount of energy before it ruptured. The fracture surface also contains features such as dimples and shear lips (Fig. 5-15(d)), which are indicative of the deformation mechanisms that occurred during fracture.

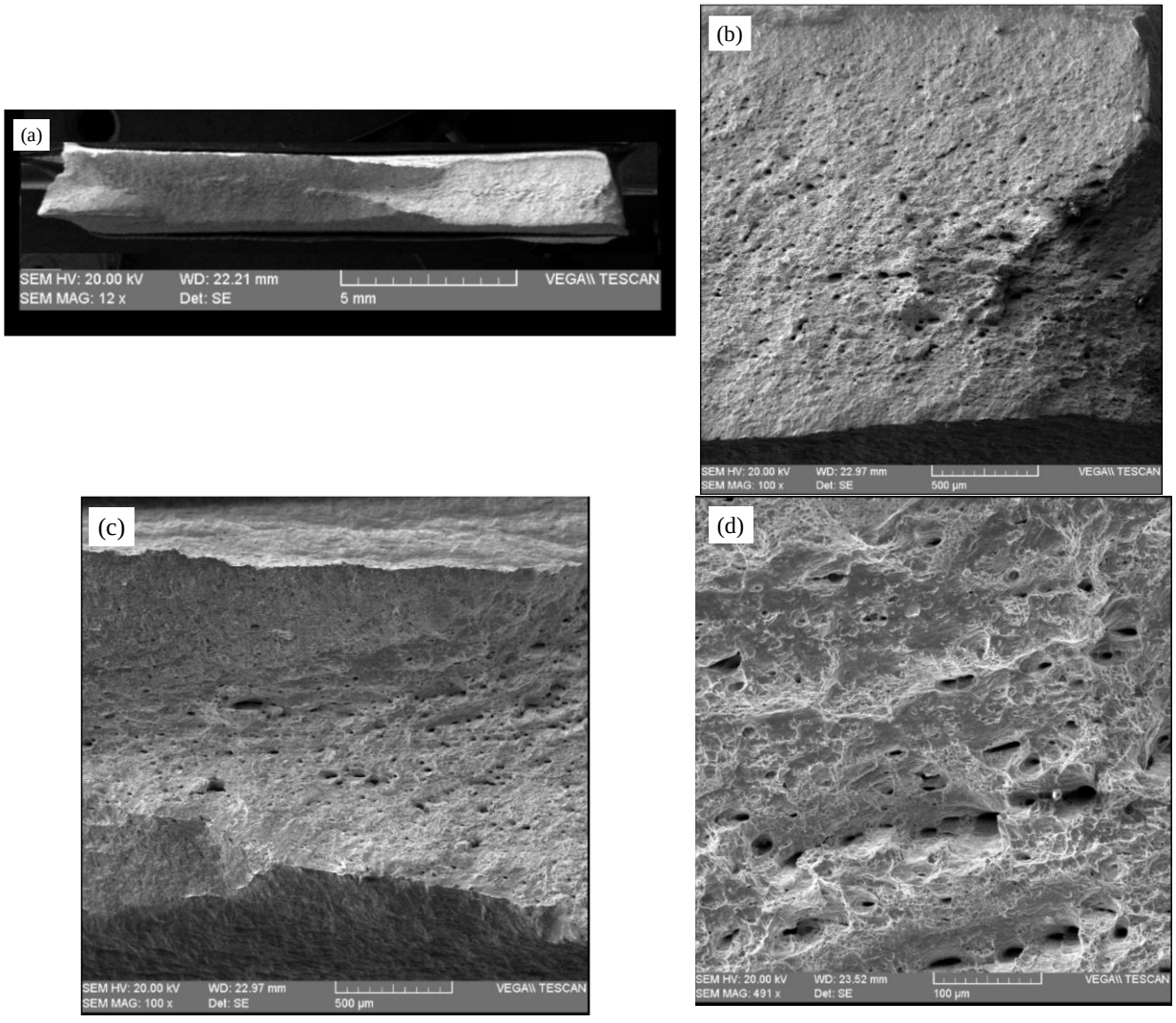

Figure 5-15. SEM images of the fracture surface of the Inconel 600 PM under tensile loading

In the case of weldments, the fractography of the ruptured samples can be influenced by the welding process and the properties of the parent material. The weldment exhibits a different microstructure compared to the parent material, which can affect its fracture behavior. For example, the heat-affected zone (HAZ) of the weldment may exhibit a different microstructure compared to the base metal, which can lead to a different fracture behavior. Figure 5-16 illustrates the SEM images of different regions of the fracture surface of the weldments undergoing static loading. The overall view of the fracture surface of the weld seam is illustrated in Figure 5-16(a). This image provides a broad perspective, showcasing the general morphology of the fracture. A more detailed examination is presented in Figure 5-16(b), which offers a zoomed-in view of the rough fracture surface. This closer inspection highlights the intricate features and characteristics of the fracture, such as the rough texture and irregularities. The presence of defects such as porosity and lack of fusion can also affect the fracture behavior of the weldment as shown in Figures 5-16(d) and 5-16(e).

In fatigue loading, the fracture surface of Inconel 600 exhibits a different appearance compared to tensile loading. Fatigue loading involves the repeated application of cyclic loading, which can lead to the initiation and propagation of cracks in the material. The fracture surface of the material exhibits a mixture of both ductile and brittle features, depending on the stage of crack propagation. As shown in Figure 5-17, the fracture surface shows beach marks, which are concentric ridges that form around the crack initiation site, as well as fatigue striations, which are fine lines that are perpendicular to the direction of crack growth.

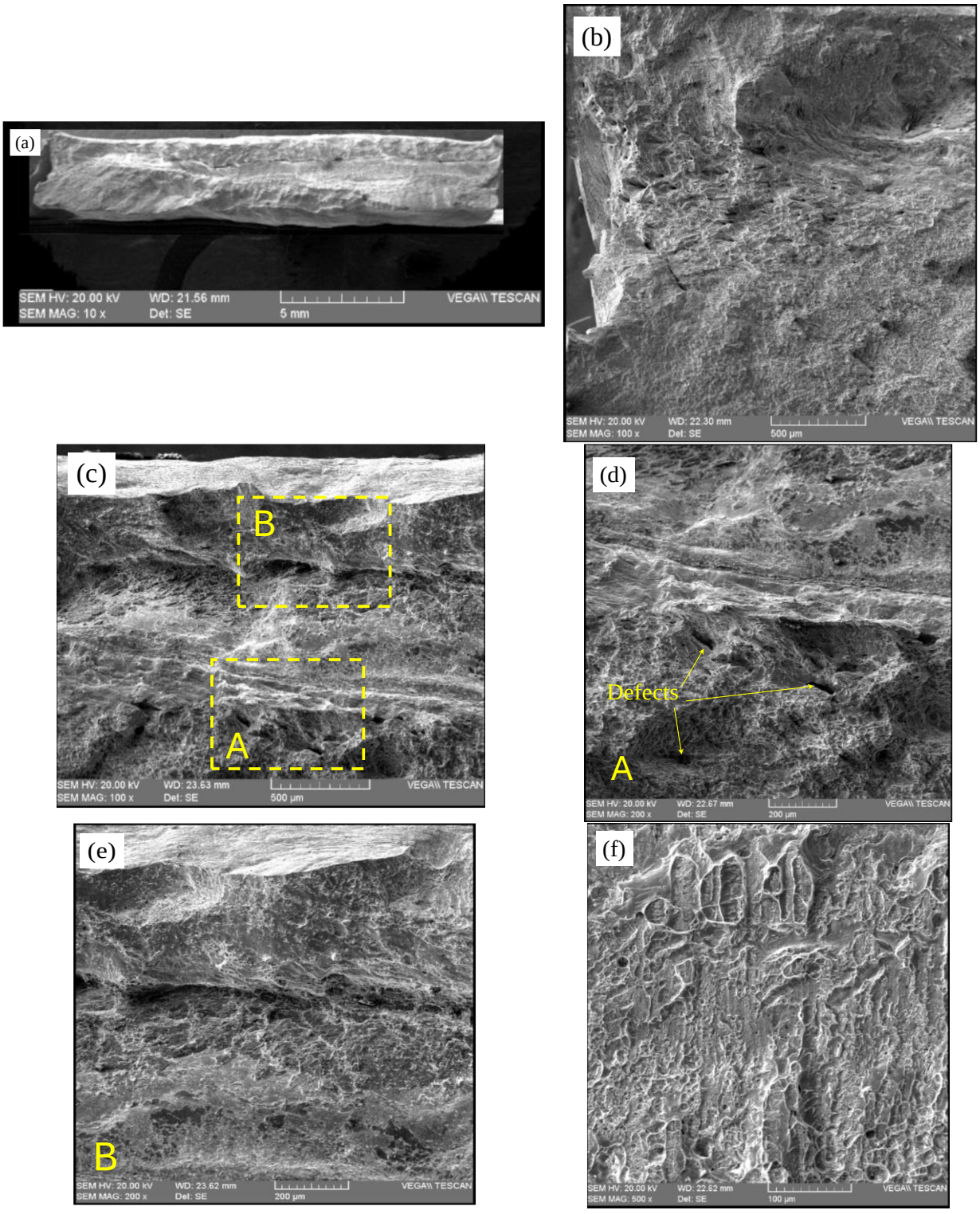

Figure 5-16. SEM images of the fracture surface of the weldment under tensile loading

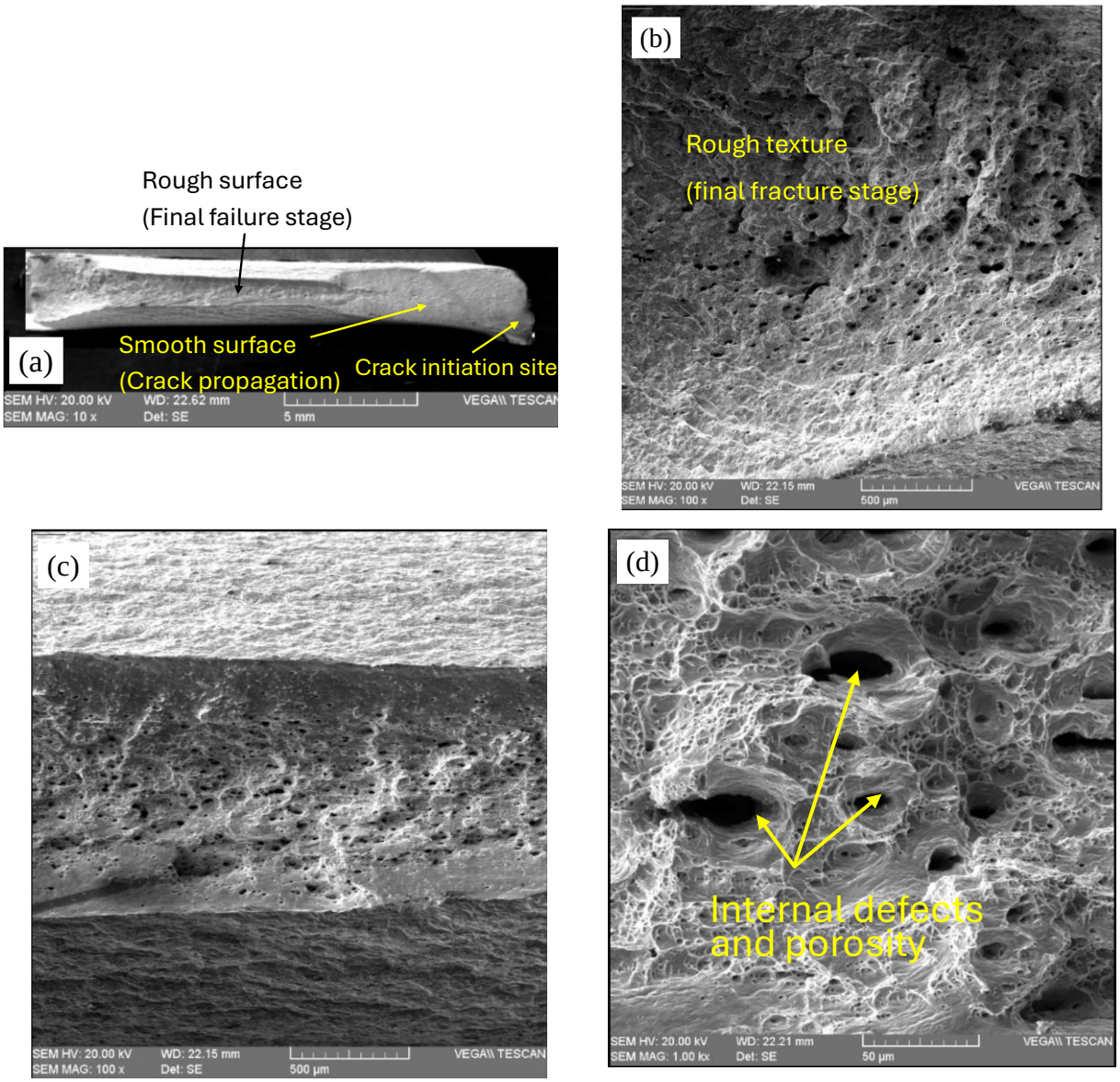

Figure 5-17. SEM images of the fracture surface of the Inconel 600 under cyclic loading

In the case of weldment (refer to Figure 5-18), the fractography of the ruptured surface under fatigue loading also shows a mix of ductile and brittle features, but with some differences compared to standard parent material. The microstructure of the weldment, particularly in the HAZ, can affect the fatigue behavior of the material. The HAZ exhibits a different microstructure compared to the base metal, which can lead to different fatigue crack initiation and propagation mechanisms. For example, the presence of brittle phases such as martensite or intermetallic compounds in the HAZ can lead to crack initiation and propagation along the grain boundaries, which can result in a brittle fracture surface.

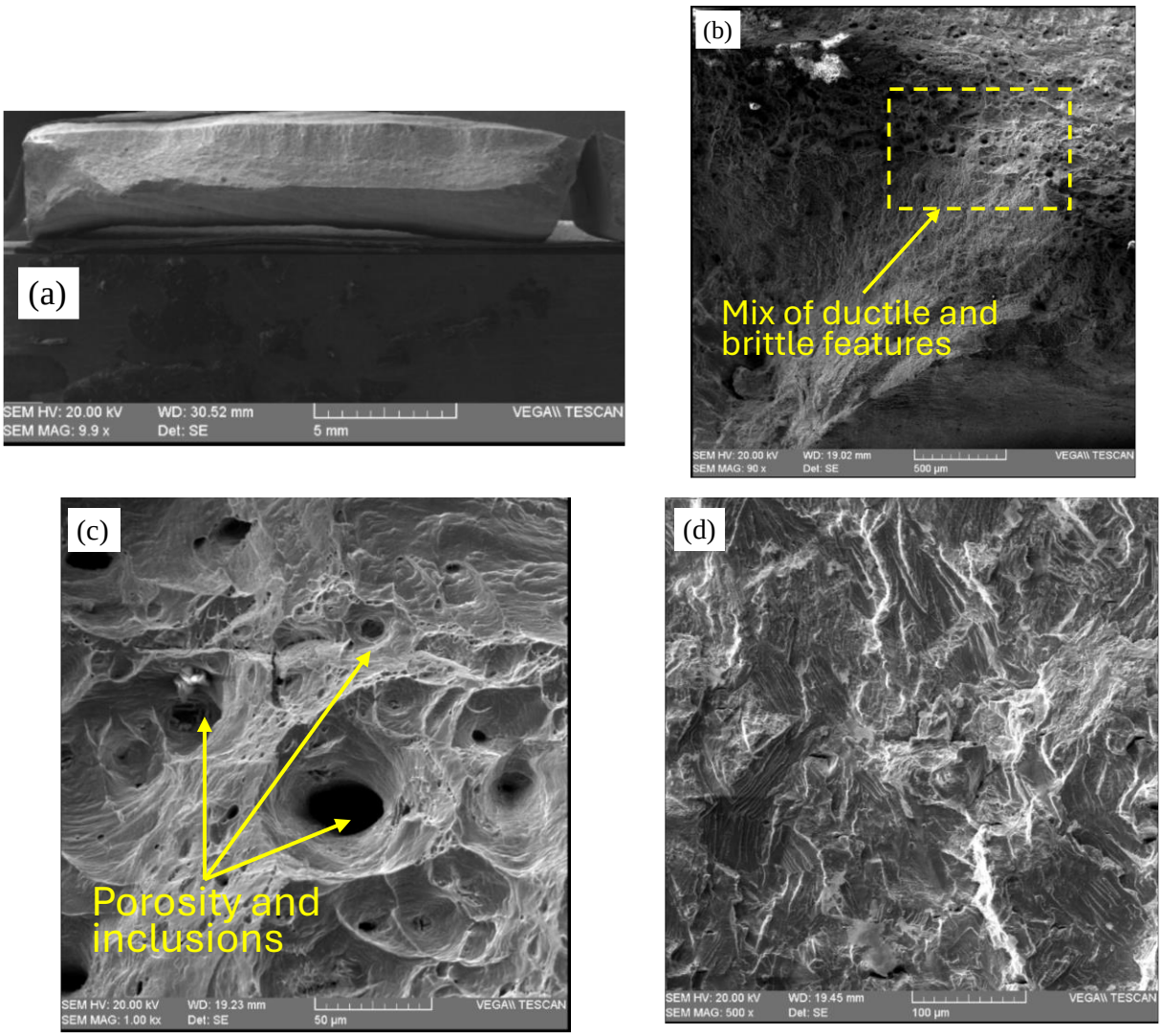

Figure 5-18. SEM images of the fracture surface of the weldment under cyclic loading

In addition to the differences in crack initiation and propagation mechanisms, the presence of defects in the weldment can also affect the fractography of the ruptured surface under fatigue loading. The presence of porosity, inclusions, or lack of fusion in the weldment can act as stress concentrators and lead to the initiation and propagation of fatigue cracks. The fractography of the ruptured surface in the presence of these defects exhibits different features compared to a defect-free weldment, such as multiple crack initiation sites, coalescence of cracks, or crack branching.

SEM images of the fractured surface in Inconel 600 weldment under fatigue loading can reveal the presence of different microstructural features compared to the base metal. In

addition to microstructural differences, the presence of defects in the Inconel 600 weldment can also influence the fractography of the ruptured surface under fatigue loading. SEM images of the fracture surface of Inconel 600 weldment under cyclic loading shown in Figure 5-18 illustrate the presence of multiple crack initiation sites due to the presence of inclusions or lack of fusion, as well as coalescence of cracks or branching of cracks, resulting in a fracture surface with more complex features.

In this section, FE simulations of Inconel 600 specimens subjected to various loading conditions were performed. The loading includes cyclic tension and torsion applied at different phases with a 10-degree increment. The loadings were considered to be completely reversed with tension from -480 MPa to 480 MPa, while cyclic torsion stress of 280 MPa was applied at different phase angles from 0º (in-phase) to 90º (out-of-phase) with 10º apart intervals. Hysteresis loops were then obtained from the sample under each loading condition. Figure 5-19 shows the hysteresis loops generated in complete loading-unloading combined tension and torsion at each phase angle.

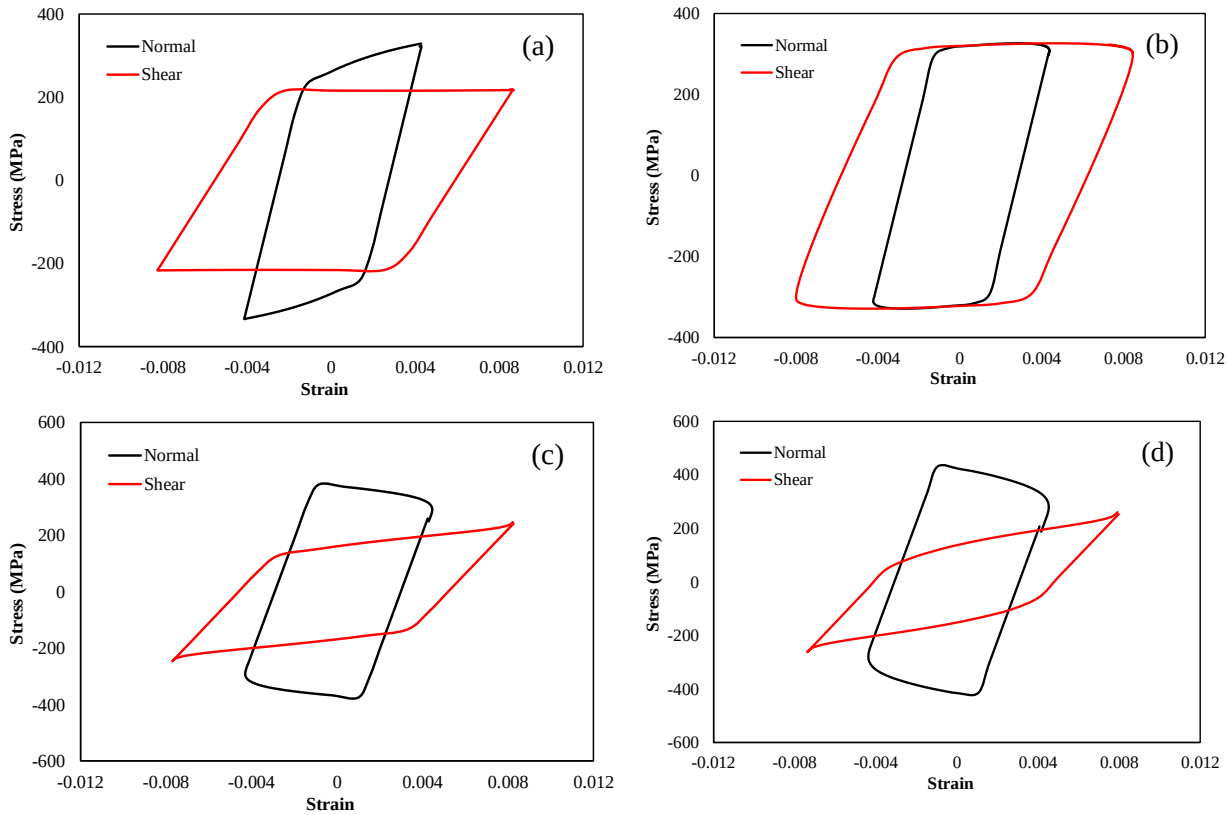

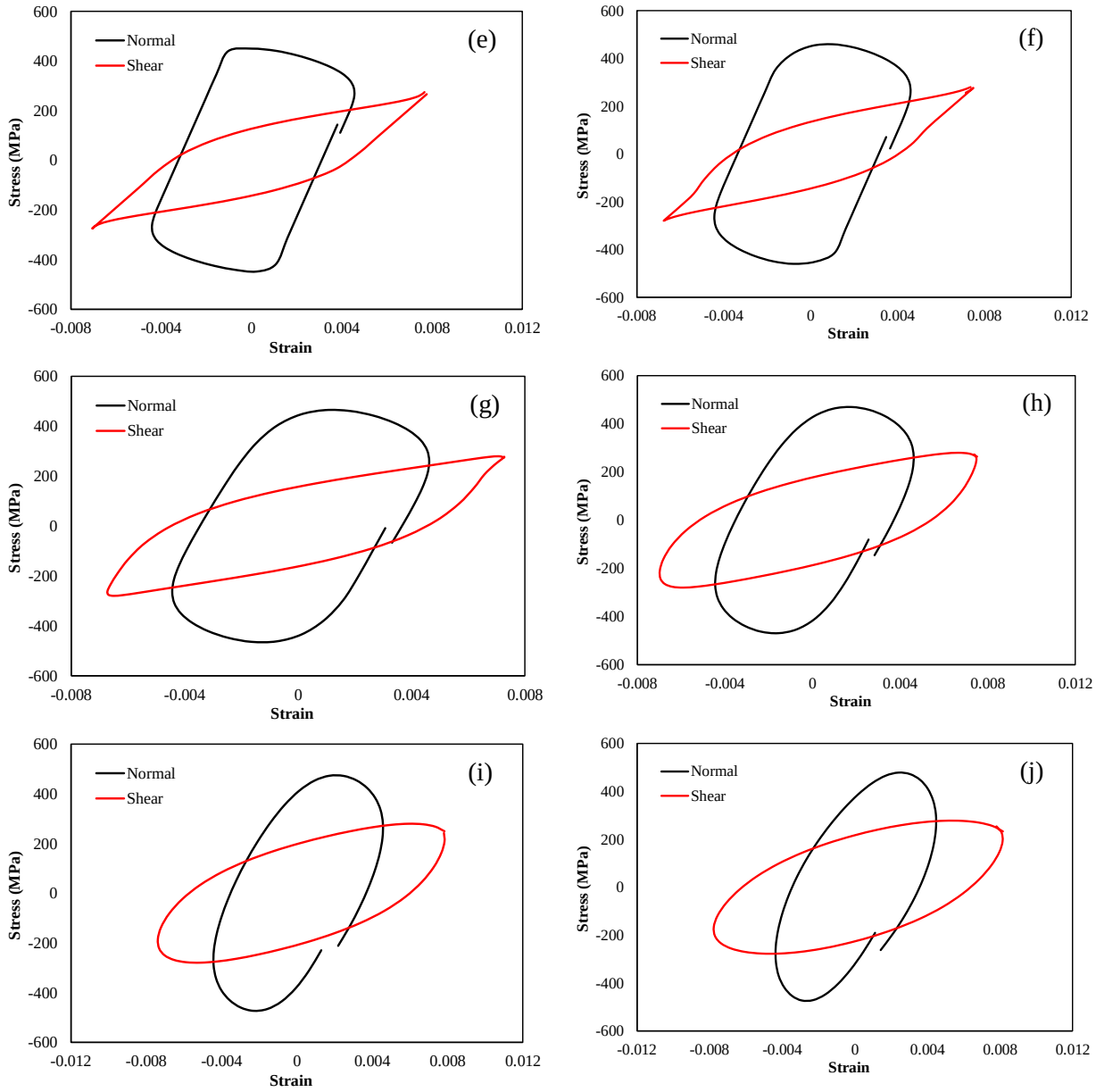

Figure 5-19. Hysteresis loops generated in complete loading-unloading combined tension and torsion at various phase angles, (a) in-phase, (b) 10º, (c) 20º, (d) 30º, (e) 40º, (f) 50º, (g) 60º, (h) 70º, (i) 80º, and (j) 90º.

The stress and strain contours at a 50º phase angle between tension and torsion loading are shown in Figure 5-20.

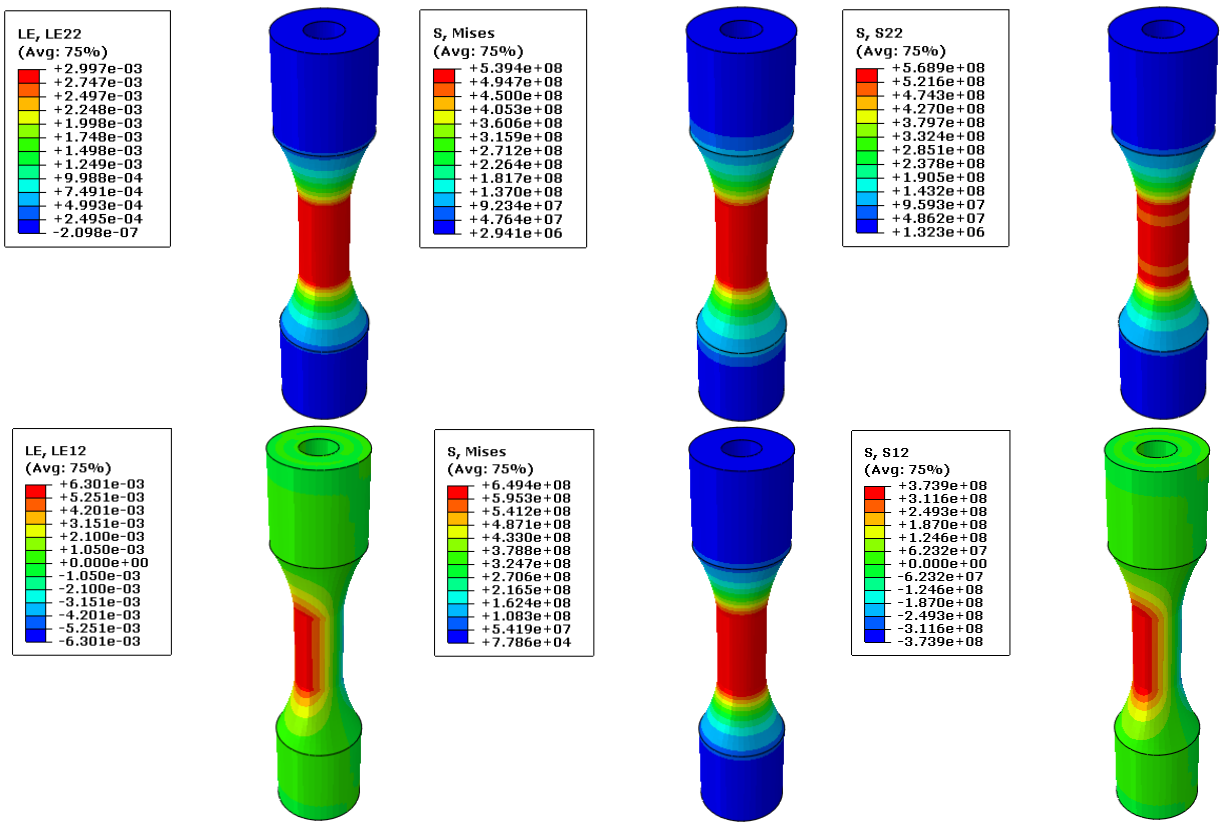

Figure 5-20. Stress and strain contours at a 50º phase angle between tension and torsion loading

Using the hysteresis loops, and the required parameters, different fatigue damage models were applied, including the FS approach, SWT approach, maximum stress, and maximum strain fatigue damage models. Each of these models uses a different critical plane approach to calculate the fatigue life of the material. The FE stress and strain results as input data are imported to MSC fatigue software to predict the fatigue lives based on the previously mentioned critical plane approaches. Figure 5-21 illustrates the predicted fatigue lives at all phase angles.

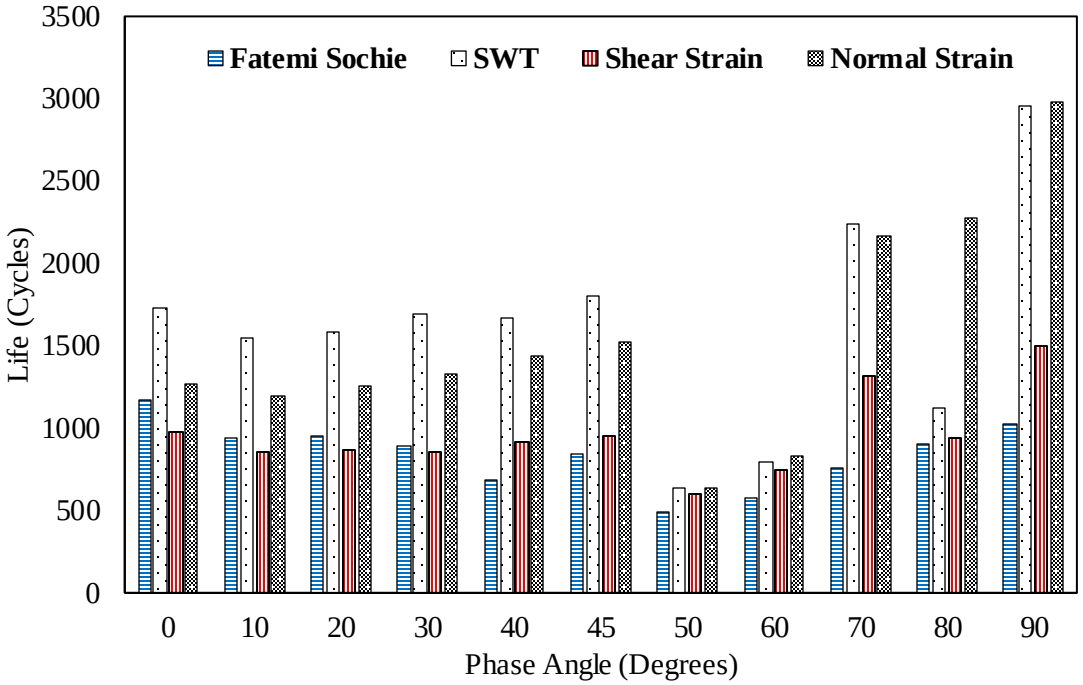

Figure 5-21. Comparison between the predicted fatigue lives obtained based on the critical plane approaches.

It was found that the fatigue life of the Inconel 600 sample was the lowest when subjected to a 50º out-of-phase loading condition. This indicates that the sample was most susceptible to fatigue failure under this loading condition, and the fatigue life of the sample would be the shortest when subjected to this particular loading condition.

The analysis began by obtaining stress-strain data through hysteresis loops, which depict the material's response to cyclic loading. Each critical plane approach calculates the fatigue life by identifying the plane within the material that experiences the maximum damage. The FE simulations provide detailed stress and strain distributions, which are then used in conjunction with the fatigue damage models to predict the lifespan of the material under different loading conditions.

The results show a significant variation in fatigue life depending on the phase angle of the applied load. Specifically, the 50º out-of-phase loading condition emerges as the most detrimental, causing the shortest fatigue life. This information is crucial for engineers and designers as it highlights the need for careful consideration of loading conditions in the design and analysis of components made from Inconel 600, particularly in applications

where cyclic loading is prevalent. Understanding these factors ensures that components are designed to endure the most challenging operational conditions, thereby enhancing their reliability and longevity.

5.7. Case Study: FE Analysis for Turbine Blade

5.7.1. Effects of Laser Shock Peening

Laser shock peening (LSP) is a surface treatment technique that uses high-intensity laser pulses to create shock waves on a material's surface [75, 86-90]. These shock waves induce compressive residual stresses [91-93], which can improve the material's fatigue life [94-96], wear resistance [97, 98], and corrosion resistance [99, 100]. LSP is widely used in various industries, including aerospace, automotive, and medical, to improve the performance of components [101, 102].

With regards to micro-turbines, LSP has emerged as a promising technique to enhance the durability and reliability of turbine blades made of Inconel 600, a high-temperature alloy with excellent mechanical properties. The blades of micro-turbines are subjected to high-speed and high-temperature conditions, which can cause fatigue cracks and other damage that compromise the turbine's performance. By applying LSP to the blades' surfaces, the compressive stresses generated by the shock waves can offset the tensile stresses generated by the operating conditions, thus reducing the risk of fatigue failure and increasing the blade's lifespan.

In this section, a combined heat and power micro-turbine underwent thermal and structural loadings, with a focus on the turbine blades. The resulting stress and temperature distributions are shown for the specified boundary conditions. Specifically, the study selected the KJ66 micro-turbine model for detailed analysis of static, fatigue, fracture, and creep behavior. To perform the analysis, the FE model of all turbine blades was imported into ABAQUS software, with one blade separated for further investigation. The simulated model of the turbine, one single blade, and its meshed model have been shown in Figure 5-22.

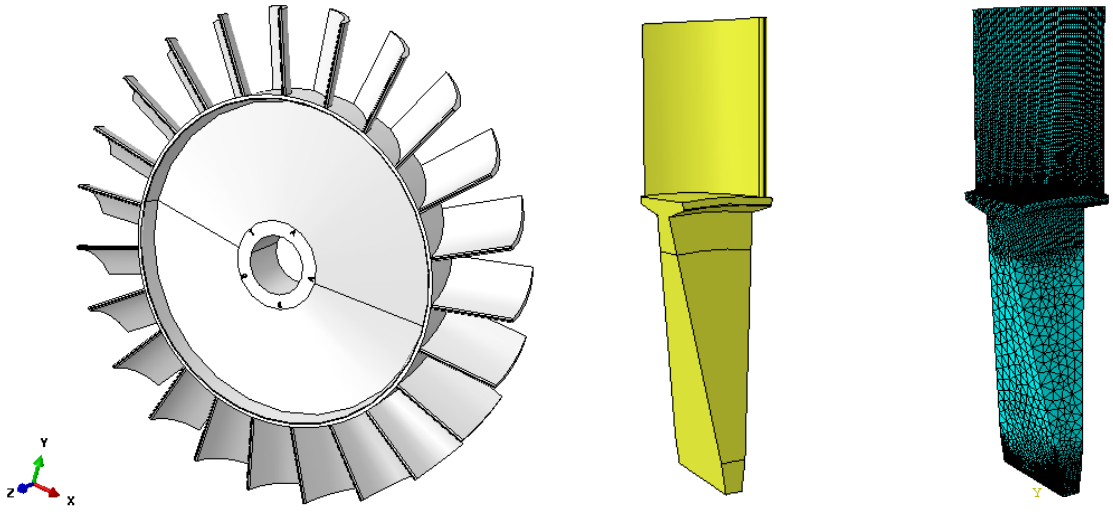

Figure 5-22. Geometry of the turbine, a single turbine blade, and meshed model of turbine blade

The following thermal and structural boundary conditions were applied to the turbine-blade structure and summarized in Table 5-1:

Table 5-1. Applied boundary conditions.

Blade temperature	1073℃
Shaft temperature	953℃
Blade pressure-front	130 kPa
Blade pressure-rear	100 kPa
Rotational speed	80000 rpm

The results of thermal analysis were imported to the structural analysis, and after applying the structural boundary conditions, the stress and strain fields were obtained in the turbine blade. Figures 5-23 to 5-25 illustrate the temperature distribution, von-Mises stress contour, and equivalent plastic strain contour in the blade respectively.

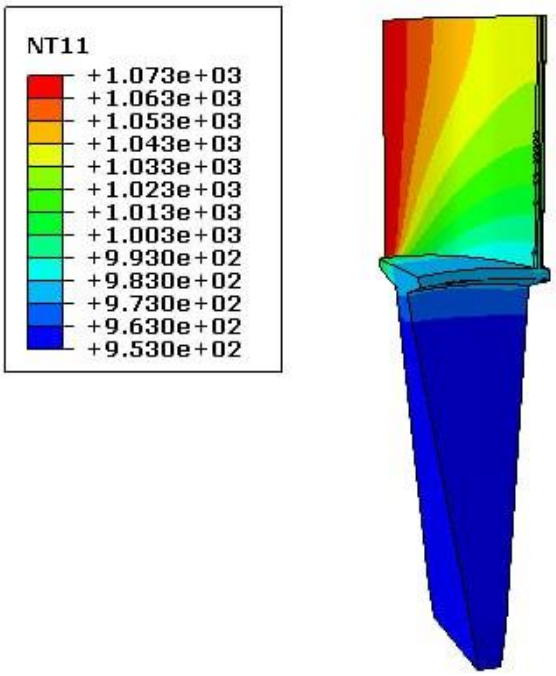

Figure 5-23. Temperature distribution in the turbine blade

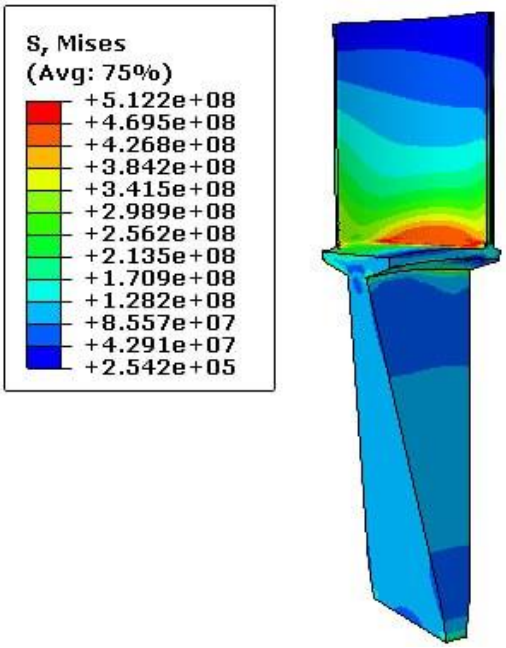

Figure 5-24. Von-Mises stress contour in the turbine blade

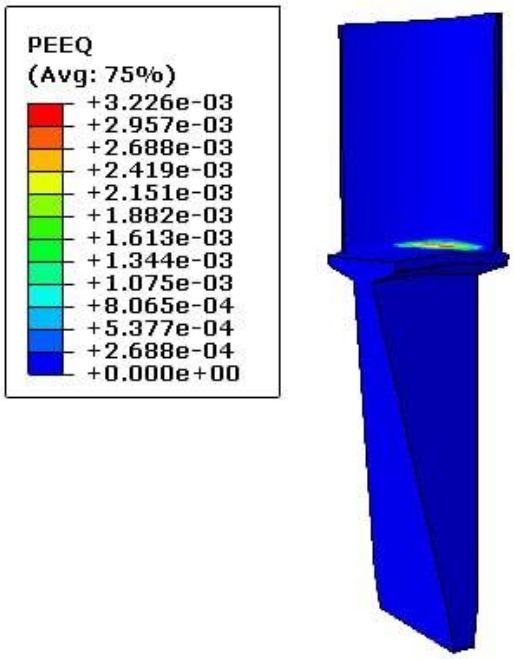

Figure 5-25. Equivalent plastic strain contour in the turbine blade

Figures 5-26 and 5-27 compares the von-Mises stress contours and fatigue lives of the blade with and without LSP operation, respectively. As seen, after applying LSP, the maximum value of von-Mises stress reduced significantly in the blade. It can also be observed that LSP enhanced fatigue life of the blade more than 10 times and shifted the critical area of the blade prone to cracking from the root to other regions of the blade.

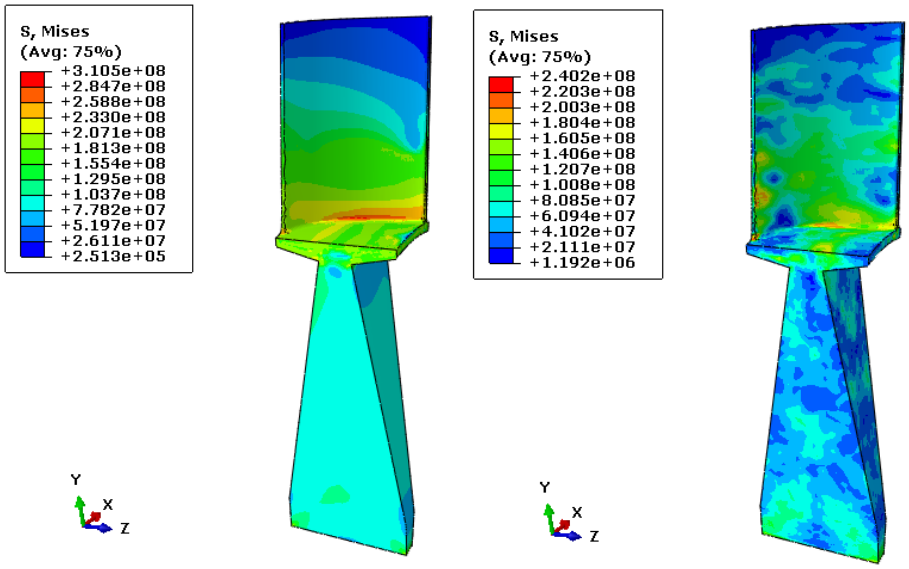

Figure 5-26. Von-Mises stress contours in the blade without LSP in the left, and with LSP in the right.

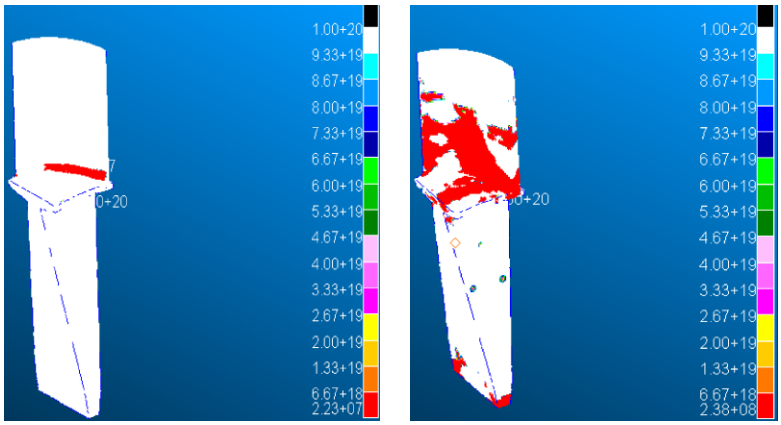

Figure 5-27. The contours of fatigue life in the blade without LSP in the left, and with LSP in the right.

In summary, LSP is a powerful surface treatment technique that has numerous applications in various industries, including micro-turbines. By inducing compressive residual stresses on the material's surface, LSP can improve the material's fatigue life, making it a valuable tool for enhancing the durability and reliability of critical components. In the case of Inconel 600 turbine blades, LSP can help mitigate the effects of high-speed and high-temperature operating conditions, thereby increasing the blade's lifespan and reducing maintenance costs. Supporting this, studies on surface treatments like severe shot peening and laser shock peening on Inconel 718 showed that proper parameters and increased kinetic energy can significantly enhance mechanical properties and fatigue behavior. This underscores the importance of these surface treatments in promoting surface grain refinement and inducing deep compressive residual stress fields for improved material performance and longevity [96].

5.8. Fatigue Crack Growth: Mixed Mode Fracture

Fatigue crack growth is a critical phenomenon that occurs in materials subjected to cyclic loading. It is a prevalent cause of failure in engineering structures and components. Fatigue cracks typically initiate at stress concentrations, such as notches or defects, and propagate gradually under repeated loading, leading to catastrophic failure. The study of fatigue crack growth has been extensively investigated under various loading conditions [103, 104]. One particular and important loading scenario is known as mixed mode condition [105-107]. In mixed mode, the crack experiences a combination of both tensile

and shear stresses, unlike traditional uniaxial loading where the stress state is primarily tensile. The presence of shear stresses in addition to tensile stresses creates a complex stress field around the crack tip, influencing the crack growth behavior. In engineering applications, mixed mode loading is common, and understanding the crack growth under such conditions is crucial for ensuring structural integrity and safety.

The behavior of a crack under mixed mode loading differs significantly from that under pure mode I (tensile) or mode II (shear) loading. The interaction between the two modes affects the crack propagation rate and direction, making it more challenging to predict the crack growth accurately.

Researchers and engineers have developed various experimental and numerical techniques to study fatigue crack growth at mixed mode conditions [108, 109]. These methods involve creating controlled crack configurations and subjecting them to cyclic loading with a combination of tensile and shear components. The resulting crack growth data are analyzed to determine the crack growth rates and paths, providing valuable information into the material's resistance to mixed mode loading.

Understanding the behavior of fatigue crack growth at mixed mode condition enables the development of more accurate fatigue life prediction models, which are essential for designing reliable and safe engineering structures. Additionally, it helps identify critical areas prone to mixed mode loading, facilitating targeted inspection and maintenance practices to prevent catastrophic failures.

To investigate the fatigue crack growth (FCG) behavior of Inconel 600, a custom-made fixture similar to an Arcan fixture [110-112] was utilized, as depicted in Figure 5-28.

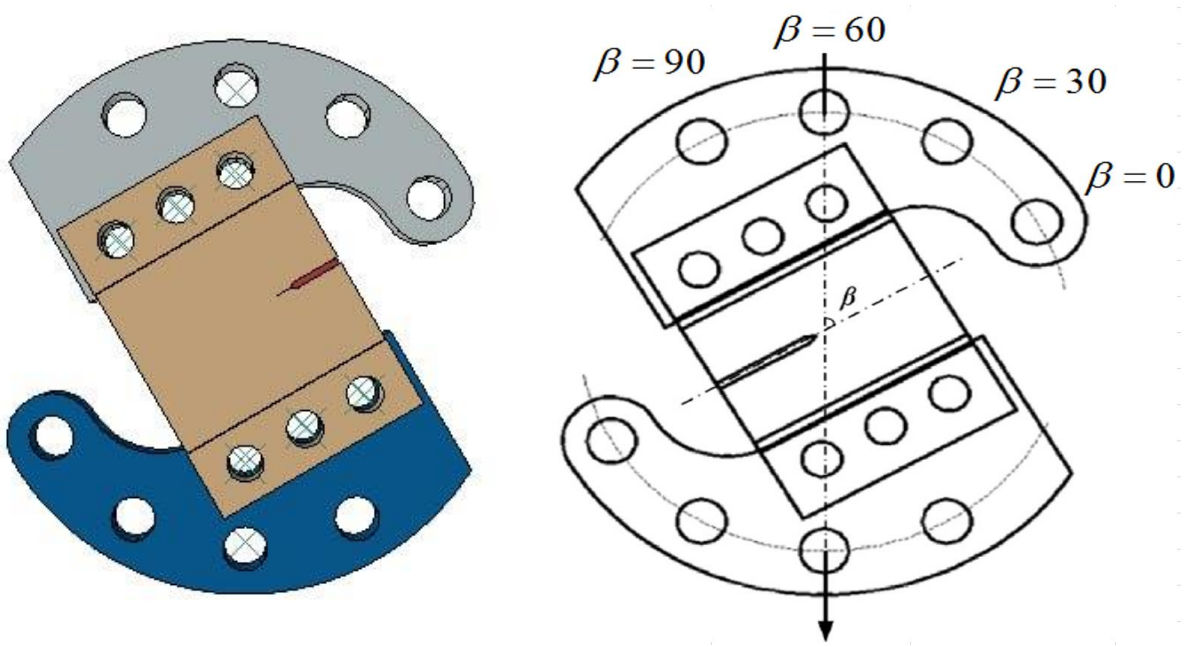

Figure 5-28. Fixture used in FCG mixed mode loading in FEA analysis

The study involved selecting four different conditions to induce mixed modes of loading: 0 degrees (pure mode I), 30 degrees, 60 degrees, and 90 degrees (pure mode II). The samples were then subjected to zero-to-maximum stress cyclic loading.

The obtained results are presented in Figures 5-29 to 5-32, illustrating the crack paths under different loading conditions. Additionally, Figure 5-33 displays the crack propagation versus the number of applied cycles until final failure. As observed, the sample under pure mode I condition exhibited the longest fatigue life before rupture, indicating its higher resistance to crack propagation. Conversely, the sample subjected to pure mode II loading demonstrated the least fatigue life before reaching failure.

These findings shed light on the material's susceptibility to fatigue crack growth under varying loading conditions and highlight the significance of mode mixity in influencing the FCG behavior of Inconel 600. The study's outcomes provide useful information about optimizing design strategies and enhancing the durability of components made from this alloy, particularly in scenarios where mixed-mode loading conditions are encountered.

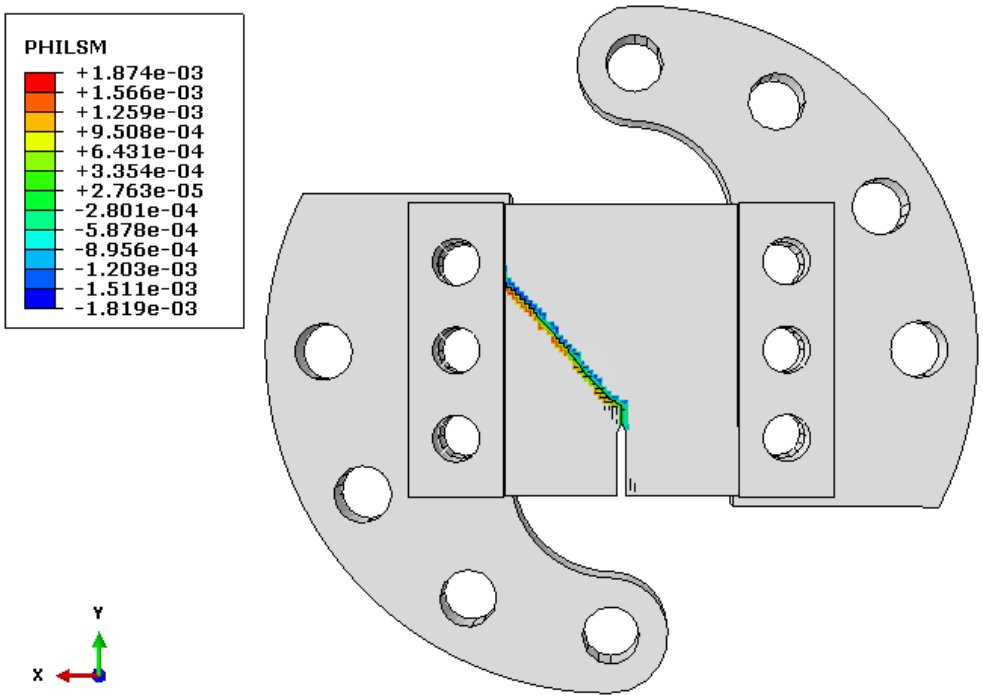

Figure 5-29. Crack path under pure mode I (0 Degree) condition

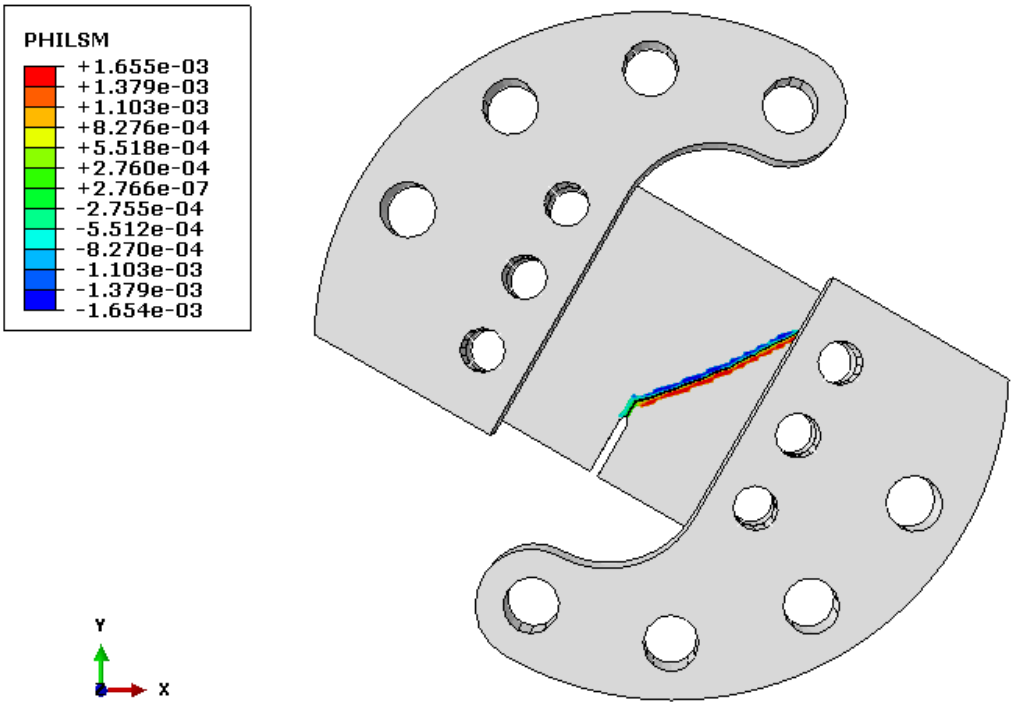

Figure 5-30. Crack path under mixed mode I and II (30 Degree) condition

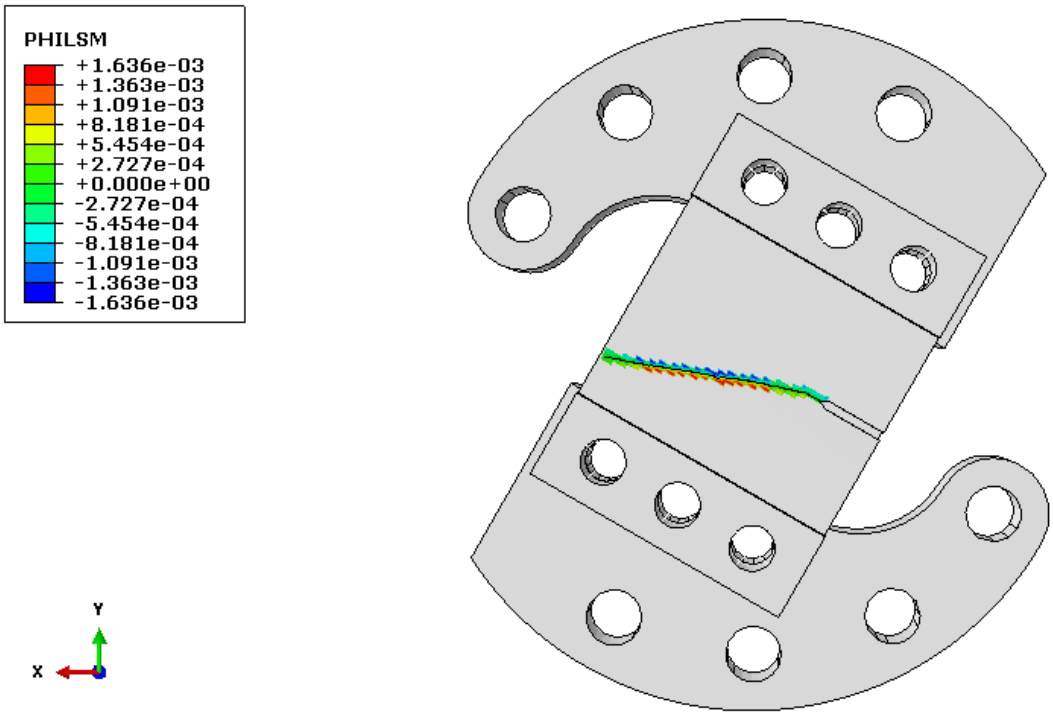

Figure 5-31. Crack path under mixed mode I and II (60 Degree) condition

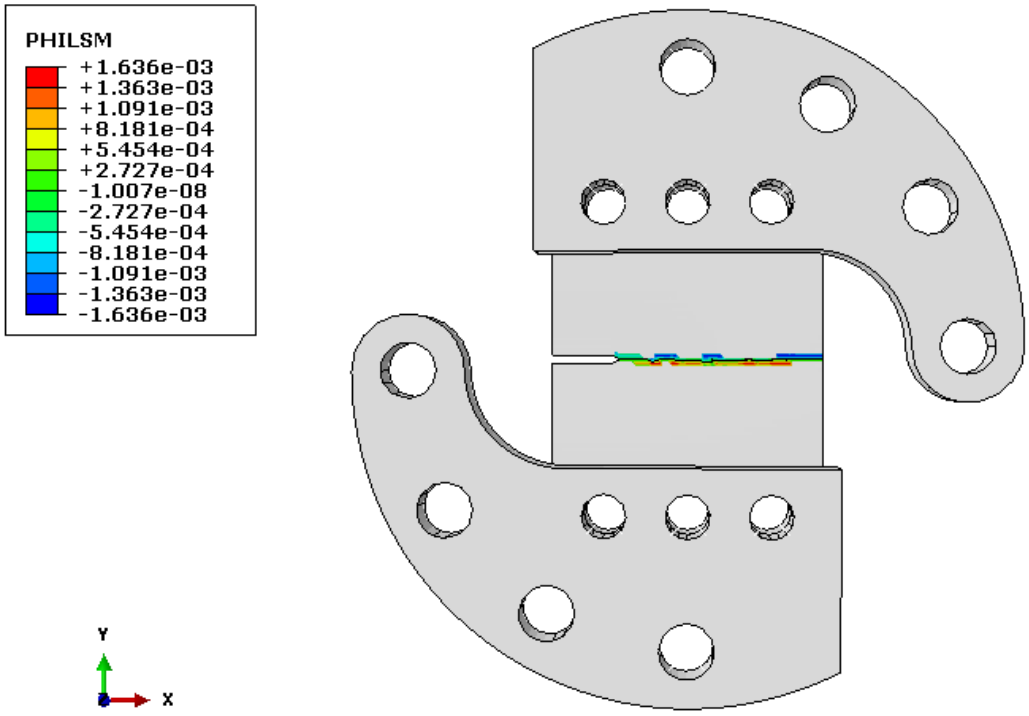

Figure 5-32. Crack path under pure mode II (90 Degree) condition

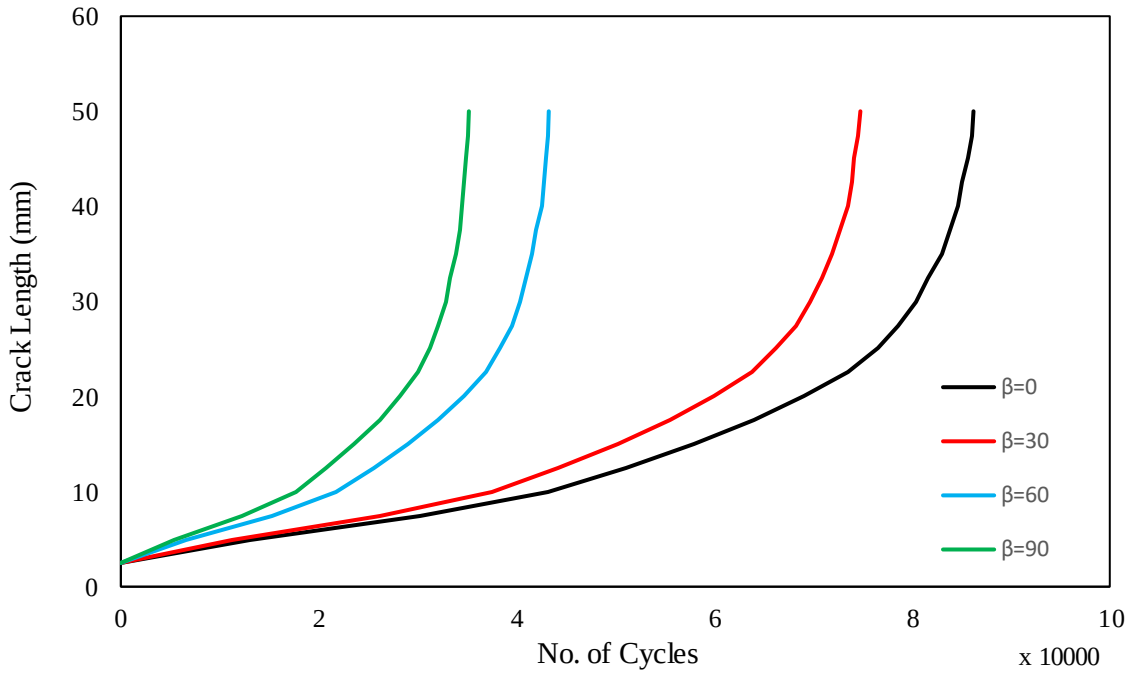

Figure 5-33. Crack propagation versus the number of applied cycles until final failure

5.9. Creep Response of Inconel 600 Un-notched and Notched Welded Samples

One essential aspect of characterizing creep is the development of creep constitutive equations, which describe the relationship between the applied stress, time, and the resulting strain. The process of obtaining creep constitutive equations is to determine the constitutive parameters that best fit experimental data using numerical optimization methods such as using least square method, and minimizing error:

$$Error = [\sum_{i=1}^{n}(\dot{\varepsilon_{exp}} - A\sigma^{n}\exp(-Q/RT))^{2}]^{1/2} \quad (5\text{-}3)$$

Figure 5-34 compares the experimentally obtained creep strain for un-notched samples with those obtained via FEA analysis. As seen in Figure 5-34, a relatively good agreement can be observed between the results.

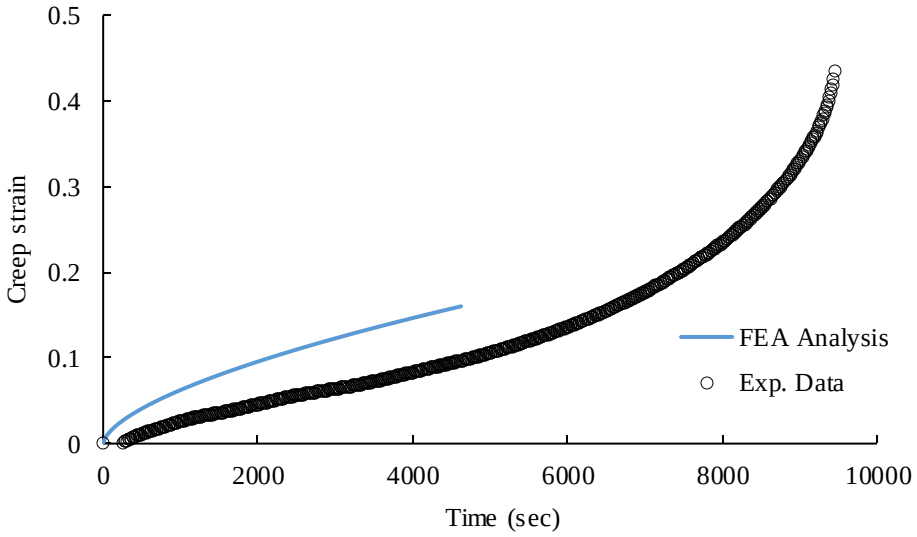

Figure 5-34. Comparison between creep strain obtained through FEA analysis and experimental data

Creep strains were obtained using ABAQUS software for un-notched and notched samples (single-edge and double-sided edge notches) at 250, 300, 350, and 400 MPa, respectively. Figures 5-35 to 5-37 illustrate the creep strain versus time for respectively un-notched, single-edge, and double-edge notched samples.

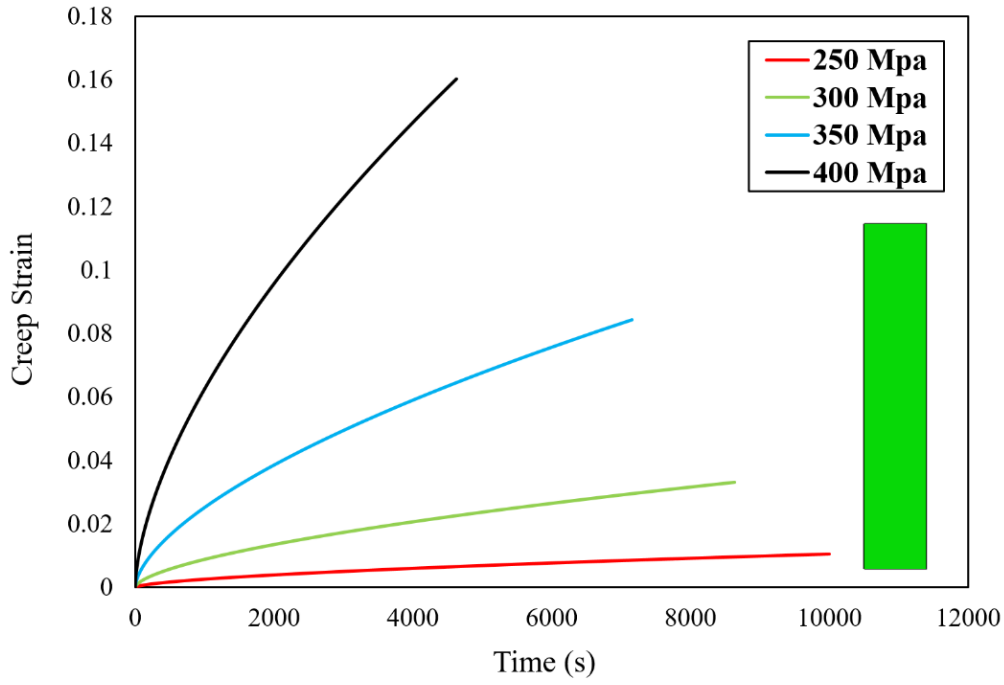

Figure 5-35. Creep strain versus time for un-notched sample

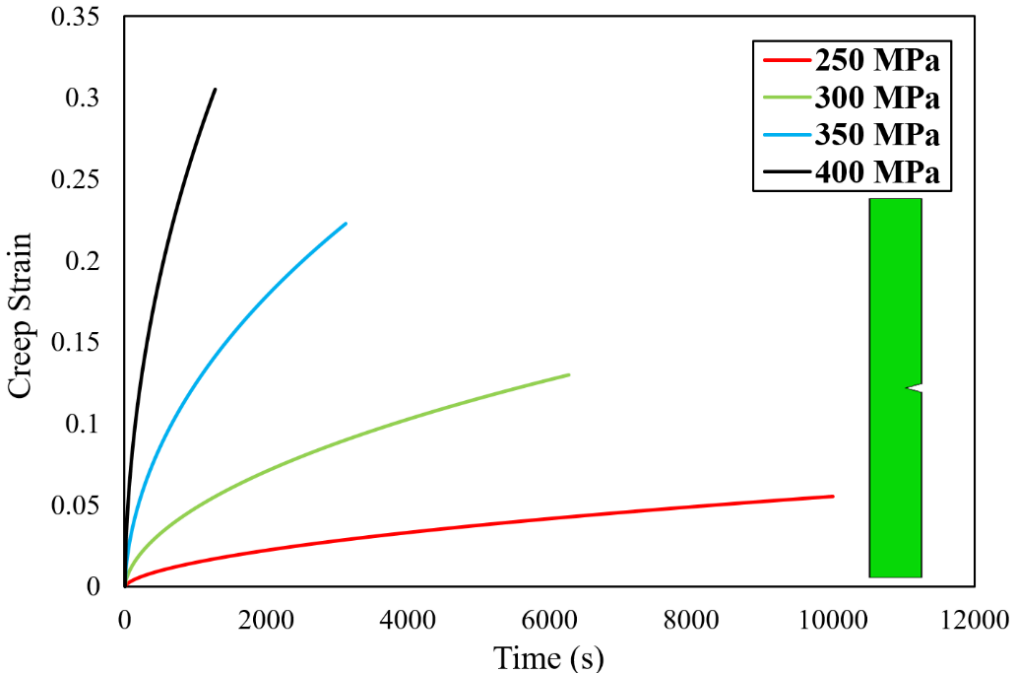

Figure 5-36. Creep strain versus time for single-edge notched sample

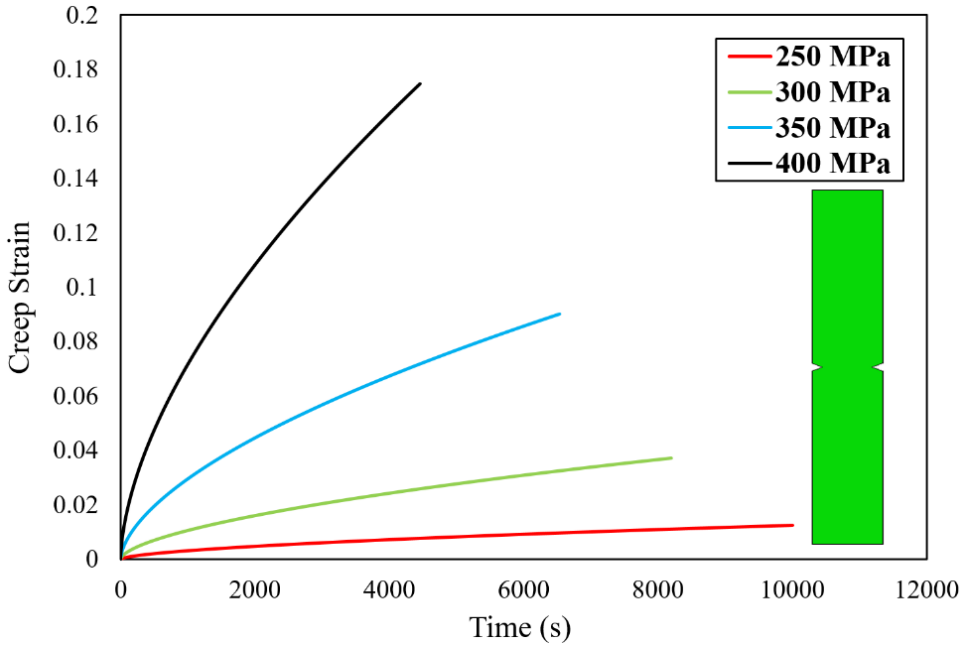

Figure 5-37. Creep strain versus time for double-edge notched sample

As seen in Figures 5-35 to 5-37, smooth samples under all applied stresses possessed the highest creep lives, while single-edge notched samples showed the least creep lives at all stress levels.

In Figures 5-38 and 5-39, the SEM images of Inconel 600 smooth (un-welded) and welded samples fractured under a creep environment at 650 ℃ and 400 MPa stress are presented. The analysis of SEM images revealed that the un-welded samples exhibited more pronounced necking compared to the welded samples. Necking is a localized deformation process that occurs before fracture and results in a reduction of the cross-sectional area in the material. The higher degree of necking in the un-welded samples indicates enhanced plastic deformation and ductility during the creep process. While both samples showed some degree of intergranular failure, it was more prominent in the welded samples. The presence of welding can introduce additional stress concentration points, which may lead to preferential crack initiation and propagation along grain boundaries.

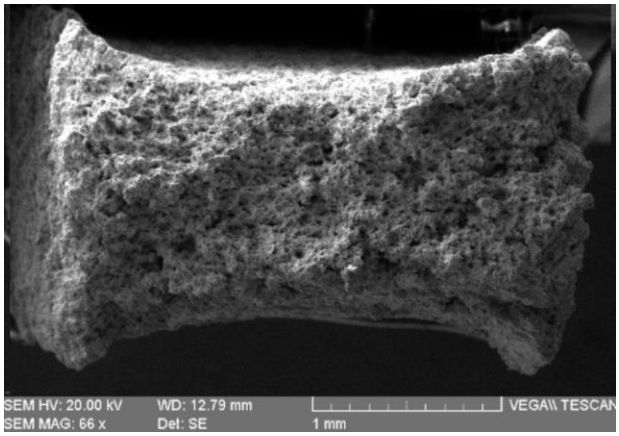

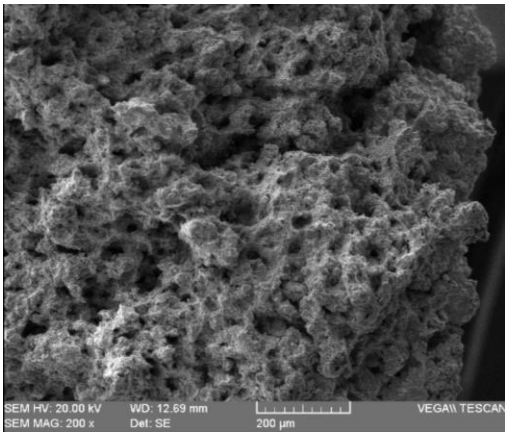

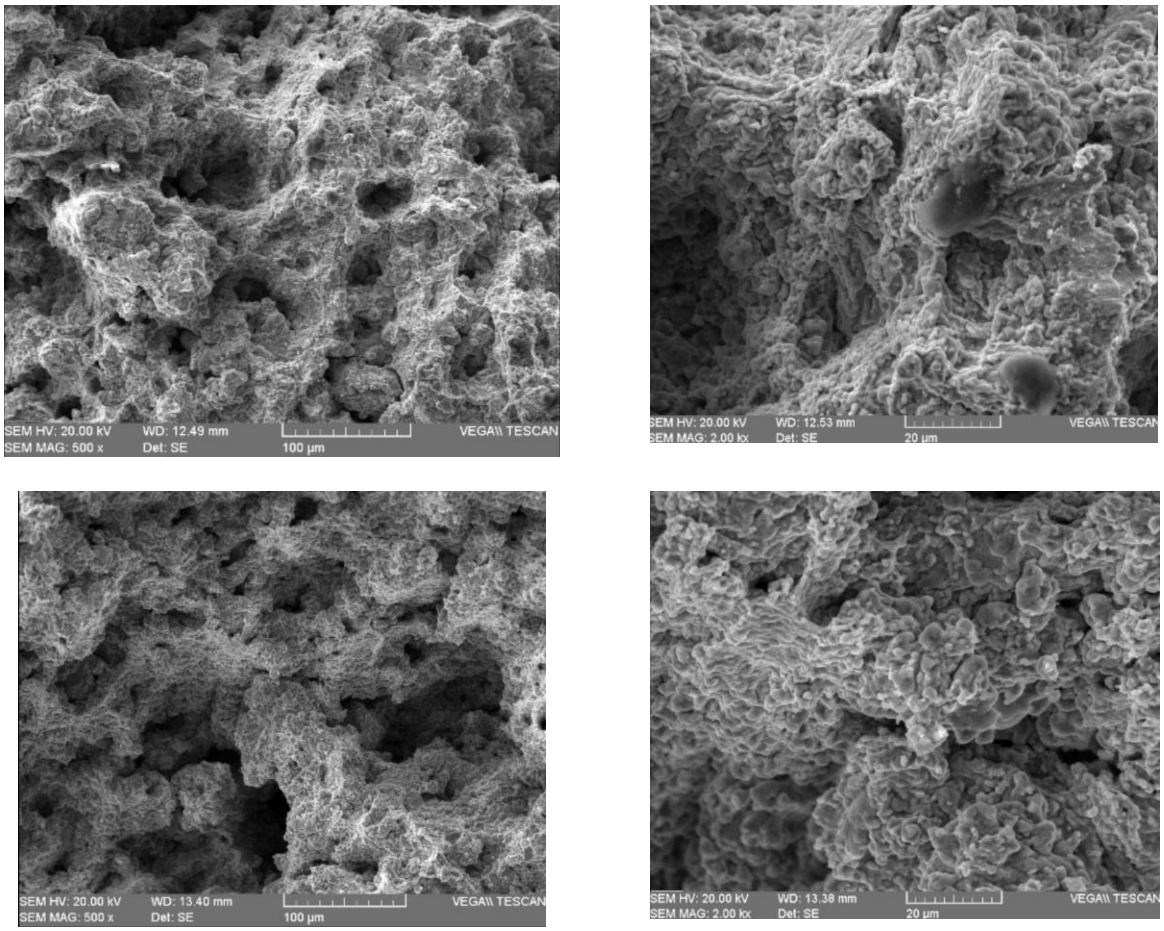

Figure 5-38. SEM images of Inconel 600 smooth sample fractured under a creep environment at 650 ℃ and 400 MPa stress

Further examination of the SEM images revealed that the un-welded samples predominantly exhibited ductile transgranular features, which are rough fracture surfaces with evidence of extensive plastic deformation. On the other hand, the welded samples showed more prominent brittle intergranular features, characterized by cleavage-like fractures along grain boundaries.

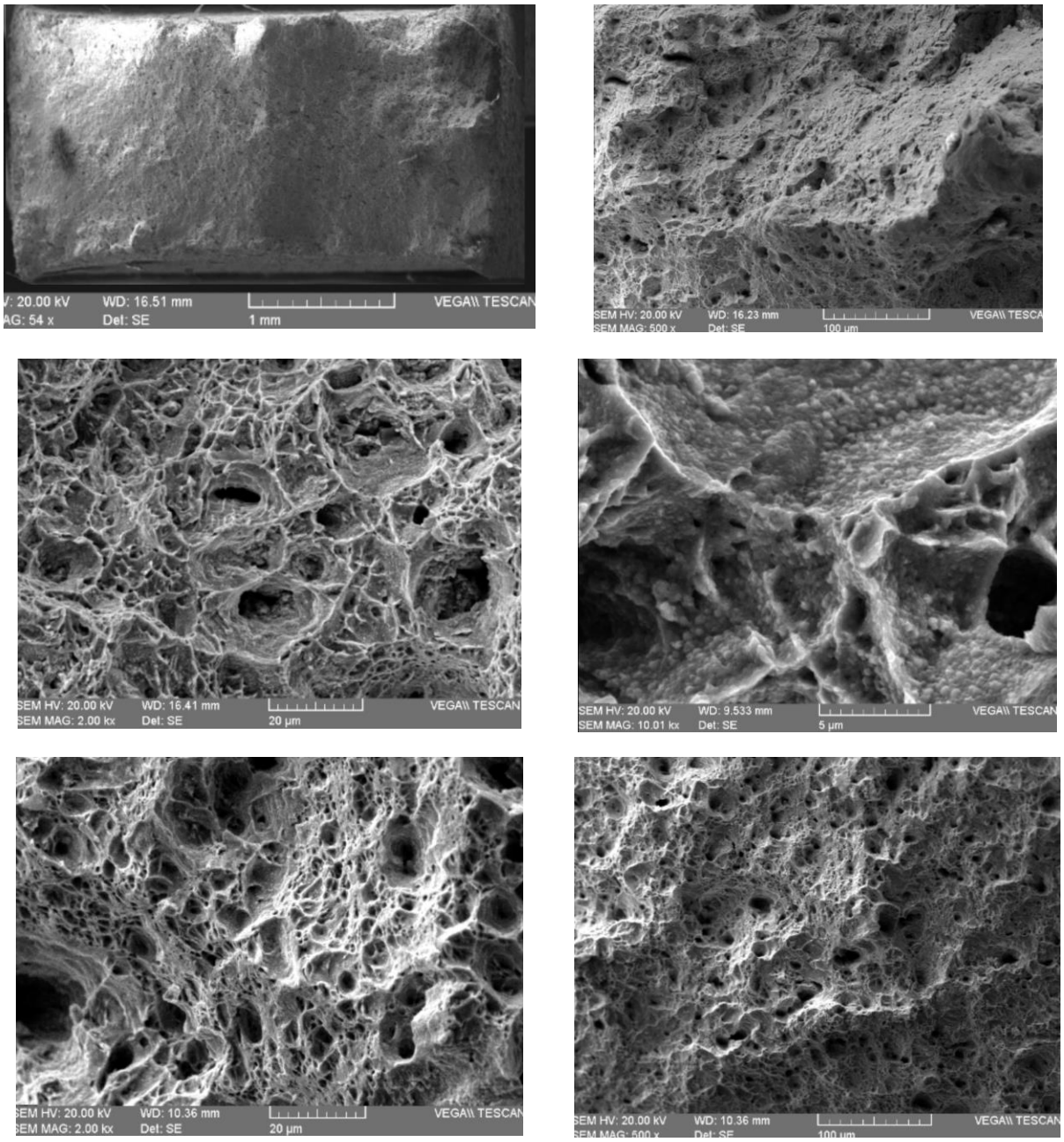

Figure 5-39. SEM images of Inconel 600 welded sample fractured under a creep environment at 650 ℃ and 400 MPa stress

Figure 5-39 shows that a brittle fracture is characterized by minimal plastic deformation and a smooth, cleavage-like fracture surface. SEM images revealed that welded samples exhibited more evidence of brittle-type fracture than un-welded samples, as shown in Figure 5-38. This observation indicates that the welding process can induce a more brittle fracture mode under creep conditions. The presence of welding introduces stress

concentration points and alters the microstructure, making the material more susceptible to brittle fracture.

6. Conclusions and Future Work

6.1. Conclusion

- The mechanical behavior and fatigue characteristics of Inconel 600 were comprehensively investigated through experimental tests and FE simulations.
- Experiments provided information on the material's mechanical properties, fatigue life, and fracture behavior.
- FE simulations, along with empirical fatigue damage models, allowed for accurate fatigue life predictions and identification of critical loading conditions.
- Quasi-static tests revealed the stress-strain behavior, determining yield strength, ultimate tensile strength, elongation, and modulus of elasticity, using the Ramberg-Osgood equation.
- Microstructural analysis detailed grain size and variations in the welded joints, with distinct HAZ microstructures affecting mechanical properties and fracture behavior.
- Fatigue tests under smooth and notched conditions unveiled fatigue life variations based on loading scenarios.
- FE analysis showed a close correlation with experimental fatigue data, indicating simulation reliability, despite some discrepancies due to internal welding defects.
- The study emphasized mixed-mode loading's influence on fatigue life and the importance of notch strength reduction factors for precise fatigue predictions.
- Fractographic analysis using SEM images provided insights into fracture behavior under tensile and fatigue loading conditions.
- Welding influenced the fracture mode, with welded samples showing more brittle-type fractures due to stress concentration points and preferential crack initiation along grain boundaries, leading to brittle intergranular features.

6.2. Recommendations and Future Work

- Based on the findings from this study, several areas for future research and improvement can be identified. Firstly, further investigation into the influence of

internal defects related to the welding process on fatigue behavior could be conducted. Identifying and understanding the role of these defects in fatigue crack initiation and propagation would enhance the accuracy of fatigue life predictions.

- Additionally, exploring the effects of different welding techniques and parameters on the microstructure and mechanical properties of weldments can provide useful information about optimizing welding processes and improving the performance of welded structures.
- Further studies on the creep behavior of Inconel 600 at lower temperatures, such as 300-400℃, would be beneficial in understanding the material's suitability for high-temperature applications. This could provide valuable information for engineering applications where creep may occur at lower temperature levels.
- To expand the understanding of fatigue behavior under complex loading conditions, more extensive FE simulations and experimentation with different combinations of loading scenarios could be conducted. This would enable the identification of critical loading conditions for a wider range of practical engineering applications.
- Lastly, investigating the long-term durability and fatigue life of Inconel 600 weldments in real-world engineering applications, such as in gas turbines, can provide valuable data for material selection and design optimization.
- In conclusion, this study has provided valuable information about the mechanical behavior, fatigue characteristics, and fracture behavior of Inconel 600. The findings contribute to the overall understanding of the material's performance under different loading conditions, aiding in the optimization of design strategies and enhancing the durability of components made from this alloy. The identified areas for future research can further advance the knowledge and applicability of Inconel 600 in various engineering applications.

References

1. Pilavachi, P.A., *Mini- and micro-gas turbines for combined heat and power.* Applied Thermal Engineering, 2002. **22**: p. 2003–2014.
2. Beith, R., *Small and Micro Combined Heat and Power (CHP) Systems: Advanced Design, Performance, Materials and Applications*. 2011: Woodhead Publishing Series in Energy.
3. Pirkandi, J. and e. al., *Simulation and multi-objective optimization of a combined heat and power (CHP) system integrated with low-energy buildings.* 2016. **5**: p. 13-23.
4. Kalam, A. and e. al., *Combined heat and power systems: economic and policy barriers to growth.* Chemistry Central Journal, 2012. **6**.
5. Backman, J.L.H. and J. Kaikko, *Microturbine systems for small combined heat and power (CHP) applications*, R. Beith, Editor. 2011, Woodhead Publishing Series in Energy.
6. Holmes, A.S. and e. al., *Laser Profiling of 3-P Microturbine Blades*, in *Fourth International Symposium on Laser Precision Microfabrication*. 2003.
7. Gajalappa, Y. and e. al., *Flow behaviour kinetics of Inconel 600 superalloy under hot deformation using gleeble 3800.* Materials Today: Proceedings, 2021. **45**: p. 5320-5322.
8. Nanaware, A. and e. al., *Mechanical Characterization of Nickel Alloys on Turbine Blades.* REST Journal on Emerging trends in Modelling and Manufacturing, 2015. **1**(1): p. 15-19.
9. Chavez, S.A., et al., *High-temperature tensile and creep data for Inconel 600, 304 stainless steel and SA106B carbon steel.* Nuclear Engineering and Design, 1994. **148**: p. 351-363.
10. Akca, E. and A. Gursel, *A Review on Superalloys and IN718 Nickel-Based INCONEL Superalloy.* PERIODICALS OF ENGINEERING AND NATURAL SCIENCES, 2015. **3**(1): p. 15-27.
11. Pollock, T.M. and S. Tin, *Nickel-Based Superalloys for Advanced Turbine Engines: Chemistry, Microstructure, and Properties.* JOURNAL OF PROPULSION AND POWER, 2006. **22**(2).
12. https://www.phase-trans.msm.cam.ac.uk/2003/Superalloys/superalloys.html.
13. Deepanraj, B. and e. al., *Theoretical Analysis of Gas Turbine Blade by Finite Element Method.* Scientific World, 2011. **9**(9): p. 29-33.
14. Hou, J., B.J. Wicks, and R.A. Antoniou, *An investigation of fatigue failures of turbine blades in a gas turbine engine by mechanical analysis.* Engineering Failure Analysis, 2002. **9**: p. 201–211.
15. Singh, H.P. and e. al., *Computational analysis of a gas turbine blade with different materials.* Materials Today: Proceedings, 2021. **44**: p. 63-69.
16. Chintala, G. and P. Gudimetla, *Optimum material evaluation for gas turbine blade using Reverse Engineering (RE) and FEA.* Procedia Engineering, 2014. **97**: p. 1332 – 1340.
17. Findley, W.N., *A Theory for the Effect of Mean Stress on Fatigue of Metals Under Combined Torsion and Axial Load or Bending.* ASME. J. Eng. Ind. , 1959. **81**(4): p. 301-305.
18. Maddox, S.J., *The effect of mean stress on fatigue crack propagation A literature review.* International Journal of Fracture, 1975. **11**(3): p. 389-408.
19. Dowling, N.E., C.A. Calhoun, and A. Arcari, *Mean stress effects in stress-life fatigue and the Walker equation.* Fatigue & Fracture of Engineering Materials & Structures, 2009. **32**: p. 163–179.
20. Barbosa, J.F. and e. al., *Fatigue life prediction of metallic materials considering mean stress effects by means of an artificial neural network.* International Journal of Fatigue, 2020. **135**.
21. Dowling, N.E., *Mean Stress Effects in Stress-Life and Strain-Life Fatigue.* SAE Technical Paper, 2004.
22. Nihei, M. and e. al., *Evaluation of mean stress effect on fatigue life by use of damage parameters* International Journal of Fatigue, 1986. **8** (3): p. 119-126.
23. Hanlon, T., Y.-N. Kwon, and S. Suresh, *Grain size effects on the fatigue response of nanocrystalline metals.* Scripta Materialia, 2003. **49**: p. 675–680.

24. Hanlon, T., E.D. Tabachnikova, and S. Suresh, *Fatigue behavior of nanocrystalline metals and alloys.* International Journal of Fatigue, 2005. **27**: p. 1147–1158.
25. Colin, J., A. Fatemi, and S. Taheri, *Fatigue Behavior of Stainless Steel 304L Including Strain Hardening, Prestraining, and Mean Stress Effects.* Journal of Engineering Materials and Technology, 2010. **132**.
26. F Brenne and T. Niendorf, *Effect of notches on the deformation behavior and damage evolution of additively manufactured 316L specimens under uniaxial quasi-static and cyclic loading.* International Journal of Fatigue, 2019. **127**: p. 175-189.
27. K Solberg, D Wan, and F. Berto, *Fatigue assessment of as-built and heat-treated Inconel 718 specimens produced by additive manufacturing including notch effects.* Fatigue Fract Eng Mater Struct., 2020. **43**: p. 2326–2336.
28. Nicoletto, G., *Directional and notch effects on the fatigue behavior of as-built DMLS Ti6Al4V.* International Journal of Fatigue 2018. **106**: p. 124-131.
29. S M J Razavi, et al., *Fatigue strength of blunt V-notched specimens produced by selective laser melting of Ti-6Al-4V.* Theoretical and Applied Fracture Mechanics, 2018. **97**: p. 376-384.
30. Hajshirmohammadi, B. and M.M. Khonsari, *Application of thermoelectricity in fatigue of metals.* Fatigue Fract Eng Mater Struct., 2021. **44**: p. 1162–1177.
31. Kuk, J.M. and e. al., *Effects of temperature and shielding gas mixture on fatigue life of 5083 aluminum alloy.* Journal of Materials Processing Technology, 2004. **155-156**: p. 1408–1414.
32. Ragab, A., H. Alawi, and K. Sorein, *Corrosion Fatigue of Steel in Various Aqueous Environments* Fatigue Fract. Engng Mater. Struct., 1989. **12**(6): p. 469-479.
33. Zhang, Y. and e. al., *Research on corrosion and fatigue performance of weathering steel and High-Performance steel for bridges.* Construction and Building Materials, 2021. **289**.
34. Hudson, C.M. and S.K. Seward, *A Literature Review and Inventory of the Effects of Environment on the Fatigue Behavior of Metals* Engineering Fracture Mechanics, 1976. **8**: p. 315-329.
35. Bennett, J.A., *Changes in the Influence of Atmospheric Humidity During Fatigue of an Aluminum Alloy.* JOURNAL OF RESEARCH of the National Bureau of Standards- C. Engineering and Instrumentation, 1964. **68C**(2).
36. Jeddi, D. and T. Palin-Luc, *A review about the effects of structural and operational factors on the gigacycle fatigue of steels.* Fatigue Fract Eng Mater Struct., 2018. **41**: p. 969–990.
37. Bag, A. and e. al., *Effect of different shot peening conditions on the fatigue life of 300 M steel submitted to high stress amplitudes.* International Journal of Fatigue, 2020. **130**.
38. Croccolo, D. and e. al., *Fatigue Response of As-Built DMLS Maraging Steel and Effects of Aging, Machining, and Peening Treatments.* Metals, 2018. **8**(505).
39. Sirin, S.Y., K. Sirin, and E. Kaluc, *Effect of the ion nitriding surface hardening process on fatigue behavior of AISI 4340 steel.* Materials Characterization, 2008. **59**: p. 351 – 358.
40. Suresh, S., *Fatigue of Materials*. 2 ed. 1998: Cambridge University Press.
41. Kim, S., *Factors Influencing Fatigue Crack Propagation Behavior of Austenitic Steels.* Met. Mater. Int., 2013. **19**(4): p. 683-690.
42. Ritchie, R.O., *Mechanisms of Fatigue Crack Propagation in Metals, Ceramics and Composites: Role of Crack Tip Shielding.* Materials Science and Engineering A, 1988. **103**: p. 15-28.
43. Tokaji, K. and e. al., *LIMITATIONS OF LINEAR ELASTIC FRACTURE MECHANICS IN RESPECT OF SMALL FATIGUE CRACKS AND MICROSTRUCTURE.* Fatigue Fract. Engng Mater. Struct., 1986. **9**(1): p. 1-14.
44. A. Pineau, et al., *Failure of metals II: Fatigue.* Acta Materialia, 2016. **107**: p. 484-507.
45. Dowling, N.E., *Mechanical Behavior of Materials, Engineering methods for Deformation, Fracture, and Fatigue*. Fourth Edition ed. 2013: Angshuman Chakraborty.

46. Gough, H.J. and H.V. Pollard, *The Strength of Metals under Combined Alternating Stresses.* Proceedings of the Institution of Mechanical Engineers, 1935. **13**(1): p. 3-103.
47. Lee, B. and S.-B. Lee, *A stochastic modeling of multiaxial fatigue life and damage accumulation of sm45c steel*, in *Proc. Fifth International Conference on Biaxial/Multiaxial Fatigue and Fracture*. p. 593-607.
48. Carpinteri, A., A. Spagnoli, and S. Vantadori, *A critical plane-based criterion for high-cycle multiaxial fatigue using averaged principola stress directions*, in *Proceedings of the Workshop on:"Progettazione a fatica in presenza di multiassialità tensionali*. 2005: Italy.
49. Matake, T., *An explanation on fatigue limit under combined stress.* Bulletin of the JSME, 1977. **20**(141): p. 745-755.
50. Papadopoulos, I.V., *Long life fatigue under multiaxial loading.* International Journal of Fatigue, 2001. **23**: p. 839-849.
51. Backstrom, M. and G. Marquis, *A review of multiaxial fatigue of weldments: experimental results, design code and critical plane approaches.* Fatigue Fract Engng Mater Struct, 2001. **24**: p. 279–291.
52. Fatemi, A. and D.F. Socie, *A Critical Plane Approach to Multiaxial Fatigue Damage Including Out-of-Phase Loading.* Fatigue Fract. Engng Mater. Struct., 1988. **11**(3): p. 149-165.
53. Riemer, A. and e. al., *On the fatigue crack growth behavior in 316L stainless steel manufactured by selective laser melting.* Engineering Fracture Mechanics, 2014. **120**: p. 15-25.
54. Dahar, M.S. and e. al., *Effects of test orientation on fracture and fatigue crack growth behavior of third generation as-cast Tie48Ale2Nbe2Cr.* Intermetallics, 2015. **57**: p. 73-82.
55. Ritchie, R.O. and J.F. Knott, *Mechanisms of fatigue crack growth in low alloy steel.* ACTA METALLURGICA, 1973. **21**: p. 639-648.
56. Jr., W.A.Z. and J.J. Lewandowski, *Effects of R-Ratio on the Fatigue Crack Growth of Nb-Si(ss) and Nb-10Si In Situ Composites.* METALLURGICAL AND MATERIALS TRANSACTIONS A 1998. **29A**: p. 1749-1757.
57. Maiti, S. and P.H. Geubelle, *A cohesive model for fatigue failure of polymers.* Engineering Fracture Mechanics, 2005. **72**: p. 691–708.
58. Kirane, K. and Z.P. Bazˇant, *Size effect in Paris law and fatigue lifetimes for quasibrittle materials: Modified theory, experiments and micro-modeling.* International Journal of Fatigue, 2016. **83**: p. 209-220.
59. Kujawski, D., *Correlating R-ratio effects on FCG behavior using ΔKd function.* Theoretical and Applied Fracture Mechanics 2022. **118**.
60. Ding, J., R. Hall, and J. Byrne, *Effects of stress ratio and temperature on fatigue crack growth in a Ti–6Al–4V alloy.* International Journal of Fatigue, 2005. **27**: p. 1551–1558.
61. Boyle, J.T. and J. Spence, *Stress analysis for creep*. 2013: Elsevier.
62. Kassner, M.E., *Fundamentals of creep in metals and alloys*. 2015: Butterworth-Heinemann.
63. Blum, W., P. Eisenlohr, and F. Breutinger, *Understanding Creep—a Review.* METALLURGICAL AND MATERIALS TRANSACTIONS A, 2002. **33A**: p. 291-303.
64. Naumenko, K. and A. Holm, *Modeling of creep for structural analysis*. 2007: Springer Science & Business Media.
65. He, H. and e. al., *Failure analysis of steam turbine blade roots.* Engineering Failure Analysis, 2020. **115**.
66. Isobe, N. and S. Nogami, *Micro-crack growth behavior and life in high temperature low cycle fatigue of blade root and disc joint for turbines.* International Journal of Pressure Vessels and Piping, 2009. **86**: p. 622–627.
67. Krechkovska, H. and e. al., *Peculiarities of fatigue fracture of high-alloyed heat-resistant steel after its operation in steam turbine rotor blades.* International Journal of Fatigue 2023. **167**.

68. Epishin, A. and T. Link, *Mechanisms of high-temperature creep of nickelbased superalloys under low applied stresses.* Philosophical Magazine, 2004. **84**(19): p. 1979-200.
69. Rae, C.M.F. and R.C. Reed, *Primary creep in single crystal superalloys: Origins, mechanisms and effects.* Acta Materialia, 2007. **55**: p. 1067–1081.
70. Boehlert, C.J., *The effect of thermomechanical processing on the creep behavior of Alloy 690.* Materials Science and Engineering A, 2008. **473**: p. 233–237.
71. Li, Z. and e. al., *Experimental investigation on creep-fatigue behaviours of as-received and service-exposed turbine blades: Mechanism and life evaluation.* Fatigue Fract Eng Mater Struct. , 2020. **43**: p. 2892–2906.
72. Sugahara, T. and e. al., *Creep and Mechanical Behavior Study of Inconel 718 Superalloy.* Materials Research, 2022. **25**.
73. Vakili-Tahami, F. and M.R. Adibeig, *Investigating the possibility of replacing IN 738LC gas turbine blades with IN 718.* Journal of Mechanical Science and Technology, 2015. **29**(10): p. 4167~4178.
74. Zhang, J. and e. al., *Characterization of mechanical properties of in-service nickel-based alloy by continuous indentation.* Structures 2023. **48**: p. 1346-1355.
75. Karthik, D. and S. Swaroop, *Laser shock peening enhanced corrosion properties in a nickel based Inconel 600 superalloy.* Journal of Alloys and Compounds, 2017. **694**: p. 1309-1319.
76. Makuch, N. and M. Kulka, *Microstructural characterization and some mechanical properties of gas-borided Inconel 600-alloy.* Applied Surface Science, 2014. **314**: p. 1007-1018.
77. *Standard Test Methods for Tension Testing of Metallic Materials*, in *ASTM E8-04*. 2004.
78. Skelton, R.P., H.J. Maier, and H.-J. Christ, *The Bauschinger effect, Masing model and the Ramberg–Osgood relation for cyclic deformation in metals.* Materials Science and Engineering A, 1997. **238**: p. 377–390.
79. Niesłony, A. and e. al., *New method for evaluation of the Manson–Coffin–Basquin and Ramberg–Osgood equations with respect to compatibility.* International Journal of Fatigue, 2008. **30**: p. 1967–1977.
80. Weixing, Y., X. Kaiquan, and G. Yi, *On the fatigue notch factor, Kf.* International Journal of Fatigue, 1995. **17**(4): p. 245-251.
81. Kim, K.S. and e. al., *Estimation methods for fatigue properties of steels under axial and torsional loading.* International Journal of Fatigue, 2002. **24**: p. 783–793.
82. Baumel, A.J.R. and T. Seeger, *Materials data for cyclic loading.* Materials science monographs, 1990. **61**.
83. *ASTM E466 – FORCE CONTROLLER CONSTANT AMPLITUDE AXIAL FATIGUE TESTING OF METALLIC MATERIALS*.
84. Zhang, Y., J.C. Outeiro, and T. Mabrouki, *On the selection of Johnson-Cook constitutive model parameters for Ti-6Al-4V using three types of numerical models of orthogonal cutting* Procedia CIRP, 2015. **31**: p. 112 – 117.
85. Buzyurkin, A.E., I.L. Gladky, and E.I. Kraus, *Determination and verification of Johnson–Cook model parameters at high-speed deformation of titanium alloys.* Aerospace Science and Technology, 2015. **45**: p. 121-127.
86. Pretorius, J.G. and e. al., *Effect of Laser Shock Peening on Fatigue Life at Stress Raiser Regions of a High-Speed Micro Gas Turbine Shaft: A Simulation Based Study.* International Journal of Engineering Research in Africa, 2019. **45**: p. 15-27.
87. Zhang, X. and e. al., *A comprehensive review of fatigue behavior of laser shock peened metallic materials.* Theoretical and Applied Fracture Mechanics, 2022. **122**.
88. Pan, X. and e. al, *Microstructure and residual stress modulation of 7075 aluminum alloy for improving fatigue performance by laser shock peening* International Journal of Machine Tools and Manufacture, 2023. **184**.

89. Z. Tang, e.a., *An investigation on the effect of change in experimental sequence of warm laser shock peening and laser shock peening on the performance of DD6 nickel-based single-crystal superalloy.* Surface & Coatings Technology, 2023. **464**.
90. Y. Vamsi, e.a., *Investigation of surface structural modifications caused by the influence of the ablative layer in Inconel718 Ni-base superalloy through laser shock peening.* Materials Letters, 2024. **354**.
91. Brockman, R.A. and e. al., *Prediction and characterization of residual stresses from laser shock peening.* International Journal of Fatigue, 2012. **36**: p. 96-108.
92. Maawad, E. and e. al., *Investigation of laser shock peening effects on residual stress state and fatigue performance of titanium alloys.* Materials Science and Engineering A, 2012. **536**: p. 82-91.
93. Y. Li, e.a., *Thermal evolutions of residual stress and strain hardening of GH4169 Ni-based superalloy treated by laser shock peening.* Surface & Coatings Technology, 2023. **467**.
94. Chahardehi, A., F.P. Brennan, and A. Steuwer, *The effect of residual stresses arising from laser shock peening on fatigue crack growth.* Engineering Fracture Mechanics, 2010. **77**: p. 2033–2039.
95. Rodopoulos, C.A. and e. al., *Effect of Controlled Shot Peening and Laser Shock Peening on the Fatigue Performance of 2024-T351 Aluminum Alloy.* Journal of Materials Engineering and Performance, 2003. **12**: p. 414-419.
96. Maleki, E. and e. al., *The effects of shot peening, laser shock peening and ultrasonic nanocrystal surface modification on the fatigue strength of Inconel 718.* Materials Science & Engineering A, 2021. **810**.
97. Yin, M. and e. al., *Improving impact wear resistance of Ti–6Al–4V alloy treated by laser shock peening.* Trans. Nonferrous Met. Soc. China, 2019. **29**: p. 1439−1448.
98. Li, X. and e. al., *Research on Wear Resistance of AISI 9310 Steel with Micro-Laser Shock Peening.* Metals 2022, 12, 2022. **12**.
99. Lim, H. and e. al., *Enhancement of abrasion and corrosion resistance of duplex stainless steel by laser shock peening.* Journal of Materials Processing Technology, 2012. **212**: p. 1347–1354.
100. Lu, J.Z. and e. al., *Corrosion behaviour of AISI 304 stainless steel subjected to massive laser shock peening impacts with different pulse energies.* Corrosion Science, 2014. **80**: p. 53-59.
101. Sundar, R. and e. al., *Laser Shock Peening and its Applications: A Review.* Lasers in Manufacturing and Materials Processing, 2019. **6**: p. 424–463.
102. Zhang, C., Y. Dong, and C. Ye, *Recent Developments and Novel Applications of LaserShock Peening: A Review.* Adv. Eng. Mater., 2021. **23**.
103. Bold, P.E., M.W. Brown, and R.J. Alle, *A review of fatigue crack growth in steels under mixed mode I and II loading* Fatigue Fract. Engng Mater. Struct., 1992. **15**(10): p. 965-977.
104. Schackert, S.M. and C. Schweizer, *Investigation of damage mechanisms and short fatigue crack growth during thermomechanical fatigue loading of the nickel-based superalloy Inconel 100.* Fatigue Fract Eng Mater Struct., 2022. **45**: p. 2261–2276.
105. Seifi, R. and N. Omidvar, *Fatigue crack growth under mixed mode I + III loading.* 2013. **34**: p. 1-15.
106. Jesus, J.S. and e. al, *Fatigue crack growth under mixed mode I + II in Ti-6Al-4V specimens produced by Laser powder Bed fusion.* Engineering Fracture Mechanics, 2022. **264**.
107. Mirsayar, M.M., *A novel multiscale model for mixed-mode fatigue crack growth in laminated composites.* International Journal of Mechanical Sciences, 2023. **255**.
108. Sajith, S., K.S.R.K. Murthy, and P.S. Robi, *Experimental and numerical investigation of mixed mode fatigue crack growth models in aluminum 6061-T6.* International Journal of Fatigue, 2020. **130**.
109. Rozumek, D. and e. al., *Experimental and numerical investigation of mixed mode I + II and I + III fatigue crack growth in S355J0 steel.* International Journal of Fatigue, 2018. **113**: p. 160-170.

110. Oskui, A.E., N. Choupani, and M. Shameli, *3D Characterization of Mixed-Mode Fracture Toughness of Materials Using a New Loading Device.* Latin American Journal of Solids and Structures, 2016. **13**: p. 1464-1482.
111. Choupani, N., *Experimental and numerical investigation of the mixed-mode delamination in Arcan laminated specimens.* Materials Science and Engineering A, 2008. **478**: p. 229–242.
112. Q. Xie, e.a., *Experimental and numerical investigation of mixed-mode fatigue crack growth in nickel-based superalloy at high temperature.* Engineering Fracture Mechanics, 2022. **273**.